# A comprehensive and internally consistent mineral dissolution rate database: Part I: Primary silicate minerals and glasses

Matylda Heřmanská, Martin Voigt, Chiara Marieni, Julien Declercq, Eric Oelkers

*Submitted to Chemical Geology*

# A comprehensive and internally consistent mineral dissolution rate database: Part I: Primary silicate minerals and glasses

Matylda Heřmanská[1], Martin J. Voigt[2], Chiara Marieni[1], Julien Declercq[3], and Eric H. Oelkers[1]

**AFFILIATION** :

[1] Géosciences Environnement Toulouse, CNRS, 14 Avenue Edouard Belin, 31400 Toulouse (France)

[2] Institute of Earth Sciences, University of Iceland, Sturlugötu 7, 101 Reykjavík (Iceland)

[3]SRK Consulting (UK) Limited, Churchill House, 17 Churchill Way, Cardiff, CF10 2HH, Wales, UK

**Keywords:** mineral dissolution rates, database, primary silicates, PHREEQC, TOUGHREACT

## Abstract

Mineral dissolution rates control the temporal evolution of many natural processes on the surface and upper crust of the Earth. This is the first of a series of papers describing the development and implementation of a comprehensive and internally consistent database of the dissolution rates of the major rock-forming minerals. In this paper, we describe the retrieval and regression of the dissolution rates of the primary rock-forming silicates, including quartz and other $SiO_2$ polymorphs, feldspars, pyroxenes, amphiboles, micas, volcanic glass, and olivines. Owing to the limited fluid chemistry data available for many of the published experimental studies, BET surface area normalized mineral and most glass dissolution rates ($r$) were regressed using

$$r = \sum_i \left( A_i a_{\mathrm{H}^+}^{n_i} e^{\frac{E_{a_i}}{RT}} \right) \left( 1 - \exp(-\frac{\mathbf{A}}{\sigma RT}) \right)$$

where $A_i$ stands for pre-exponential factors, $a_{H^+}$ corresponds to the hydrogen ion activity, $n_i$ refers to reaction orders, $T$ designates absolute temperature, $R$ denotes the gas constant, $E_{ai}$ represents activation energies, $\sigma$ stands for Temkin's average stoichiometric number, and **A** denotes the chemical affinity of the dissolution reaction. Where relevant data were lacking, rates were extrapolated assuming that mineral dissolution follows similar trends within the same mineral group. Regression was performed using least-squares algorithms. The average difference between calculated and measured rates ranged from 0.2 to 0.8 log units depending on the mineral. The obtained rate equations were implemented into the *carbfix.dat* database for direct use in the PHREEQC software but can be extended to other geochemical modeling software, such as TOUGHREACT.

# 1. Introduction

The dissolution of primary minerals plays a crucial role in many natural geological processes in the upper crust, including surface weathering, soil evolution, and mass transfer in surface waters and hydrothermal systems (e.g., Berner and Holdren, 1979; Colman, 1982; Berner et al., 1983; Eggleton, 1987; Drever, 1988; Banfield et al., 1991; Brady, 1991; Nesbitt and Wilson, 1992; Shoji et al., 1993; Brady and Carroll, 1994; Lasaga et al., 1994; Gislason et al., 1996; Kump et al., 2000; Chadwick and Chorover, 2001; Beig and Lüttge, 2006; Maher et al., 2009; Xiao et al., 2018). Mineral dissolution rates are also critical to geoengineered systems such as carbon capture and storage, nuclear waste management, and industrial waste neutralization (e.g., Malow et al., 1984; Crovisier et al., 1988; Van Herk et al., 1989; Jercinovic et al., 1990; Morgenstein and Shettel, 1993; Jonckbloedt, 1998; Xiao et al., 1999; Berg and Banwart, 2000; Oelkers and Schott, 2005; Bertier et al., 2006; McGrail et al., 2006; Stopar et al., 2006; Matter et al., 2007, 2016; Goldberg et al., 2008; Hausrath et al., 2008; Oelkers et al., 2008; Oelkers and Cole, 2008; Olsen and Rimstidt, 2008; Kampman et al., 2009; Matter and Kelemen, 2009; Prigiobbe et al., 2009; Schaef and McGrail, 2009; Schaef et al., 2009, 2010; Gislason et al., 2010; Hausrath and Brantley, 2010; King et al., 2010; Guyot et al., 2011; Köhler et al., 2013; Lu et al., 2013; Wang et al., 2013; Sissmann et al., 2013, 2014; Wang et al., 2013; Dehouck et al., 2014; Velbel, 2014; Olsen et al., 2015; Tutolo et al., 2015; Niles et al., 2017; Li et al., 2018). The quantification of mineral dissolution rates at conditions of major geochemical processes, including surface weathering and fluid-rock interaction, is, therefore, a major step towards constraining the temporal evolution of these processes.

Numerous experimental studies have reported the dissolution rates of primary and secondary minerals at various temperatures and initial fluid composition. Much of this work has been summarized in the literature (e.g., Blum and Stillings, 1995; Brantley, 2003; Marini, 2007; Brantley et al., 2008; Ganor et al., 2009; Crundwell, 2015). As noted by White and Brantley (1995) and Brantley et al. (2008), however, the interpretation and interlaboratory comparisons of mineral dissolution rates are challenging due to several factors, including changing aqueous solution and mineral surface compositions, secondary phase precipitation, and surface area variations as a function of elapsed time (c.f., Aagaard and Helgeson, 1982; Helgeson et al., 1984; Murphy and Helgeson, 1987; Oelkers, 2001a; Brantley, 2003). Moreover, experimental methods and sample preparation such as wet grinding or sieving can lead to preferential leaching and non-stoichiometric dissolution (Nagy, 1995). There has also been much debate about the consistency of laboratory-measured rates with those of natural processes (Walther and Wood, 1986; Schnoor, 1990; Swoboda-Colberg and Drever, 1993; Velbel, 1993) as summarized in White and Brantley (1995) and Brantley et al. (2008).

Several past studies have regressed some of the available mineral rate data (Sverdrup, 1990; Brantley and Chen, 1995; White and Brantley, 1995; Palandri and Kharaka, 2004; Marini, 2007;

Brantley et al., 2008; Schott et al., 2009). Zhang et al. (2019) incorporated some of these rate equations into a PHREEQC script to facilitate their use in geochemical modeling calculations, but made no effort to update or verify the internal consistency of these rates. This study builds on this past work by 1) updating the regression calculations to account for rates published over the past 20 years, 2) deriving an internally consistent database of the rate equations and parameters, and 3) formatting the database for direct use within PHREEQC (Parkhurst and Appelo, 1999) and TOUGHREACT (Xu et al., 2006, 2011). It is anticipated that this newly created database can serve as a benchmark enabling the direct comparison of the results of geochemical modeling calculations in dynamic and time-dependent fluid-mineral systems. The purpose of this manuscript is to introduce this new mineral dissolution rate database and to document the retrieval of rate parameters for the major rock-forming primary silicates. Subsequent series will provide similar documentation of the retrieval of rate parameters for other major rock-forming minerals.

# 2. Theoretical background

## Notation

| | | | |
|---|---|---|---|
| $a_{H^+}$ | Activity of aqueous $H^+$ | $R^2$ | Coefficient of determination |
| **A** | Chemical affinity of the reaction dissolution reaction (kJ $mol^{-1}$) | $r$ | Dissolution rate (mol $m^{-2}$ $s^{-1}$) |
| $A_0, A'_0$ | Temperature-independent pre-exponential factor (mol $m^{-2}$ $s^{-1}$) | $r_+$ | Forward (or far-from-equilibrium) dissolution rate (mol $m^{-2}$ $s^{-1}$) |
| $E_a$ | Activation energy (kJ $mol^{-1}$) | $S$ | Specific surface area ($m^2$ $g^{-1}$) |
| $E'_a$ | Apparent activation energy (kJ $mol^{-1}$) | $T$ | Temperature in K |
| $k$ | Rate constant (mol $m^{-2}$ $s^{-1}$) | $\bar{y}$ | Average experimentally measured experimental rate |
| $K$ | Equilibrium constant for the dissolution reaction | $y_i$ | Measured experimental rate |
| $n_i$ | Reaction order | $\sigma$ | Temkin's average stoichiometric number |
| $R$ | Gas constant (8.314 J $K^{-1}$ $mol^{-1}$) | | |

## 2.1 Fundamentals of mineral dissolution kinetics

This study focuses on quantifying the surface area normalized *steady-state* dissolution rates of minerals. Steady-state rates, rates that are proportional to the mineral surface area but do not vary with time, are thought to be most suitable for modeling natural processes. During the initial part of many mineral dissolution rate experiments, non-steady-state behaviors are observed, where the release rates of the elements vary significantly with time. Such behavior has been attributed to a number of processes including a preferential initial dissolution of fine particles adhering to larger grains in the

reactor (Holdren and Speyer, 1985; Talman and Nesbitt, 1988), the preferential removal of liable elements, such as alkali metals from feldspars (Chou and Wollast, 1985; Casey et al., 1993), and the rapid changes in reactive fluid composition including pH (Oelkers et al., 2001). Another factor that alters experimentally measured reactions rates over time are changes in mineral surface area. For example, Oxburgh et al. (1994) noted that the dissolution rates of plagioclase decreased continuously during their experiments. Such decreasing rates can potentially occur due to a decrease in the reactive surface area as the mineral dissolves (Köhler et al., 2005). Such factors make the definition of what is a steady-state rate in any experiment somewhat ambiguous. As it is not possible in most studies to determine a globally consistent definition of steady-state dissolution rates, the pragmatic approach adopted in this study is to accept the definition of steady-state as reported in each published study.

The steady-state surface area normalized dissolution rate of a mineral, $r$, can be considered to be the difference between the forward rate ($r_+$) and the reverse rate ($r_-$) such that

$$r = r_+ - r_- = r_+\left(1 - \frac{r_-}{r_+}\right) \quad . \tag{1}$$

Taking into account the law of detailed balancing, it can be shown that **Eq. (1)** is equivalent to

$$r = r_+(1 - \exp(-\mathbf{A}/(\sigma RT))) \quad , \tag{2}$$

where $\sigma$ stands for Temkin's average stoichiometric number equal to the ratio of the rate of destruction of the activated or precursor complex relative to the overall dissolution rate, **A** denotes the chemical affinity or the Gibbs free energy of the dissolution reaction, $T$ defines the absolute temperature, and $R$ signifies the gas constant (Aagaard and Helgeson, 1977, 1982; Lasaga, 1981; Schott and Oelkers, 1995). The majority of mineral dissolution rates for the major silicate minerals reported in the literature have been performed at far-from-equilibrium conditions such that $\mathbf{A} >> \sigma RT$. At such conditions, $r_- << r_+$ and thus $r \approx r_+$. As a result, the parameter $r_+$ is often reported in the literature as the far-from-equilibrium dissolution rate.

As pointed out in Lichtner (2016), Temkin's average stoichiometric number (Temkin, 1963) is widely misunderstood by the geochemical community and has often been used as an empirical fit parameter. Rather than being empirical, this number normalizes the chemical formula used to represent a mineral to the rate-controlling process. For example, if the rate-controlling process of diopside dissolution is the release of a single silica tetrahedron from its mineral surface and the chemical formula used for diopside is $Ca_{0.5}Mg_{0.5}SiO_3$, Temkin's number would be 1. If the chemical formula used for diopside is $CaMgSi_2O_6$, Temkin's number would be 2. Note that the chemical affinity for a mineral dissolution reaction scales to the mineral chemical formula such that the chemical affinity for the dissolution reaction of $CaMgSi_2O_6$ is twice that of $Ca_{0.5}Mg_{0.5}SiO_3$.

A number of studies have demonstrated the applicability of **Eq. (2)** to describe the dissolution rates as a function of chemical affinity (c.f., Schott et al., 2009). For example, Berger et al. (1994) showed that the constant temperature dissolution rates of quartz decreased systematically with decreasing chemical affinity in accord with **Eq. (2)** at 300 °C. Similarly, Pokrovsky and Schott (2004) showed the same trend for brucite at 25 °C, and Bénézeth et al. (2008) at constant pH for boehmite at 100 °C. In each case, Temkin's stoichiometric number was found to be one, consistent with the release of a single metal from the mineral structure being rate-limiting.

The forward, or far-from-equilibrium dissolution rate of a mineral ($r_+$) depends on its dissolution mechanism. Much of the early development of the field of mineral dissolution kinetics focused on the rates and dissolution mechanism of single oxide/hydroxide minerals, such as quartz and goethite. The dissolution mechanisms of these minerals require the breaking of a single type of metal-oxygen bond. Such bond breaking is promoted by the adsorption of either a proton, a hydroxide, or a water molecule onto the mineral surface (e.g., Pokrovsky et al., 2006). Several excellent examples of such behavior have been published, including the work of Furrer and Stumm (1986). They observed a close correlation between the dissolution rates of aluminum oxide and the degree of proton and/or hydroxide adsorption on the mineral surface. Other examples were presented or reviewed by Stumm et al. (1983), Wieland et al. (1988), and Stumm and Wieland (1990). Such observations lead to the conclusion that the dissolution of simple oxide/hydroxide minerals proceeds by a number of parallel mechanisms, each consisting of the adsorption of a proton, water, hydroxide, or ligand to the mineral surface. This surface species would then help destabilize the metal-oxygen bond at the surface leading to the dissolution of the mineral. Based on these mechanisms, the surface area normalized forward dissolution rates of single oxide/hydroxide minerals can be computed from

$$r_+ = \sum_i r_{+,i} \tag{3}$$

where the $r_{+,i}$ refers to the forward dissolution rate of the *i*th parallel reaction. Each term in this rate equation is proportional to the concentration of the rate accelerating adsorbed species at the mineral surface. For example, in the simplest case, several parallel rates were assumed to be dependent on the adsorption of protons, or water and/or hydroxide on mineral surfaces and could be described using (e.g., Palandri and Kharaka, 2004; Marini, 2007; Crundwell, 2014)

$$r_{+,i} = k_i a_{\mathrm{H}^+}^{n_i} \tag{4}$$

where $k_i$ refers to the rate constant of the subscripted rate equation, $a_{H^+}$ designates the activity of aqueous $H^+$, and $n_i$ represents an empirical reaction order.

The early rationale for this approach stemmed from measurements of surface charge and the identification of the zero point of charge. The zero point of charge is the pH at which the net charge of the mineral surface is equal to zero. At lower pH, the surface tends to adsorb protons and

153 at high pH, the surface tends to desorb protons. For single oxide minerals, these can be
154 related to the surface speciation of the mineral and related to its rate (c.f. Pokrovsky et al.,
155 2006). What is reported in the literature as the zero point of charge for multi-oxide minerals, however,
156 differs significantly from what is reported as the zero point of charge for the single oxide minerals.
157 The measurement of zero point of charge commonly consists of measuring the net consumption of
158 protons by the mineral surface as a function of pH. For the case of single oxide minerals, the
159 consumption or liberation of protons is dominated by the adsorption or desorption of protons to the
160 mineral surface. In contrast, in the case of multi-oxide minerals, the consumption or liberation of
161 protons can be dominated by proton-exchange reactions with metals in the mineral structure (Oelkers
162 et al., 2009). In such cases, proton-exchange reactions promote the dissolution of the minerals,
163 affecting the reported zero points of charges for multi-oxide minerals (c.f., Oelkers et al., 1994; Schott
164 et al., 2009).

165 Due to the potential for proton for metal exchange reactions, the dissolution mechanisms of multi-
166 oxide minerals tend to be more complex due to the presence of more than one type of metal-oxygen
167 bond. In multi-oxide minerals, each distinct metal-oxygen bond will break at vastly different rates. For
168 example, Na-O bonds will break orders of magnitude faster than Si-O bonds via proton exchange
169 reactions (Oelkers 2001a). Such reactions are similar to ion exchange reactions commonly observed in
170 clay minerals and zeolites (summarized in, e.g., Sposito, 1981; Drummond et al., 1983; Townsend,
171 1991; Crooks et al., 1993; Colella, 1996; Whitworth, 1998; Coker and Rees, 2005; Dyer, 2007; Zaidi,
172 2012, and references therein). In these cases, rates are promoted by the removal of some of the metals
173 from the mineral structure, distorting the adjacent slower breaking metal-oxygen bonds. This leads to
174 forward dissolution rates that can depend on the concentration in aqueous solutions of those metals
175 more readily removed from the mineral structure (Oelkers et al., 1994; Gautier et al., 1994; Oelkers
176 2001a).

177 Many experimental studies of mineral dissolution rates failed to measure and/or report the
178 complete composition of the reactive aqueous fluids used in their multi-oxide mineral dissolution
179 experiments. Instead, many reported just the dissolution rates based on Si release and the pH of the
180 reactive aqueous fluid (e.g., Busenberg and Clemency, 1976; Rimstidt and Barnes, 1980; Velbel,
181 1985; Knauss and Wolery, 1986 and 1988; Holdren and Speyer, 1987; Mast and Drever, 1987; Brady
182 and Walther, 1989; Casey et al., 1991; Wogelius and Walther, 1991; Knauss et al., 1993; Oxburgh et
183 al., 1994; Knauss and Copenhaver, 1995; Kalinowski and Schweda, 1996; Carroll and Knauss, 2001;
184 van Hees et al., 2002; Hodson, 2003; Balland et al., 2010). This greatly limits the ability to regress rate
185 data consistently as a function of aqueous solution composition or to determine the chemical affinity
186 of the reactive fluid. As a result, to generate a consistent database covering as extensively as possible
187 all major rock-forming minerals, one is obliged to fit the existing rate data based on Si release to an

empirical function of pH. This approach is limited, as it does not allow explicit quantification of the effects of individual aqueous species, including dissolved $CO_2$ or organic ligands on rates.

Numerous efforts have been made in the literature to include one or more parallel reactions to describe the influence of other aqueous species such as organic ligands and/or $CO_2$ on mineral dissolution rates. Such additional terms were not considered in this work, as it might lead to inconsistencies among the rates of different minerals (e.g., calculation of a specific effect on rates of an aqueous organic ligand on some minerals for which data was available but not for others for which data may be unavailable). Many of the available data of mineral dissolution rates as a function of some of the organic and inorganic acids have been included in the Appendix. These might serve as a starting point for a comprehensive description of the effect of these added species on rates. A promising alternative approach in this regard, which has not been verified for many minerals, is that the effect on rates of many aqueous species may stem indirectly from their effect on fluid pH or on the aqueous activities of metals such as Al, that directly affect the dissolution rates (e.g., Oelkers and Schott, 1998; Golubev et al., 2005).

The variation of mineral dissolution rates as a function of temperature has been almost exclusively described using some form of an Arrhenius equation. The application of the Arrhenius equation has, nevertheless, led to some confusion when applied to mineral dissolution rates. The Arrhenius equation suggests that the logarithm of the rate constant, $k$, which relates the rate to the concentration of the rate-controlling activated complex, should be approximately a linear function of reciprocal temperature in accord with (cf. Schott et al., 2009)

$$k = A_0 e^{-E_a/(RT)} \tag{5}$$

where $A_0$ refers to a temperature-independent pre-exponential factor, and $E_a$ stands for the activation energy. Confusion arises as many have applied a form of the Arrhenius equation to describe the temperature dependence of reaction rates rather than rate constants, for example, using

$$r = A'_0 e^{-E'_a/(RT)} \tag{6}$$

where $A'_0$ refers to a temperature-independent pre-exponential factor, but $E'_a$ stands for an apparent activation energy (see Casey and Sposito, 1992). The difference between $E_a$ and $E'_a$, therefore, stems from the temperature variation of the concentration of the activated or precursor species, for example, the temperature dependence of the concentrations of the $>Si_2O\text{-}H^+$ and/or the $>MgOH_2^+$ surface species in the Pokrovsky and Schott (2000) model for forsterite dissolution. This subtle difference is responsible in part for the inconsistencies in activation energies for mineral reactions reported in the literature (cf., Oelkers and Schott, 1999). In cases where the concentrations of the activated or rate-controlling species decrease rapidly with increasing temperature, negative apparent activation energies

can be observed, for example, for the case of carbonate mineral dissolution rates at acidic conditions (Pokrovsky et al., 2009; Schott et al. 2009).

It is commonly assumed that the overall reactivity of a mineral in water is proportional to its surface area. There is, however, considerable discussion over exactly which surface area should be considered in this regard. The simplest surface area that has been used to characterize mineral reactivity is the geometric surface area, which is the surface of a smooth geometric shape, such as a sphere or a cube of equal size to the mineral grains. A popular alternative is using the surface area measured by inert gas adsorption techniques together with the Brunauer, Emmett, and Teller (BET) approach (Brunauer et al., 1938). The advantage of this gas adsorption approach is that the size of the adsorbing gas (e.g., Kr, Ar, or $N_2$) is similar to that of $H_2O$, so is thought to be a good proxy for characterizing the interaction of a mineral surface with water. The ratio of the BET surface area to the geometric surface area is termed roughness factor, which is thus a measure of how different the BET surface area is compared to that of a smooth geometric shape of the same size.

Combining **Eqs. (2)** to **(6)** leads to the following equation that can be used to describe existing surface area normalized mineral or glass dissolution rate data:

$$r = \sum_i \left( A_i a_{\mathrm{H}^+}^{n_i} e^{\frac{E_{a_i}}{RT}} \right) \cdot (1 - \exp(-\mathbf{A}/(\sigma RT))). \quad (7)$$

where the subscript $i$ stands for either acidic, neutral, or basic conditions. These three conditions are denoted by *a*, *b,* and *c,* respectively in **Table 2**. It should be emphasized that this equation is largely empirical and should not be considered to yield mechanistic information. Note that the use of **Eq. (7)** to describe the dissolution rates of silicate minerals as a function of chemical affinity requires a value of $\sigma$, Temkin's average stoichiometric number. Consistent with the studies of single oxide minerals detailed above and the assumption that the rate-limiting step for the dissolution of silicate minerals is the release of a silicon atom from the mineral structure, the value of $\sigma$ adopted in the study is equal to the number of Si in the chemical formula chosen to represent the mineral. Another major caveat to using **Eq. (7)** to fit available rate data is that a large percentage of the published mineral dissolution rates 1) were generated rates at far-from-equilibrium conditions, where the final term in **Eq. (7)** is indistinguishable from 1, and/or 2) did not provide sufficient reactive fluid chemistry data to calculate the chemical affinity term. Consequently, only rates performed at 'far-from-equilibrium conditions' ($r_+$) are considered in this study, which includes the vast majority of the published rates. For the purposes of geochemical modeling, for example, using the PHREEQC computer code, the chemical affinity of the dissolution reaction can be calculated using the *carbfix.dat* thermodynamic database (Voigt et al., 2018).

The form of **Eq. (7)** suggests that once it is parameterized to describe the dissolution rates for any mineral, it could also provide estimates of the precipitation rates of this mineral by taking into

account the change in sign in the term for the chemical affinity in the equation. The final term in **Eq. (7)** is positive in undersaturated solutions. At equilibrium, this term is zero, and in supersaturated solutions, this term is negative. As a result, as one crosses equilibrium from undersaturation to supersaturation, rates calculated using **Eq. (7)** will change sign and yield what appear to be precipitation rates. Although precipitation rates calculated this way may be applicable to some minerals, such an approach gives clearly inconsistent results compared to natural and laboratory observations for many rock-forming minerals (Schott et al., 2009). This inconsistency likely stems from differences in the mechanism of dissolution compared to that of precipitation. The dissolution of a mineral continuously creates new active sites on the mineral surface, which further removes material from these sites. Precipitation, however, in many cases destroys these active sites. In such cases, for precipitation to proceed, new active sites must be nucleated on the mineral surface (e.g., De Yoreo and Vekilov, 2003). As nucleation is a distinct process from the removal or attachment of material at an existing site, **Eq. (7)** is likely insufficient to describe the precipitation rates of many rock-forming minerals.

In contrast to the fitting of the dissolution rates of other solids in this study, sufficient data is available to account directly for the effect of aqueous Al basaltic glass dissolution rates. As such, the dissolution rates of basaltic glass, based on Si release can be quantified using (Oelkers and Gislason, 2001)

$$r_+ = \left( A * \exp\left(\frac{Ea}{RT}\right)\left(\frac{(a_{H+})^3}{(a_{Al^{3+}})}\right)^{\frac{1}{n}} \right) \quad (8)$$

where $a_{Al^{3+}}$ is the activity of aqueous $Al^{3+}$. Aqueous aluminum activities considered in this study considered the formation of the $AlOH^{2+}$, $Al(OH)_2^+$, $Al(OH)_3$, and $Al(OH)_4^-$ species.

## 2.2 Data selection

Experimental data were regressed using **Eq. (7)** or **(8).** The parameters $A$, $E_a$, and $n$ in these equations were obtained via a two-step process, and the final chemical affinity term in **Eq.(7)** was set to 1 consistent with the far-from-equilibrium conditions considered in most published dissolution rate studies. To generate rate parameters, first, experimental datasets containing rates determined at far-from-equilibrium conditions were tabulated as a function of temperature and pH. All collected experimental datasets for each mineral group discussed here are listed in **Table S1** in **Appendix A**. These experimental data were evaluated critically to assess the quality of the starting materials, their compositions, and their experimental conditions. Only rates obtained at a steady-state, performed at far-from-equilibrium conditions, and normalized to the initial surface area measured by the BET technique were retained for regression. This latter choice was pragmatic as relatively few studies reported BET surface areas after the completion of their experiments. For example, Gautier et al.

(2001) reported that the BET surface areas of quartz increased by a factor of 5.6 during its dissolution at a temperature of 200 and 250 °C over the course of 95 days. To ensure consistency, all rates used for the regression are based on silicon release rates unless stated otherwise. This too is a pragmatic choice as many studies failed to measure or report rates based on the release of other elements from the dissolving minerals.

It should be noted, however, that in some cases, certain elements may be preferentially retained or released either initially or during the complete dissolution of the mineral. For example, Schott et al.( 2012) observed the complete preferential removal of Ca from wollastonite at ambient temperatures and pH<2.2 during experiments lasting 3000 hours. Experimental data that were accelerated or slowed due to the presence of organic ligands, those where rates were affected by the formation of secondary minerals, or experimental data obtained from minerals containing major impurities, were not included in the regression calculations unless otherwise noted in the text below. Similar to Rimstidt et al. (2012), for some minerals, two parallel rate mechanisms were used to fit rate data as a function of pH and temperature; rates were fit by separating the experimental data into two groups divided by their point of zero charge. This choice is somewhat arbitrary but adequately works for some of the minerals. For other minerals, e.g., the feldspars or micas, three parallel rate mechanisms were considered, where the published rates were divided into three sets according to pH. For each subset, the activation energies, pre-exponential factors, and reaction orders were fit from selected dataset using **Eqs. (7)** and **(8)** and method of the least-squares minimization. These parameters are listed in **Table 2**. In cases where insufficient experimental data are available to regress these parameters for a given mineral, regression parameters are estimated based on the results of regression fits of similarly structured and composited minerals. When such an approach is used, it is noted explicitly below when describing the regression of a given dataset.

The quality of regression fits is evaluated in the present study by the differences between measured rates and those calculated from the regression equations. The difference between measured and calculated rates is referred to as residuals. The coefficient of determination ($R^2$) for each fit is calculated as

$$R^2 = 1 - \frac{\sum \text{residuals}^2}{\sum (y_i - \bar{y})^2} \tag{9}$$

where $\bar{y}$ is the value obtained from the regression equation, and $y_i$ is its corresponding measured experimental value. $R^2$ values for each fit are reported in **Table 2,** along with the regressed rate constants.

To further characterize the quality of the regression fits, 95% confidence level bands ($y_{95}$) of regressed rates were determined using:

$$y_{95} = \bar{y} \pm 1.96 \frac{SD}{\sqrt{N}} \quad (10)$$

where *SD* symbolizes the standard deviation of the regression fit and *N* refers to the number of data points considered in the regression.

# 3. Regression of the experimental dissolution rate equations for primary silicate minerals

## 3.1 Amphiboles

Experimentally measured amphibole dissolution rates have been reviewed and summarized by Brantley and Chen (1995), Marini (2007), and Brantley et al. (2008). It is reasonable to assume similar dissolution mechanisms for all the minerals in the amphibole group. However, measured amphibole dissolution rates vary significantly due to Al content in the mineral structure. To account for the effect of Al in the mineral structure, we summarize amphibole dissolution in two subsections, one focused on Al-free amphiboles and the other on Al-bearing amphiboles. The former group was regressed assuming two parallel mechanisms (pH-dependent and pH-independent trends at acidic and basic conditions, respectively), while the latter three independent parallel mechanisms as a function of pH were considered.

### 3.1.1. Al-free amphiboles

Sources of experimentally measured dissolution rates of Al-free amphiboles (e.g., tremolite, anthophyllite) are summarized in **Table 1**. To date, there have been relatively few studies of the dissolution rates of the amphiboles compared to many of the other major rock-forming minerals. Most available studies reported rates at 25 ºC and pH from 1 to 9. At elevated temperatures, Diedrich et al. (2014) reported tremolite dissolution rates at temperatures from 25 °C to 150 °C, and Chen and Brantley (1998) reported anthophyllite dissolution rates from 25 °C to 90 °C. **Figure 1 A-D** shows experimentally measured Al-free amphibole dissolution rates as a function of pH and temperature. Substantial scatter is evident. For example, anthophyllite dissolution rates at pH 3 at 25 °C range over two orders of magnitude from $10^{-13.5}$ to $10^{-11.6}$ mol $m^{-2}$ $s^{-1}$. As is the case for most mineral-forming minerals, constant temperature dissolution rates decrease with increasing pH to at least neutral conditions. Tremolite dissolution rates decrease continuously with increasing pH from $10^{-11.4}$ mol $m^{-2}$ $s^{-1}$ at pH 1 to $10^{-12.4}$ mol $m^{-2}$ $s^{-1}$ at pH 9. Experimental data from Mast and Drever (1987) and Schott et al. (1981) were not included in the regression calculations as the solids used in these studies likely included impurities, and the experiments exhibited non-stoichiometric dissolution. Data from these two studies are indicated in **Figure 1** by circles and arrows.

***Table 1**: Sources of experimentally measured Al-free amphibole dissolution rates considered in this study*

| | T °C | pH | Mineral Composition |
|---|---|---|---|
| ***Anthophyllite*** | | | |
| Brantley and Chen (1995) | 25 | 1.1-3.6 | $Mg_{5.7}Fe_{1.0}Al_{0.1}Si_{7.8}O_{22}(OH)_2$ |
| Chen and Brantley (1998) | 25-90 | 1.2-3.4 | $Mg_{5.7}Fe_{1.0}Al_{0.1}Si_{7.8}O_{22}(OH)_2$ |
| Mast and Drever (1987) | 25 | 2.0-9.2 | $Mg_{1.88}Ca_{0.08}Na_{0.04}(Mg_{4.51}Mn_{0.42}Fe_{0.02}Al_{0.02})Si_8O_{22}(OH)_2$ |
| ***Ferroactinolite*** | ---------- *no reported data* ---------- | | |
| ***Riebeckite*** | ---------- *no reported data* ---------- | | |
| ***Tremolite*** | | | |
| Diedrich et al. (2014) | 25-150 | 1.9-7.5 | $Ca_{2.10}Mg_{4.97}Fe_{0.07}Si_8O_{22}(OH)_2$ |
| Mast and Drever (1987) | 22 | 2.0-9.0 | $Ca_{0.07}Mg_{6.4}Si_8O_{22}(OH)_2$ |
| Schott et al. (1981) | 22 | 1.0-6.0 | $Ca_{1.91}Mg_{5.09}Fe_{0.03}Si_8O_{22}(OH)_2$ |

The rate parameters for anthophyllite were generated from regression of the experimental results of Chen and Brantley (1998) with an activation energy based on the variation of rates over the 25 to 90 °C temperature range. The rate parameters for tremolite were derived from a regression of the experimental rates reported by Diedrich et al. (2014) over the 37 to 90 °C temperature range. The activation energy at neutral and higher pH was set equal to that of anthophyllite due to a lack of relevant experimental data.

The resulting kinetic parameters are listed in **Table 2,** and rates calculated using these parameters can be compared with corresponding experimental rates in **Figures 1** and **2.** The rates displayed in this figure span the 25 °C to 150 °C temperature range and pH. The average difference between the measured and calculated far-from-equilibrium dissolution rates for anthophyllite is 0.14 log units, and 50% of the rates are within 0.09 log units of their corresponding calculated values. The average difference between the measured and calculated far-from-equilibrium dissolution rates of tremolite regression equation is 0.35 log units, and 50% of the rates are within 0.28 log units of their corresponding calculated values.

No experimentally measured dissolution rates have been reported for the minerals riebeckite and ferroactinolite. Owing to a lack of experimental data, we recommend adopting a first approximation of the rates of tremolite dissolution to estimate the dissolution rates for ferroactinolite and riebeckite due to their similar structures and compositions until such rates might become available.

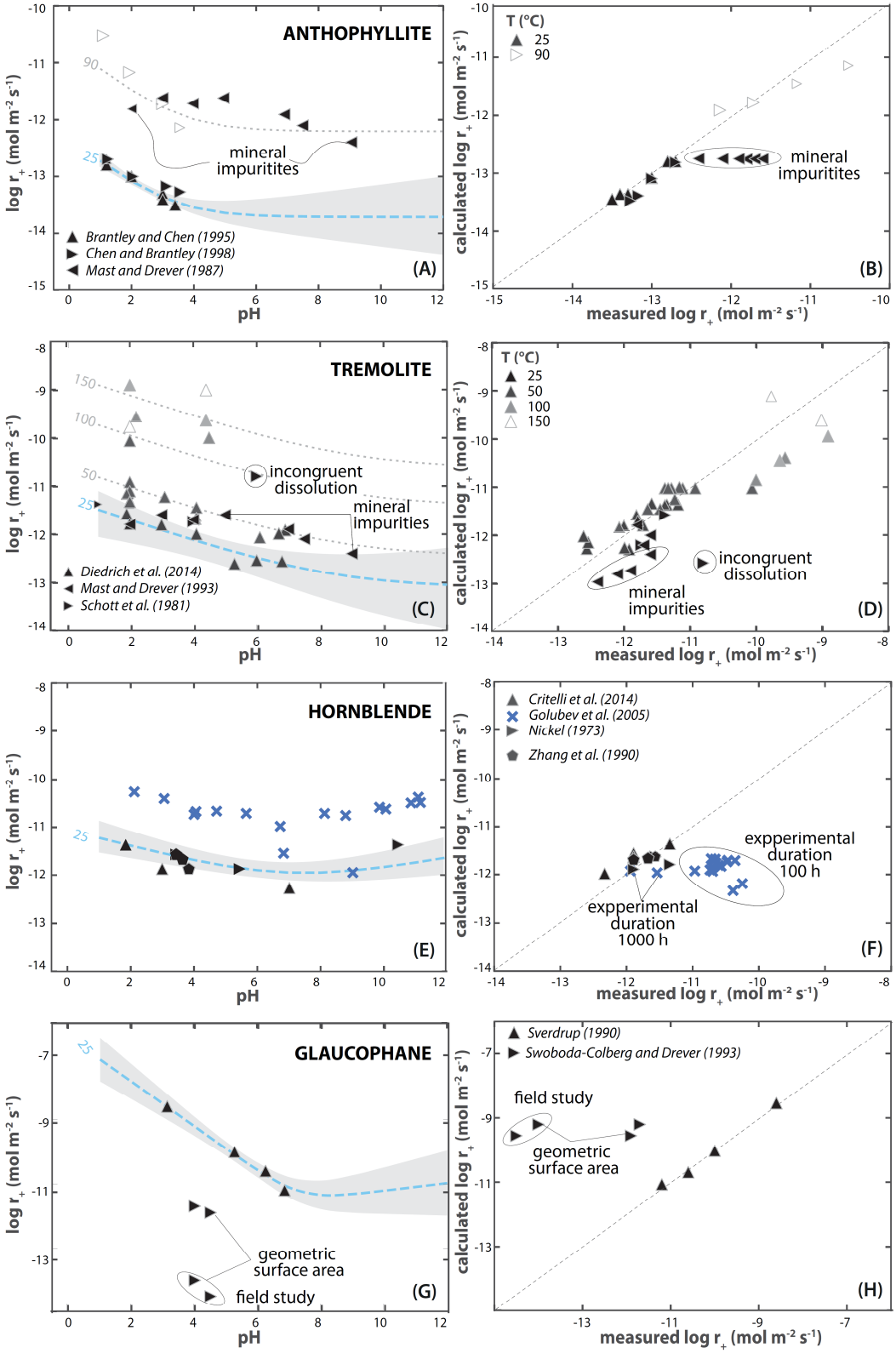


***Figure 1:*** *Far-from-equilibrium dissolution rates of the amphiboles. Experimental data shown as symbols can be compared with computed rates shown as curves as a function of pH in the left plots. Plots in the right column directly compare calculated versus measured rates. The symbol shape indicates the source of the data, whereas the shading of the symbol indicates the experimental temperature, where black symbols indicate 25 °C. The shaded regions in the left plots illustrate the 95% confidence limits of the regression fits performed at 25 °C.*

376

***Table 2:*** *Summary of parameters describing the far-from-equilibrium dissolution rates with* ***Eq (7).***

| | ***Acid mechanism*** | | | | ***Neutral mechanism*** | | | ***Basic mechanism*** | | | | $R^2$ |
|---|---|---|---|---|---|---|---|---|---|---|---|---|
| | $logk_{25}$ mol $m^{-2}$ $s^{-1}$ | $A_a$ mol $m^{-2}$ $s^{-1}$ | $E_{a_a}$ kJ $mol^{-1}$ | $n_a$ | $logk_{25}$ mol $m^{-2}$ $s^{-1}$ | $A_b$ mol $m^{-2}$ $s^{-1}$ | $E_{a_b}$ kJ $mol^{-1}$ | $logk_{25}$ mol $m^{-2}$ $s^{-1}$ | $A_c$ mol $m^{-2}$ $s^{-1}$ | $E_{a_c}$ kJ $mol^{-1}$ | $n_c$ | |
| ***Amphiboles*** | | | | | | | | | | | | |
| Anthophyllite | -12.4 | $5.7x10^{-4}$ | 52.0 | 0.4 | -13.7 | $5.0x10^{-6}$ | 48.0 | - | - | - | - | 0.94 |
| Ferroactinolite | -11.3 | $3.0x10^{-3}$ | 50.0 | 0.2 | -13.1 | $2.0x10^{-5}$ | 48.0 | - | - | - | - | - |
| Riebeckite | -11.3 | $3.0x10^{-3}$ | 50.0 | 0.2 | -13.1 | $2.0x10^{-5}$ | 48.0 | - | - | - | - | - |
| Tremolite | -11.3 | $3.0x10^{-3}$ | 50.0 | 0.2 | -13.1 | $2.0x10^{-5}$ | 48.0 | - | - | - | - | 0.77 |
| Glaucophane | -6.10 | $2.2x10^{2}$ | 50.0 | 0.7 | - | - | - | -12.8 | $1.0x10^{-4}$ | 48.0 | -0.1 | 0.99 |
| Hornblende | -10.7 | $5.0x10^{-3}$ | 50.0 | 0.2 | - | - | - | -13.4 | $2.1x10^{-5}$ | 48.0 | -0.1 | 0.16 |
| ***Feldspars*** | | | | | | | | | | | | |
| Albite | -10.3 | 0.70 | 58.0 | 0.3 | -11.19 | 0.21 | 60.0 | -13.6 | $1.5x10^{-5}$ | 50.0 | -0.3 | 0.83 |
| Andesine | -7.99 | 147 | 58.0 | 0.7 | -11.23 | 0.19 | 60.0 | -13.6 | $1.5x10^{-5}$ | 50.0 | -0.3 | - |
| Anorthite | -5.17 | $9.8x10^{4}$ | 58.0 | 1.2 | -11.34 | 0.15 | 60.0 | -13.6 | $1.5x10^{-5}$ | 50.0 | -0.3 | 0.81 |
| Bytownite | -5.88 | $1.9x10^{4}$ | 58.0 | 1.1 | -11.28 | 0.17 | 60.0 | -13.6 | $1.5x10^{-5}$ | 50.0 | -0.3 | - |
| K-feldspar | -10.4 | $5.0x10^{-2}$ | 51.7 | 0.5 | -12.48 | $1.1x10^{-2}$ | 60.0 | -20.8 | $1.2x10^{-10}$ | 62.0 | -0.8 | 0.23 |
| Microcline | -10.4 | $5.0x10^{-2}$ | 51.7 | 0.5 | -12.48 | $1.1x10^{-2}$ | 60.0 | -20.8 | $1.2x10^{-10}$ | 62.0 | -0.8 | - |
| Labradorite | -6.39 | $5.9x10^{3}$ | 58.0 | 1.0 | -11.28 | 0.17 | 60.0 | -13.6 | $1.5x10^{-5}$ | 50.0 | -0.3 | - |
| Oligoclase | -9.33 | 6.8 | 58.0 | 0.4 | -11.21 | 0.20 | 60.0 | -13.6 | $1.5x10^{-5}$ | 50.0 | -0.3 | - |
| ***Glass*** | | | | | | | | | | | | |
| Basalt | See section 3.3.1 and **Eq. (10)** | | | | | | | | | | | |
| Rhyolite | -9.10 | $1.6x10^{-3}$ | 36.0 | 0.5 | - | - | - | -16.3 | $7.0x10^{-8}$ | 52.0 | -0.6 | |
| ***Mica*** | | | | | | | | | | | | |
| Annite | -9.42 | $5.9x10^{-7}$ | 18.2 | 0.5 | -12.2 | $5.00x10^{-9}$ | 22.0 | -13.9 | $4.00x10^{-10}$ | 25.5 | -0.2 | |
| Biotite* | -9.42 | $5.9x10^{-7}$ | 18.2 | 0.5 | -12.2 | $5.00x10^{-9}$ | 22.0 | -13.9 | $4.00x10^{-10}$ | 25.5 | -0.2 | 0.38 |
| Phlogopite | -9.42 | $5.9x10^{-7}$ | 18.2 | 0.5 | -12.2 | $5.00x10^{-9}$ | 22.0 | -13.9 | $4.00x10^{-10}$ | 25.5 | -0.2 | |
| Muscovite | -11.1 | $1.3x10^{-4}$ | 41.3 | 0.4 | -12.1 | $6.31x10^{-6}$ | 39.0 | -14.5 | $3.16x10^{-5}$ | 57.0 | -0.2 | 0.67 |
| ***Olivines*** | | | | | | | | | | | | |
| Fayalite | -6.26 | $1.20x10^{6}$ | 70.4 | 0.4 | - | - | - | -7.39 | $1.91x10^{3}$ | 60.9 | 0.2 | 0.29 |
| Forsterite | -7.16 | $1.48x10^{5}$ | 70.4 | 0.4 | - | - | - | -8.33 | $2.20x10^{2}$ | 60.9 | 0.2 | 0.92 |
| Larnite | -3.61 | $5.25x10^{8}$ | 70.4 | 0.4 | - | - | - | -4.75 | $8.25x10^{5}$ | 60.9 | 0.2 | 0.43 |
| ***Pyroxenes*** | | | | | | | | | | | | |
| Augite | -8.20 | $1.52x10^{6}$ | 81.8 | 0.7 | -12.8 | 350 | 83.0 | - | - | - | - | 0.32 |
| Bronzite | -9.80 | $9.5x10^{-4}$ | 38.5 | 0.6 | -11.7 | $7.6x10^{-1}$ | 66.1 | - | - | - | - | 0.63 |
| Diopside | -9.80 | $8.55x10^{-5}$ | 32.7 | 0.3 | -11.0 | $4.3x10^{-4}$ | 43.9 | - | - | - | - | 0.75 |
| Enstatite | -8.30 | 0.574 | 46.1 | 0.5 | -11.9 | $6.3x10^{3}$ | 89.5 | - | - | - | - | 0.84 |
| ***$SiO_2$ polymorphs*** | | | | | | | | | | | | |
| Cristobalite-alpha | -11.4 | $4.03x10^{-4}$ | 45.6 | 0.3 | - | - | - | -15.0 | 0.105 | 80.0 | -0.4 | 0.89 |
| Cristobalite-beta | -11.4 | $4.03x10^{-4}$ | 45.6 | 0.3 | - | - | - | -15.0 | 0.105 | 80.0 | -0.4 | 0.89 |
| Quartz | -11.4 | $4.03x10^{-4}$ | 45.6 | 0.3 | - | - | - | -15.0 | 0.105 | 80.0 | -0.4 | 0.89 |
| Amorphous $SiO_2$ | -10.6 | $4.56x10^{-4}$ | 41.6 | 0.3 | - | - | - | -14.2 | $3.53x10^{-2}$ | 73.0 | -0.4 | 0.95 |

*Biotite here corresponds to generic mica ($KFe_{1.5}Mg_{1.5}AlSi_3O_{10}(OH)_2$)

### 3.1.2 Al-bearing amphiboles

Available experimentally measured dissolution rates of Al-bearing amphiboles (glaucophane and hornblende) are summarized in **Table 3**. Nickel (1973), Golubev et al. (2005), and Critelli et al. (2014) reported hornblende dissolution rates at pH up to 12and up to 1 atm $CO_2$. The variation of constant temperature far-from-equilibrium dissolution rates of the Al-bearing amphiboles exhibits minimum values near pH ~6. Such behavior may be attributed to the rates being controlled by a precursor complex created by a proton for Al exchange reactions (Oelkers, 2001a). Hornblende dissolution rates vary from $10^{-8.4}$ at pH 1.6 to $10^{-12.3}$ mol $m^{-2}$ $s^{-1}$ at pH 7.0. The glaucophane dissolution rates are similar to those of hornblende, decreasing from $10^{-8.6}$ to $10^{-11.2}$ mol $m^{-2}$ $s^{-1}$ with increasing pH from 3.23 to 6.83 (Sverdrup, 1990). Swoboda-Colberg and Drever (1993) compared glaucophane dissolution rates at laboratory and field conditions at pH 4.0 to 4.5. However, these data were not included in the regression calculations as they were normalized to geometric surface area. The effect of mineral chemical composition, the presence of organic ligands, and/or the presence of aqueous $CO_2$ on Al-amphibole dissolution rates have not yet been reported in the literature.

***Table 3**: Sources of experimentally measured Al-amphibole dissolution rates considered in this study*

| | **T °C** | **pH** | **Mineral Composition** |
|---|---|---|---|
| ***Glaucophane*** | | | |
| Sverdrup (1990) | 25 | 3.1-6.8 | $Na_{0.14}K_{0.09}Ca_2Fe_{1.78}Mg_2Al_2Si_7O_{22}(OH)_2$ |
| Swoboda-Colberg and Drever (1993) | 25 | 4.0-4.5 | $Na_{0.14}K_{0.09}Ca_2Fe_{1.78}Mg_2Al_2Si_7O_{22}(OH)_2$ |
| ***Hornblende*** | | | |
| Critelli et al. (2014) | 25 | 2.0-12.3 | $Na_{0.4}Mg_{3.1}Ca_{2.7}Fe_{1.0}Al_{0.9}Si_{7.4}O_{22}(OH)_2$ |
| Golubev et al. (2005) | 25 | 2.1-11.1 | - |
| Nickel (1973) | 25 | 3.6-10.6 | $Na_{0.8}Ca_{1.8}Mg_{3.7}Fe_{0.9}Al_{0.1}Si_{7.1}Al_{0.9}O_{22}(OH)_2$ |
| Zhang et al. (1990) | 25 | 3.6-4.0 | $K_{0.11}Na_{0.66}Ca_{1.66}Mg_{3.11}Fe_{1.34}Al_{0.79}Si_{6.36}Al_{1.64}O_{22}(OH, F)_2$ |

Regression of these data yielded the kinetic parameters listed in **Table 2.** Rates generated using the regression parameters produced in this study are compared with experimentally measured rates in **Figure 1**. The dissolution rate equation for glaucophane describes the experimentally measured rate data with an average difference of 0.07 log units. The mineral hornblende was regressed assuming its chemical formula is $(Ca_2Mg_4Al_{0.75}Fe_{0.25}(Si_7AlO_{22})(OH)_2)$. The average difference between measured and calculated dissolution rates of hornblende is 0.183 log unit, and 50% of the calculated rates are within 0.13 log unit of their corresponding measured rates.

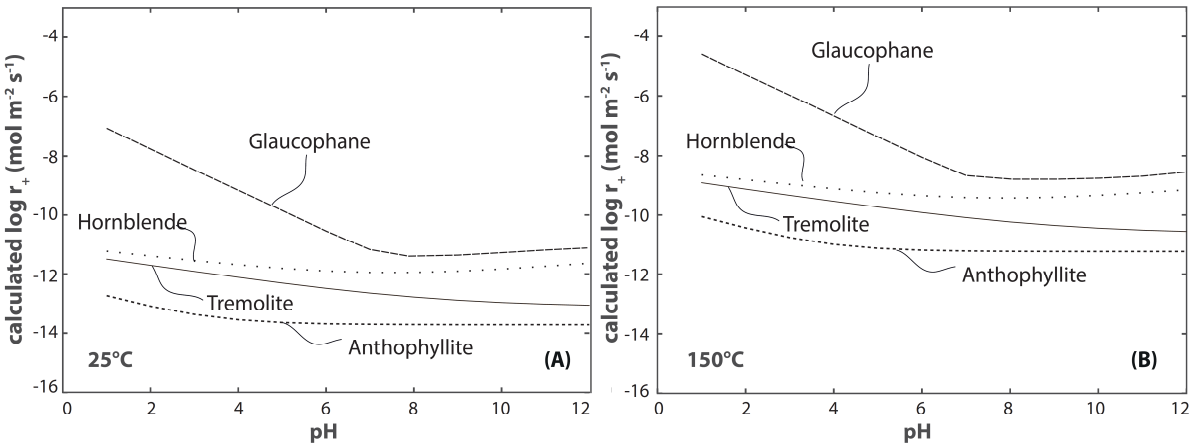


***Figure 2:*** *Summary of the calculated far-from-equilibrium dissolution rates of amphiboles as a function of pH. Illustrated rates were calculated using* ***Eq (7)*** *and parameters listed in* ***Tables 2*** *at* ***(A)*** *25 °C, and* ***(B)*** *150 °C.*

The quantification of amphibole dissolution rates is challenging due to the lack of experimental data, particularly at neutral to basic conditions and at temperatures above 25 °C. Although there is a general agreement among amphibole dissolution rates generated using the various regression equations available in the literature at acidic conditions and near to ambient temperature, these equations differ significantly at neutral to basic conditions suggesting either continuously decreasing rates as a function of pH (Brantley and Chen, 1995; Brantley et al., 2008; Diedrich et al., 2014) or pH-independent rates at neutral to basic conditions (Palandri and Kharaka, 2004). Such interpretative differences are largely due to the limited datasets available at these conditions and inconsistencies among these data. Moreover, suggested activation energies span the range of 18.9 up to 94.4 kJ $mol^{-1}$ (Brantley and Chen, 1995; Chen and Brantley, 1998; Palandri and Kharaka, 2004; Brantley et al., 2008; Diedrich et al., 2014). As a result, the various rate equations available in the literature generate rates for pH greater than pH 6 and elevated temperature that can differ by up to two orders of magnitude from one another. To address this issue, we recommend adopting the activation energies of tremolite dissolution to approximate the dissolution rates for glaucophane and hornblende to higher temperature due to their similar structures and compositions. A comparison of calculated dissolution rates generated in this study for both Al-free and Al-amphiboles for 25 and 150 °C can be seen in **Figure 2**. Due to the presence of Al in the framework, dissolution rates of Al-amphiboles appear to minimize as a function of pH at near to neutral pH, whereas this minimum is not evident in the Al-free amphiboles.

## 3.2 Feldspars

Experimentally measured feldspar dissolution rates have been reviewed and summarized by Blum and Stillings (1995), Marini (2007), Brantley et al. (2008), and Gudbrandsson et al. (2014). A list of the sources of experimentally measured feldspar dissolution rates is provided in **Table 4.** Due to the presence of Al in the feldspar structure, their rates minimize as a function of pH at near to neutral

conditions. To address this variation, feldspars dissolution rates were regressed assuming three parallel dissolution mechanisms dominating at acidic (pH<5), neutral (5<pH<7), and basic (pH >7) conditions.

### 3.2.1 Plagioclases

Experimentally measured albite dissolution rates have been reported for temperatures from 5 to 300 ºC, and pH from 1.0 to 12.5. **Figures 3A** and **3B** illustrate far-from-equilibrium albite dissolution rates over a temperature range from 25 to 300 °C. Measured rates at 25 °C vary from as low as $10^{-11.8}$ mol $m^{-2}$ $s^{-1}$ at pH 5.6 to as high as $10^{-9.40}$ mol $m^{-2}$ $s^{-1}$ at pH 11.3. Constant pH rates increase by approximately two orders of magnitude as the temperature increases from 25 to 100 °C. Albite dissolution rates obtained by Gudbrandsson et al. (2014) are up to an order of magnitude faster than corresponding rates reported by Chou and Wollast (1985) and up to two orders of magnitude faster than dissolution rates reported by Knauss and Wolery (1986). As noted by Gudbrandsson et al. (2014), such a scatter can stem from several factors, including differences in experiment duration as dissolution rates tend to decrease with time in many experiments (Oxburgh et al. 1994), variability in mineral composition (0-12 An%), formation of non-stoichiometric layers on the surfaces of the dissolving feldspars (Chou and Wollast, 1985), a decrease in the reactive surface area as the mineral dissolves (Köhler et al., 2005), or a large range of grain size of the initial material used in the experiments (2µm up to 3 mm). See **Table 4 and Appendix** for further details on each experimental study.

Experimentally measured dissolution rates of the intermediate plagioclases, including oligoclase, andesine, bytownite, and labradorite, are listed in **Table 4** and displayed in **Figure 3.** Most of these rates were obtained at 22-25 °C. Corresponding rates scatter significantly. Some of this scatter may be due to the presence of exsolution textures in the solids considered in the experiments (e.g., Gudbrandsson et al., 2014 and references therein). It appears that the measured dissolution rates may be independent of plagioclase composition at basic pH. The rates, however, increase with increasing anorthite content at acidic conditions. For example, bytownite dissolution rates were found to be more than an order of magnitude faster than those of oligoclase at pH 2. Similar to albite, experimental rates for the intermediate plagioclases from Oxburgh et al. (1994) are up to one order of magnitude slower than those presented in Gudbrandsson et al. (2014).

Additionally, Busenberg and Clemency (1976), Welch and Ullman (1993), Sillings and Brantley (1995), Stillings et al. (1996), and Blake and Walther (1999) reported plagioclase dissolution rates in the presence of organic acids and $CO_2$. The addition of $CO_2$ into the aqueous solution increased labradorite dissolution rates by approximately two orders of magnitude. The presence of organic acids both increased and decreased plagioclase dissolution rates, depending on acid composition and concentration as well as solution pH and mineral composition (see **Figure 3**). Oelkers and Schott

(1998) attributed the effects of aqueous organic ligands on rates to the formation of complexes with aqueous Al.

Experimentally measured anorthite dissolution rates are summarized in **Table 4** and **Figure 3.** This dataset consists of 11 studies with 149 reported rates of plagioclases having an anorthite component greater than 89 mol%. The majority of such studies were performed at ambient temperature conditions and at pH ranging up to 11.3 (Bailey, 1974; Fleer, 1982; Holdren and Speyer, 1987; Brady and Walther, 1989; Casey et al., 1991; Amrhein and Suarez, 1988, 1992; Oelkers and Schott, 1995; Hodson, 2003; Gudbrandsson et al., 2014). Berg and Banwart (2000) reported anorthite dissolution rates as a function of $CO_2$ concentration from 0.01 to 0.1 atm, and Oelkers and Schott (1995) reported rates at pH below 4 and temperatures ranging from 45 to 95 °C. Rates reported by Amrhein and Suarez (1992) and those from Gudbrandsson et al. (2014) scatter over two orders of magnitude at near to neutral pH conditions. This scatter may be the result of different experiment duration, the presence of aqueous $CO_2$, and secondary mineral precipitation. The anorthite dissolution rates reported by Hodson (2003) are likely slowed due to the presence of a Fe-rich coating, resulting in rates that are 3 log units lower than most of the other corresponding rates. At the same time, the rates obtained from Berg and Banwart (2000) are 3 log units higher on average than corresponding anorthite dissolution rates, potentially due to the presence of aqueous $CO_2$.

Plagioclase dissolution rates affected by $CO_2$ and organic acids in the aqueous solutions, secondary precipitation, mineral coating, and data influenced by the approach to chemical equilibrium are not considered in the regression calculations. These datasets are indicated in **Figure 3**.

***Table 4****: Sources of experimentally measured plagioclase dissolution rates considered in this study.*

| References | T<br>°C | pH | Anorthite content (in mol%) | Comments |
|---|---|---|---|---|
| ***Albite*** | | | | |
| Burch et al. (1993) | 80 | 8.7-8.9 | 5 | Function of Gibbs free energy of dissolution, experimental duration 1200 h, grain size 2-20µm |
| Busenberg and Clemency (1976) | 25 | 5.0 | 1.1 | + 1atm $CO_2$, experimental duration 1160 hours, grain size <37 µm |
| Casey et al. (1991) | 25 | 2.0 | 2 | Grain size 25-75 µm, experimental duration 556 hours |
| Chen and Brantley (1997) | 5-90 | 1-4.5 | 3 | Grain size 75-150 µm, experimental duration 4000-6000 hours |
| Chou and Wollast (1984) | 25 | 2.5-3.5 | 3 | Grain size 50-200 µm, experimental duration 280 hours on average |
| Chou and Wollast (1985) | 25 | 1.0-12.5 | 3 | Grain size 50-100 µm, experimental duration 280 hours on average |
| Gudbrandsson et al. (2014) | 22 | 1.8-11.3 | 2 | Grain size 45-125 µm, experimental duration 75-600 hours |
| Hellmann (1994) | 100-300 | 1.3-10.0 | 1 | Grain size <1 mm, experimental duration 24-248 hours |
| Hellmann et al. (1989) | 225 | 0.9-8.1 | 1 | Grain size 150-180 µm, experimental duration 500-600 hours |
| Hellmann and Tisserand (2006) | 150 | 9.2 | 1 | Function of Gibbs free energy of dissolution; grain size 1-3 mm, experimental duration 2400 hours |

| | | | | |
|---|---|---|---|---|
| Holdren and Speyer (1987) | 25 | 3.0 | N/R | Function of grain size (<37 to >600 µm), experimental duration 72 hours |
| Knauss and Copenhaver (1995) | 70 | 4.0-9.5 | 1 | Grain size 75-125 µm, experimental duration 1385 hours |
| Knauss and Wolery (1986) | 25-70 | 1.4-11.8 | 1 | Grain size 75-125 µm, experimental duration over 1200 hours |
| Lagache (1965) | 200 | 7.3 | N/R | Grain size 10-55 µm, experimental duration over 290 hours |
| Oelkers et al. (1994) | 150 | 9.2 | N/R | Effect of Al and chemical affinity |
| Rose (1991) | 25 | 1.4 | 0.5 | Grain size 50-100 µm, experimental duration 8-500 hours |
| Stillings and Brantley (1995) | 25 | 3.0-3.6 | 2 | Grain size 75-100 µm, experimental duration 3000 hours, added NaCl and organic acids |
| Welch and Ullman (1996) | 25 | 3.0-6.0 | 2 | Grain size 125 – 250 µm; added 1mM oxalate |
| ***Oligoclase*** | | | | |
| Casey et al. (1991) | 25 | 3.0 | 20 | |
| Gudbrandsson et al. (2014) | 22 | 2.01-11.1 | 19 | |
| Holdren and Speyer (1987) | 25 | 3.0 | 24 | |
| Mast and Drever (1987) | 22 | 4.0-9.3 | 13 | |
| Oxburgh et al. (1994) | 25 | 3.0-5.1 | 12 | |
| Stillings and Brantley (1995) | 25 | 3.0-5.0 | 22 | +NaCl, + organic acids |
| Stillings et al. (1996) | 25 | 2.9-5.7 | 22 | + 1 mM oxalate |
| ***Andesine*** | | | | |
| Busenberg and Clemency (1976) | 25 | 5.0 | 43 | + 1atm $CO_2$ |
| Casey et al. (1991) | 25 | 2.0 | 47 | Batch experiments |
| Holdren and Speyer (1987) | 25 | 3.0 | N/R | |
| Mast and Drever (1987) | 25 | 3.1-9.0 | 46 | |
| Oxburgh et al. (1994) | 25 | 3.0-5.1 | 43 | |
| Stillings et al. (1996) | 25 | 3.0-7.2 | 43 | +organic acids |
| Stillings and Brantley (1995) | 25 | 3.0-3.1 | 43 | +organic acids, + NaCl |
| Sun (1994) | 25 | 3.0-7.7 | 47 | + organic acids |
| Welch and Ullman (1993) | 25 | 3.0-9.0 | 49 | + organic acids |
| ***Labradorite*** | | | | |
| Blake and Walter (1999) | 80 | 6.0 | 70 | + organic acids, +NaCl |
| Busenberg and Clemency (1976) | 25 | 5.0 | 53 | + 1atm $CO_2$ |
| Carroll and Knauss (2001) | 30-150 | 3.20-3.37 | 60 | + added $CO_2$ (aq) |
| Casey et al. (1991) | 25 | 2.0 | 60 | |
| Gudbrandsson et al. (2014) | 22 | 2.1-11.0 | 61-71 | |
| ***Bytownite*** | | | | |
| Brady and Walther (1989) | 25 | 2.1-12.1 | N/R | |
| Casey et al. (1991) | 25 | 3.0 | 76 | |
| Gudbrandsson et al. (2014) | 22 | 2.0-11.2 | 76-78 | |
| Holdren and Speyer (1987) | 25 | 3.0 | N/R | |
| Oxburgh et al. (1994) | 25 | 3.1-7.2 | 86 | |
| Siegel and Pfannkuch (1984) | 25 | 4.0 | 72 | |
| Stillings and Brantley (1995) | 25 | 3.2-3.6 | 76 | +NaCl, +organic acids |
| Welch and Ullman (1993) | 25 | 3.2-10.0 | 77 | +NaCl, +organic acids |
| ***Anorthite*** | | | | |
| Amrhein and Suarez (1988) | 25 | 3.0-10.0 | 93 | +$CO_2$, secondary mineral precipitation |
| Amrhein and Suarez (1992) | 25 | 3.6-7.4 | 96 | +$CO_2$, secondary mineral precipitation |
| Bailey (1974) | 25 | 3.0-4.5 | N/R | |
| Berg and Banwart (2000) | 25 | 5.7-8.4 | 93 | +$CO_2$ |
| Brady and Walther (1989) | 25 | 1.9-12.0 | 95 | |
| Casey et al. (1991) | 25 | 2.0 | 92 | |
| Fleer (1982) | 25 | 2.0-5.6 | N/R | Underestimated surface area |
| Gudbrandsson et al. (2014) | 22 | 1.8-11.3 | 89 | |
| Hodson (2003) | 25 | 2.6 | 93 | Influence of Fe-rich coating |
| Holdren and Speyer (1987) | 25 | 3.0 | N/R | Secondary mineral precipitation |
| Oelkers and Schott (1995) | 45-95 | 2.5-3.1 | 96 | |

N/R = not reported

To assure internal consistency among the dissolution rates of the plagioclase mineral regression, the equation in this study is based on that of Gudbrandsson et al. (2014), who performed a systematic analysis of the dissolution rates of plagioclases of distinct compositions. Specifically, we used the

equations to describe dissolution rates as a function of pH for albite, oligoclase, andesine, labradorite, bytownite, and anorthite. Gudbrandsson et al. (2014) reported that far-from-equilibrium plagioclase dissolution rates depend strongly on the Ca content of the mineral at acidic conditions, whereas these rates were found to be independent of this composition at basic pH. As such, the dissolution rates for the plagioclases are here assumed to be mineral composition independent at basic pH but depend increasingly on pH as the aqueous fluids become more acidic at pH<6. In addition, the activation energies of all of the plagioclases were taken to be identical. Although this might seem arbitrary, regression of the plagioclase rate data for the individual compositions yielded scattered activation energies as a function of composition, and the activation energy for anorthite was significantly lower than that of albite. This latter difference would lead to albite dissolution rates that are substantially faster than those of anorthite at elevated temperatures, which is inconsistent with observations of natural systems. The choice of single activation energies for all plagioclases prevents such inconsistencies in the resulting database and is within the uncertainty in published rate data.

A comparison of far-from-equilibrium plagioclase dissolution rates calculated using **Eq. (7)** and parameters provided in **Table 2** with corresponding experimentally measured values can be made with the aid of **Figures 3** and **4.** At pH<5, anorthite dissolves significantly faster than the more albitic plagioclases but dissolves at close to identical rates at basic conditions. The dissolution rate equation for albite describes the experimentally measured rate data with an average difference of 0.63 log units; 50% of the experimental data are within 0.54 log units of the corresponding calculated rates. The dissolution rate equation for anorthite describes the experimentally measured rate data with an average difference of 0.61 log units; 50% of the experimental data are within 0.41 log units of the corresponding calculated rates. The significant scatter in these experimental datasets may be due to effects of aqueous solution composition (Burch et al., 1993; Knauss and Copenhaver, 1995; Oelkers et al., 1994), due to the different methods used to measure rates, or be related to sample preparation. In addition, the dissolution rates of the plagioclases are affected by the aqueous activity of Al and, consequently, any aqueous ligand that might complex this metal in the aqueous phase. Oelkers et al. (1994), Blum and Stillings (1995), and Gudbrandsson et al. (2014) noted that the experimental dataset for anorthite dissolution is strongly affected by uncertainties in the measurement of the mineral surface area, for example, in the case of the data from Fleer (1982), and secondary mineral precipitation, for example in the case of the data from Amrhein and Suarez (1988, 1992) and Hodson (2003). Differences in experiment duration, as in the case of data from Oxburgh et al. (1994), may result to up to 1 log unit of difference between measured and calculated rates.

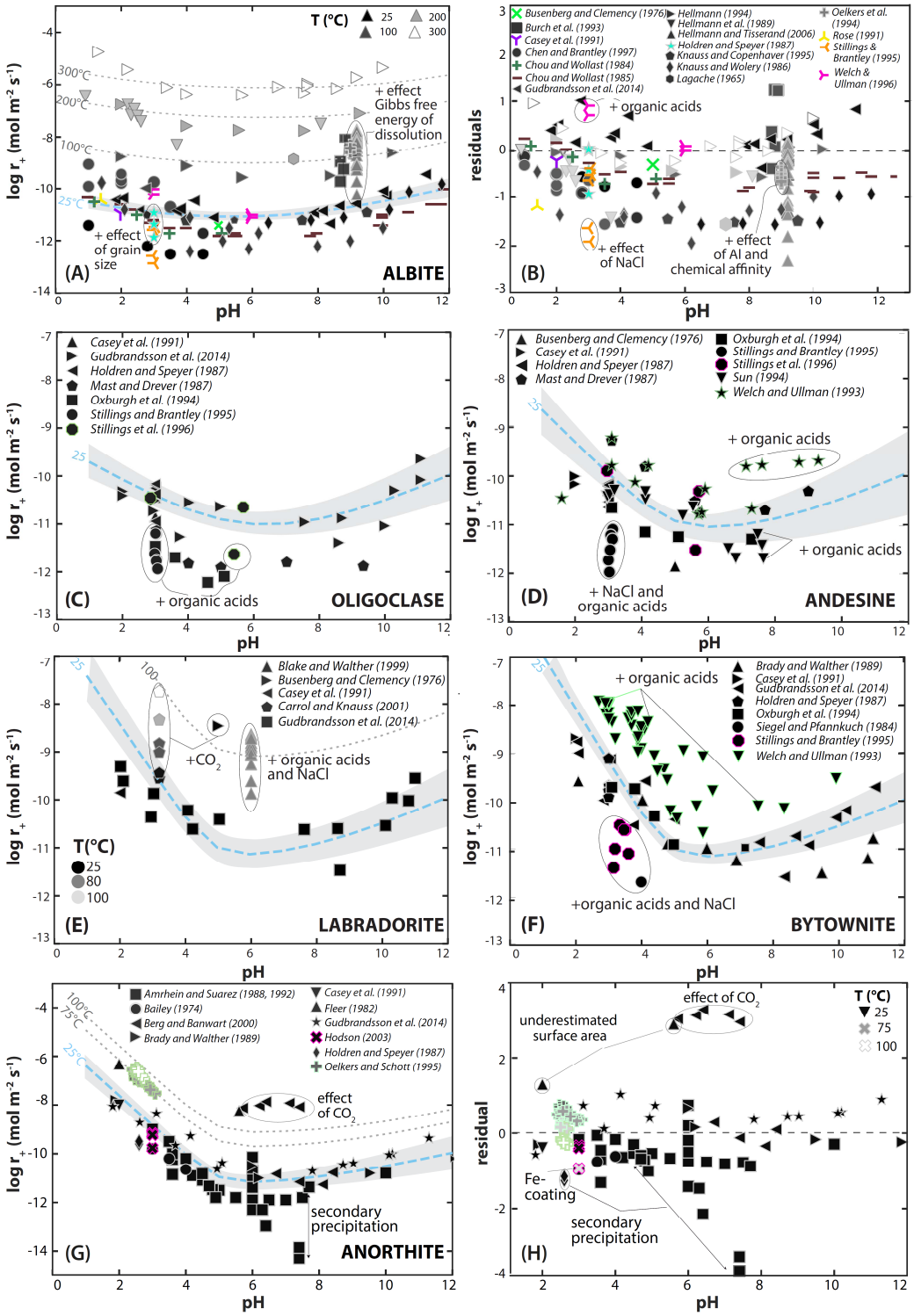


***Figure 3:*** *Far-from-equilibrium dissolution rates of plagioclase minerals:* ***A-B)*** *comparison of measured experimental rates for albite, C) oligoclase, D) andesine, E) labradorite, F) bytownite, G-H) anorthite shown as symbols with corresponding values calculated using* ***Eq. (7)*** *together with the parameters provided in* ***Table 2*** *shown as curves as a function of pH and temperature. The symbol shape and outlying color indicate the source of the data, whereas the shading of the symbol indicates the experimental temperature, with black symbols denoting 25 °C. The shaded regions in some of these plots illustrate the 95% confidence limits of the regression fits for the 25 °C data.*

There are a number of differences between the results of the regression rate equation generated in this study and those presented by Palandri and Kharaka (2004) and Brantley et al. (2008). The anorthite dissolution rate models of Palandri and Kharaka (2004) and Brantley et al. (2008) are limited to acidic to neutral conditions, mostly due to the distribution of rate data available at the time of these studies. Perhaps the most significant difference between these past studies and the present involves the activation energies of these minerals. In the past studies, the activation energies for albite and anorthite were regressed independently, and the activation energies of anorthite were lower than that for albite. The activation energies for intermediate plagioclases were then derived graphically from activation energies of anorthite and albite. As a result, the activation energy for anorthite dissolution is substantially lower than for most primary silicates.

Moreover, using parameters from Palandri and Kharaka (2004) and Brantley et al. (2008), albite-rich plagioclases are calculated to dissolve faster than anorthite-rich plagioclases at a temperature above 130 °C, which is inconsistent with field observations. This likely ambiguity was overcome in the present study by generating plagioclase dissolution rates assuming the activation energies for the plagioclase minerals are independent of the mineral composition. Such could be verified or improved with future studies.

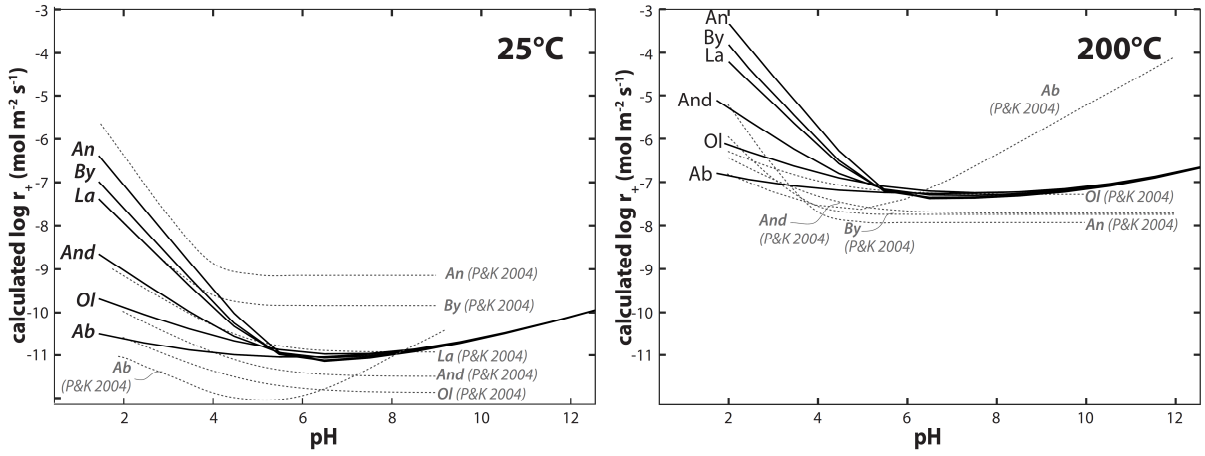


***Figure 4:*** *Far-from-equilibrium dissolution rates of the plagioclases as a function of pH calculated using* ***Eq. (7)*** *together with parameters listed in* ***Table 2,*** *compared with the rates calculated using kinetic parameters in Palandri and Kharaka (2004):* ***A)*** *25 °C and* ***B)*** *150 °C. In this figure Ab=albite, Ol=oligoclase, And=andesine, La=labradorite, By=bytownite, An=anorthite).*

### 3.2.2 K-feldspar

Experimentally measured dissolution rates of K-feldspar, including those of orthoclase and microcline, are summarized in **Figure 5** and **Table 5**. Based on the similarity of K-feldspar and albite structures and compositions, these rates might be expected to be largely similar to one another. Nevertheless, the K-feldspar dissolution rates available in the literature are scattered in part due to the variations in composition of the feldspar samples used in the various experiments. Moreover, there are

far less rate data available for K-feldspar than albite. The experimental dataset considered for the regression calculations includes rates obtained at ambient $pCO_2$ and in the absence of organic ligands. These data span in temperature from 13 to 150 °C (Siegel and Pfannkuch, 1984; Bevan and Savage, 1989; Gautier et al., 1994; Schweda, 1989; Swoboda-Colberg and Drever, 1993; Stillings and Brantley, 1995; Stillings et al., 1996; van Hees et al., 2002). Additional rates have been reported in the presence of 1 atm $pCO_2$ (Busenberg and Clemency, 1976) and in the presence of aqueous organic ligands (Tan, 1980; Manley and Evans, 1986; Welch and Ullman, 1993, 1996; Blake and Walter, 1999; Ullman and Welch, 2002). Experimentally measured rates in this dataset at 25 °C range from as high as $10^{-10.1}$ at pH 2.0 to as low as $10^{-13.3}$ mol $m^{-2}$ $s^{-1}$ at pH 5.6. Rates obtained in the presence of 1 atm $pCO_2$ and/with added aqueous organic ligands are up to 1.5 log units faster than those measured at ambient $pCO_2$ and in the absence of organic ligands (Busenberg and Clemency, 1976; Tan, 1980; Bevan and Savage, 1989). Moreover, experimental data from Swoboda-Colberg and Drever (1993) obtained at field and laboratory conditions and normalized to the geometric surface area, and data from Gautier et al. (1994) obtained at various close-to-equilibrium chemical affinities were also not considered for the regression. Experimental datasets that are not included for the kinetic fit are marked in circles in **Figure 5** and indicated in **Table S1 in Appendix A**.

***Table 5****: Sources of experimentally measured K-feldspar dissolution rates considered in this study.*

| References | T °C | pH | Composition* | Comments |
|---|---|---|---|---|
| Bevan and Savage (1989) | 70-95 | 1.0-9.0 | $Or_{93}Ab_{7}$ | Added organic acids; orthoclase |
| Busenberg and Clemency (1976) | 25 | 5.0 | $Or_{75\text{-}79}Ab_{20\text{-}24}$ | 1 atm $CO_2$; orthoclase/microcline |
| Gautier et al. (1994) | 150 | 9.0 | $Or_{81}Ab_{15}$ | Function of chemical affinity; added Ba |
| Holdren and Speyer (1987) | 25 | 2.0 – 3.0 | $Or_{78}Ab_{21}An_{1}$ | Function of grain fraction |
| Knauss and Copenhaver (1995) | 70 | 4.0-9.5 | $Or_{94}Ab_{6}$ | Added Na |
| Manley and Evans (1986) | 13 | 3.8-5.7 | $Or_{67}Ab_{31}An_{2}$ | Added organics |
| Schweda (1990) | 25 | 1.1-12.7 | N/R | - |
| Siegel and Pfannkuch (1984) | 25 | 4.0 | $Or_{66}Ab_{32}An_{2}$ | Microcline |
| Stillings and Brantley (1995) | 25 | 3.0 | $Or_{78}Ab_{22}$ | Microcline |
| Stillings et al. (1996) | 25 | 3.12 | $Or_{78}Ab_{22}$ | Microcline |
| Swoboda-Colberg and Drever (1993) | 25 | 4.0-4.5 | N/R | Laboratory and field experiments; geometric surface area |
| Tan (1980) | 25 | 7.0 | N/R | Added organic acids; microcline |
| van Hees et al. (2002) | 25 | 3.5-5.0 | $Or_{70}Ab_{25}An_{5}$ | Microcline |

N/R = not reported
*Or-orthoclase, Ab-albite

The K-feldspar experimental datasets spanning the range of temperature from 25 to 95 °C and pH from 2 to 12 were fit to **Eq (7)**. A comparison of experimentally measured rates with those generated using the regression equation and the parameters in **Table 2** can be made with the aid of **Figure 5**. The activation energies retrieved in this study, 51.7, 38.0, and 62.2 kJ $mol^{-1}$, at acidic, neutral, and basic conditions, respectively, are similar to those previously reported by Helgeson et al. (1984), Bevan and Savage (1989), Schweda (1990), Sverdrup (1990), and Blum and Stillings (1995). The activation energies of Palandri and Kharaka (2004) at basic conditions are somewhat higher as they considered

the rates of Gautier et al. (1994) in their regression. As seen in **Figure 5,** there is significant scatter among the datasets leading to differences between calculated and measured rates in some cases.

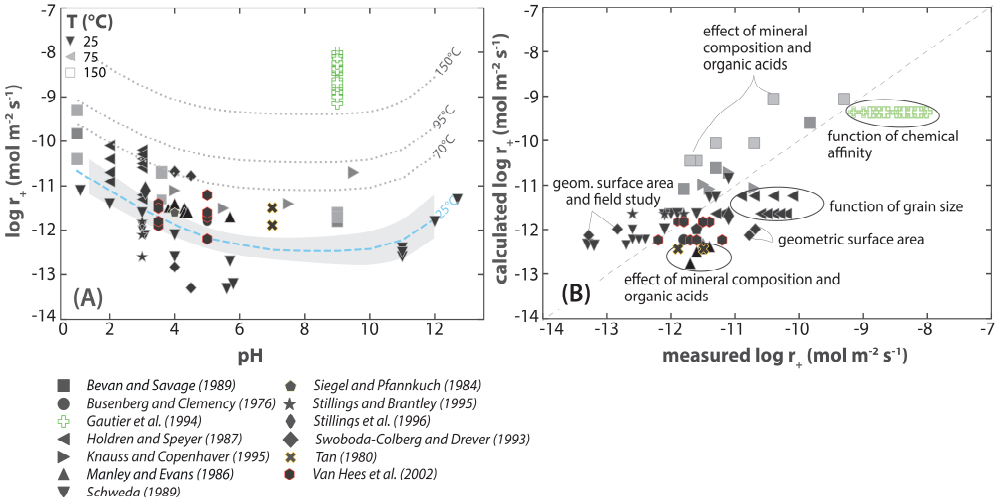


***Figure 5:*** *Far-from-equilibrium dissolution rates of K-feldspar:* ***A)*** *comparison of measured experimental rates shown as symbols with corresponding values calculated using* ***Eq. (7)*** *together with the parameters provided in* ***Table 2*** *shown as curves as a function of pH at temperatures from 25 to 95 °C.* ***B)*** *Direct comparison of measured and calculated dissolution rates. The symbol shape and outline indicate the source of the data, whereas the shading of the symbol indicates the experimental temperature, where black symbols indicate 25 °C. The shaded region in the left plot illustrates the 95% confidence limits of the regression fit of the 25 °C rates.*

The dissolution rate equation for K-feldspar describes the experimentally measured rate data with an average difference of 0.53 log units; 7% of the experimental data are more than one log unit different from the corresponding calculated rate. Many of these larger differences may be due to the composition of the studied feldspar, which ranged from $Or_{66}$ to $Or_{94}$.

### 3.3. Volcanic Glass

Numerous studies have reported volcanic glass reactivity dissolution rates at ambient temperatures to elucidate weathering rates of the oceanic and continental crust (e.g., Colman, 1982; Eggleton, 1987; Banfield et al., 1991; Nesbitt and Wilson 1992). Other studies have reported volcanic glass dissolution rates at a higher temperature and at various $pCO_2$ to assess the potential of volcanic glass to store $CO_2$ and nuclear waste (e.g., Malow et al., 1984; Crovisier et al., 1988; Jercinovic et al., 1990; Morgenstein and Shettel, 1993; Oelkers and Schott, 2005; McGrail et al., 2006; Goldberg et al., 2008; Oelkers and Cole, 2008; Oelkers et al., 2008; Schaef and McGrail, 2009; Gislason et al., 2010; Schaef et al., 2010, 2009; Matter et al., 2016). Most studies have focused on basaltic glass, yet others have described the dissolution rates of borosilicate, rhyolitic and dacitic glass (Jantzen and Plodinec, 1984; Malow et al., 1984; Petit et al., 1990; Plodinec and Wicks, 1993; Wolff-Boenisch et al., 2004).

It is reasonable to assume similar dissolution mechanisms for basaltic and rhyolitic glass; however, measured dissolution rates vary significantly with glass composition (Wolff-Boenisch et al., 2004). Therefore, to account for variability in the glass composition, we summarize volcanic glass dissolution into two subsections, one focused on basaltic glass (<52 wt% $SiO_2$) and the other focused on rhyolitic glass (>68 wt% $SiO_2$).

### 3.3.1 Basaltic glass

Measured basaltic glass dissolution rates have been collected from 9 different studies containing 146 distinct data points. Aside from field data in Gordon and Brady (2002), all rates were measured in the laboratory. Laboratory rates have been measured as functions of aqueous solution composition and temperature. Gislason and Eugster (1987), Oelkers and Gislason (2001), Gislason and Oelkers (2003), Wolff-Boenisch et al. (2004), and Stockmann et al. (2012) used basaltic glass from Iceland as an analog for the oceanic crust, while Daux et al. (1997) focused their efforts on the synthetic glass; the compositions of the glass used in each study are provided in **Table S1, Appendix A**. Most of the experiments were performed at temperatures <100 °C (Gislason and Eugster, 1987; Daux et al., 1997; Oelkers and Gislason, 2001; Wolff-Boenisch et al., 2004; Stockmann et al., 2012), although Guy (1989) and Gislason and Oelkers (2003) reported rates at temperatures ranging up to 200 °C. Oelkers and Gislason (2001) and Stockmann et al. (2012) measured basaltic glass dissolution rates in the presence of organic acids and bacteria, and Crovisier et al. (1987) reported on basaltic glass dissolution in seawater. As the presence of seawater significantly accelerates the dissolution of basaltic glass (marked in circle on **Figure 6**), the experimental data from Crovisier et al. (1987) were not considered in the regression.

The dissolution rate equation adopted in this compilation is based on Stapafell (Iceland) basaltic glass (Oelkers and Gislason, 2001; Gislason and Oelkers, 2003). As this glass is similar in composition to that of mid-ocean ridge basalt, it is representative of much of the natural glass on our planet. In their work, it is assumed that the dissolution rates of basaltic glass are controlled by the breaking of the Al-Si-rich leached layer. In the case of basaltic glass, the majority of the published rate data report sufficient fluid chemistry data to permit the regression of the rate data using (Oelkers and Gislason, 2001; Gislason and Oelkers, 2003; Wolff-Boenisch et al. 2004; Stockmann et al., 2012) yielding:

$$r_+ = \left( 1.08 \cdot 10^{-4}\ \mathrm{mol\ m^{-2} s^{-1}} * \exp\left(\frac{-21500\ \mathrm{J\ mol^{-1}}}{RT}\right) \left(\frac{(a_{\mathrm{H}^+})^3}{(a_{\mathrm{Al}^{3+}})}\right)^{\frac{1}{3}} \right) \quad (10)$$

where $R$ stands for the gas constant, $T$ signifies temperature in K, and $a_{\mathrm{H}^+}$ and $a_{\mathrm{Al}^{3+}}$ represents the activity of the subscripted aqueous species. The effect of the chemical affinity on calculated glass dissolution rates in **Eq. (10)** for use in modeling calculations was accounted for using the solubility of

635 a theoretical leached $SiO_3$-$Al(OH)_3$ glass framework. Its solubility was estimated as an ideal mixture
636 of amorphous $SiO_2$ and $Al(OH)_3$ with the same stoichiometry as the basaltic glass (Bourcier, 1990).
637 **Figure 6** illustrates the degree to which **Eq. (10)** describes the available experimental data. Rates
638 generated using **Eq. (10)** are within two orders of magnitude of corresponding rates published in the
639 literature. The average difference between calculated and measured rates is 0.49 log units, and 50% of
640 the experimental data are within 0.44 log units of those generated with **Eq. (10)**. Relatively large
641 differences were found between calculated rates and those measured by Daux et al. (1997) and Wolff-
642 Boenisch et al. (2004). These studies considered a synthetic glass or a glass with a different Si and Al
643 content than those from Stapafell (Iceland).

644 **3.3.2 Rhyolitic glass**

645 Fewer studies have focused on the dissolution rates of rhyolitic glass. The rhyolite glass
646 dissolution dataset collected in this study comprises 93 data points. Wolff-Boenisch et al. (2004)
647 compared dissolution rates of natural glasses as a function of their silica content from 25 to 74 °C, at
648 pH~4 and 10.6. Karkhanis et al. (1980), White (1983), and Declercq et al. (2013) reported rhyolite
649 glass dissolution rates over the temperature range of 40 to 200 °C as a function of pH and in the
650 presence of organic ligands. Measured rhyolitic glass dissolution rates are one to four orders of
651 magnitude slower than those of basaltic glass at corresponding temperature and pH conditions and
652 range from $10^{-10.4}$ to $10^{-11.6}$ mol $m^{-2}$ $s^{-1}$ at neutral pH and ambient temperature conditions.

653 A comparison of rhyolite glass dissolution rates calculated with **Eq. (7)** and parameters from
654 **Table 2** with their corresponding experimentally measured rates is shown in **Figure 6C**. The
655 dissolution rate equation for rhyolite glass describes the experimentally measured rate data with an
656 average difference of 0.32 log units; 50% of the experimental data are within 0.22 log units of the
657 corresponding calculated rates. Some of the differences between measured and calculated rates likely
658 stem from the variable $SiO_2$ content of dissolved rhyolitic glass samples used in Wolff-Boenisch et al.
659 (2004) and possibly uncertainties reported in surface area measurements in the experiments reported in
660 Declercq et al. (2013).

661

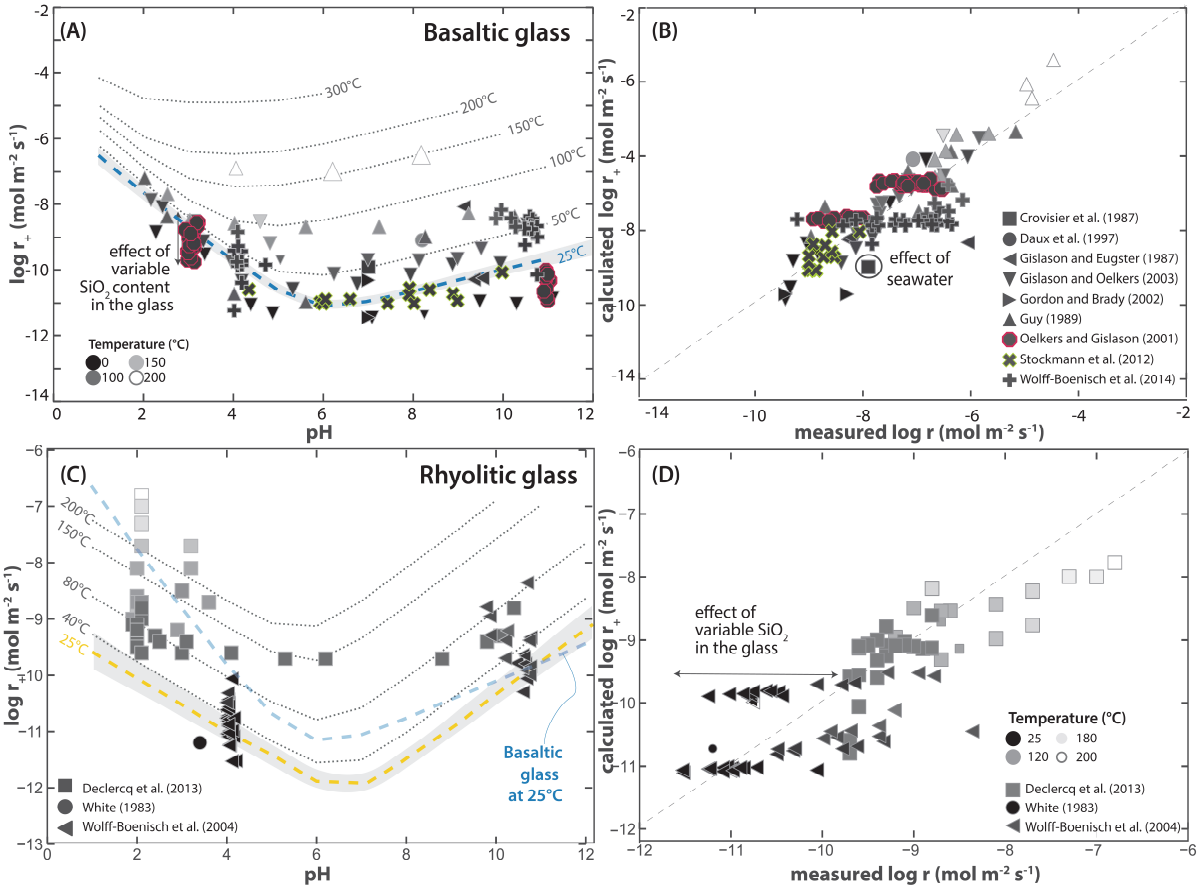


***Figure 6**: Experimentally measured far-from-equilibrium dissolution rates of silicate glass: **A-B)** Comparison of experimentally measured dissolution rates for basaltic glass with rates calculated using **Eq. (10)** at temperatures ranging from 25 to 300°C; **C-D)** Comparison of experimentally measured dissolution rates of rhyolite glass with rates calculated using **Eq. (7)** and parameters from **Table 2** for rhyolitic glass and a temperature range from 25 to 200°C. The symbol shape and outline color indicate the source of the data, whereas the shading of the symbol indicates the experimental temperature, where black symbols indicate 25 °C. The shaded regions in **Fig. 6(C)** illustrate the 95% confidence limits of the regression fit of the 25 °C data.*

## 3.4 Micas

Mica dissolution rates have been previously summarized and reviewed by Ross (1967) and Nagy (1995). The experimental datasets of biotite and muscovite dissolution considered in the present study are summarized in **Table 6** and **Figure 7**. Constant temperature far-from-equilibrium mica dissolution rates tend to minimize as a function of pH at near to neutral conditions. The published dissolution rates of biotite appear to vary more strongly with pH than those of muscovite. Although the dissolution rates of both muscovite and biotite are comparable at 25 °C, muscovite dissolution rates appear to increase faster with increasing temperature. No significant effect has been observed of the magnesium to iron ratio of the biotite on its dissolution rate to date. Magnesium content is expressed as Mg number (Mg# = Mg/(Mg+Fe)) in **Figure 7A**.

### 3.4.1 Biotite

The experimental dataset collected in this study of biotite dissolution includes 19 studies with 129 data points. These studies focused on biotite having compositions ranging between its annite and

683 phlogopite endmembers; most of these reported rates were measured at temperatures near 25 °C and
684 over the pH range of 1 to 8.5 (Sverdrup, 1990; Acker and Bricker, 1992; Kenoyer and Bowser, 1992;
685 Kalinowski and Schweda, 1996; Malmström et al., 1996; Malmström and Banwart, 1997; Murphy et
686 al., 1998; Taylor et al., 2000; Voinot et al., 2013). Samson et al. (2005) reported rates at pH up to 14.3.
687 Biotite dissolution rates at temperatures up to 280 °C have been reported by Carroll et al. (2017).
688 Other studies considered natural biotite weathering at pH from 4.0 to 6.0 at ambient temperature.
689 These studies include those of Velbel (1985), Swoboda-Colberg and Drever (1993), Clow and Drever
690 (1996), Murphy et al. (1998), and White et al. (2002). Acker and Bricker (1992) and Samson et al.
691 (2005) reported that iron oxidation results in biotite dissolution rates that are substantially faster in
692 oxidized fluids when compared to dissolution in oxygen-free conditions. Moreover, Clemency and Lin
693 (1981) and Lin and Clemency (1981) carried out biotite dissolution experiments in open and closed
694 systems in saturated $pCO_2$ aqueous solutions. According to these two studies, biotite dissolution is 67
695 times faster in an open system compared to a closed system.

696 Experimentally measured biotite far-from-equilibrium dissolution rates data are shown at
697 temperatures up to 280 °C as a function of pH in **Figure 7**. As shown in **Figure 7A,** rates at constant
698 pH scatter over up to three orders of magnitude at 25 °C. Bray et al. (2015) attributed these differences
699 to a number of factors, including the distinct biotite sample locations of the considered solids,
700 structural anisotropy, the composition of the studied biotites, the effect of aqueous fluid composition
701 on rates, and experiment duration (see **Table 6** for further details of each experimental study). Further
702 sources of scatter include the biotite iron content and the effect of oxidation. The addition of $CO_2$ to
703 the aqueous solution results in slower biotite dissolution rates (Malmström et al., 1995), whereas some
704 aqueous organic ligands can accelerate these rates (Balland et al., 2010; Bray et al., 2015). Rates
705 measured in the presence of $CO_2$ and/or the presence of organic ligands were not considered in the
706 regression calculations. Moreover, the rates from Velbel (1985) and White et al. (2002) were not
707 considered in the regression either as the surface areas in these studies are likely to be overestimated.
708 Experimental datasets not included in the regression are marked in circle or by arrow in **Figure 7** and
709 **Appendix**.

***Table 6:*** *Sources of experimentally measured mica dissolution rates considered in this study.*

| | T °C | pH | Mg/Fe Ratio | Mineral sample | Experiments |
|---|---|---|---|---|---|
| ***Biotite*** | | | | | |
| Acker and Bricker (1992) | 25 | 3.0-6.7 | 0.59 | Bancroft, Ontario, (Canada) | Fluidized-bed reactors and flow-through columns; added $H_2SO_4$; non-stoichiometric dissolution; Fe-oxidation |
| Balland et al. (2010) | 25 | 2.0-4.4 | 0.6 | Raze, Limousin, (France) with Ca/Mn/Ti impurities; | Batch (closed system) experiments |

| | | | | | |
|---|---|---|---|---|---|
| | | | | | with added organic acids |
| Bray et al. (2015) | 25 | 2.0-6.0 | 0.57 | Grasasen (Norway) | Mixed-flow and batch (closed system) experiments with varying concentrations of organic acids and grain size |
| Carroll et al. (2017) | 100-280 | 3.0-7.5 | 0.94 | | Mixed-flow reactors |
| Clemency and Lin (1981) | 25 | 3.0 | 0.93 | Madagascar | batch (open system) with added $CO_2$ |
| Clow and Drever (1996) | 25 | 4.0 | 0.5 | Field study | |
| Kalinowski and Schweda (1996) | 25 | 1.0-4.0 | 0.91 | Bancroft, Ontario, Canada | Dialysis-cell reactors |
| Kalinowski and Schweda (1996) | 25 | 1.0-4.0 | 0.51 | Grasasen (Norway) | Dialysis-cell reactors |
| Kenoyer and Bowser (1992) | 25 | 4 | 0.5 | Field study | Added $CO_2$ |
| Lin and Clemency (1981) | 25 | 5.5 | 0.93 | Madagascar | batch (closed system) with added $CO_2$ |
| Malmström and Banwart (1997) | 25 | 2.0-10.0 | 0.38 | Moen (Norway); | Flow-through reactors; Fe-oxidation at pH>7 |
| Murphy et al. (1998) | 25 | 4.5 | 0.53 | Field study | |
| Samson et al. (2005) | 22-25 | 7.2-14.3 | 0.59 | Bancroft, Ontario, Canada | Stirred flow-through reactors; rates as a function of solution composition |
| Sverdrup (1990) | 25 | 4.0-5.0 | N/R | N/R | Mixed-flow experiments, K release rates |
| Swoboda-Colberg and Drever (1993) | 25 | 4.0-4.5 | 0.5 | Field study; geometric surface area | Fluidized bed reactors |
| Taylor et al. (2000) | 25 | 3.0-4.0 | 0.8 | pegmatite deposits in the northwestern Adirondack Mountains. | Flow-through reactor |
| Velbel (1985) | 25 | 6.0 | 0.48 | Field study | |
| Voinot et al. (2013) | 20 | 3.0-4.5 | 0.74 | Bancroft, Ontario, (Canada) | Flow-through reactors |
| White et al. (2002) | 25 | 5.5-5.7 | 0.5 | Field study | |
| ***Muscovite*** | | | | | |
| Cabrera and Talibudeen (1979) | 25 | 3 | - | >1µm particles | |
| Hurd et al. (1979) | 1 | 8 | - | <100µm particles | |
| Kalinowski and Schweda (1996) | 22 | 1.1-4.1 | - | 10-20µm particle size | |
| Knauss and Wolery (1989) | 70 | 1.4-11.8 | - | 75-125µm particles | Single-pass and batch reactors |
| Lammers et al. (2017) | 100-280 | 2.1-10.9 | - | 150-250 µm particle size | |
| Nickel (1973) | 25 | 0.2-10.6 | - | 20-35 µm particle size, +impurities | |
| Oelkers et al. (2008) | 60-201 | 1.0-10.3 | - | 50-100 µm particle size | Function of Al and Si activity |
| Swoboda-Colberg and Drever (1993) | 25 | 4.0-4.5 | - | Field study; 75-150 µm, geometric surface area | |

N/R = not reported

710

**Figure 7** compares measured rates with rates calculated using **Eq. (7)** and parameters listed in **Table 2**. The dissolution rate equation for biotite describes the experimentally measured rate data with an average difference of 0.43 log units; 50% of the measured dissolution rates are within 0.35 log units of those calculated.

Previous equations describing far-from-equilibrium biotite dissolution rates have been presented by Acker and Bricker (1992), Kalinowski and Schweda (1996), Malmström and Banwart (1997), Palandri and Kharaka (2004), and Bray et al. (2015). Most of these equations were limited to acidic to neutral conditions other than that of Malmström and Banwart (1997), which described biotite dissolution rates to pH 10. However, this latter study included rates affected by Fe oxidation and therefore yields higher rates than that of other regression efforts. The regression equation generated in the present study yields rates similar to that of Bray et al. (2015) and Carroll et al. (2017) but 1) clarifies the variation of rates as a function of biotite composition, and 2) takes into consideration an increase in dissolution rates with increasing pH at pH>10, and 3) considered the rate data to temperatures up to 280 °C.

### 3.4.2 Muscovite

The experimental dataset for muscovite collected in this study includes 136 data points from 8 experimental studies. Nickel (1973) described muscovite dissolution rates measured in stirred tank reactors at 25 °C and pH 0.2, 3.6, 5.6, and 10.6. These rates were normalized to BET surface areas by Nagy (1995). Cabrera and Talibudeen (1979) and Kalinowski and Schweda (1996) investigated muscovite dissolution rates at 25 ºC over a 1 to 4.1 pH range. Lin and Clemency (1981) measured muscovite dissolution rates at pH 4.6 and 5.1 and $CO_2$-saturated solutions in closed system reactors. Moreover, Swoboda-Colberg and Drever (1993) compared muscovite dissolution rates at <25 °C observed in the field and measured in the laboratory conditions. Hurd et al. (1979) reported muscovite dissolution rates at 1 °C and pH 8 in seawater. Knauss and Wolery (1986), Oelkers et al. (2008), and Lammers et al. (2017) derived equations describing muscovite dissolution rates based on flow-through experiments over wide ranges of pH at temperatures up to 280 °C.

Published far-from-equilibrium dissolution rates are shown in **Figure 7** as a function of pH at 25, 100, 150, 200, and 250 °C. Experimental datasets from Nickel (1973), Cabrera and Talibudeen (1979), and Kalinowski and Schweda (1996) have comparable values at temperatures 22 to 25 °C, and pH ranging from 0.3 to 4.1. Rates increase with increasing temperature; the fastest rate $10^{-8.5}$ mol $m^{-2}$ $s^{-1}$ was measured at 250 °C as reported by Lammers et al. (2017). Rates reported by Swoboda-Colberg and Drever (1993) differ by up to one log unit from corresponding rates of other studies as they were normalized to the geometric surface area. Therefore, the rates reported in these studies were not considered in the regression calculations.

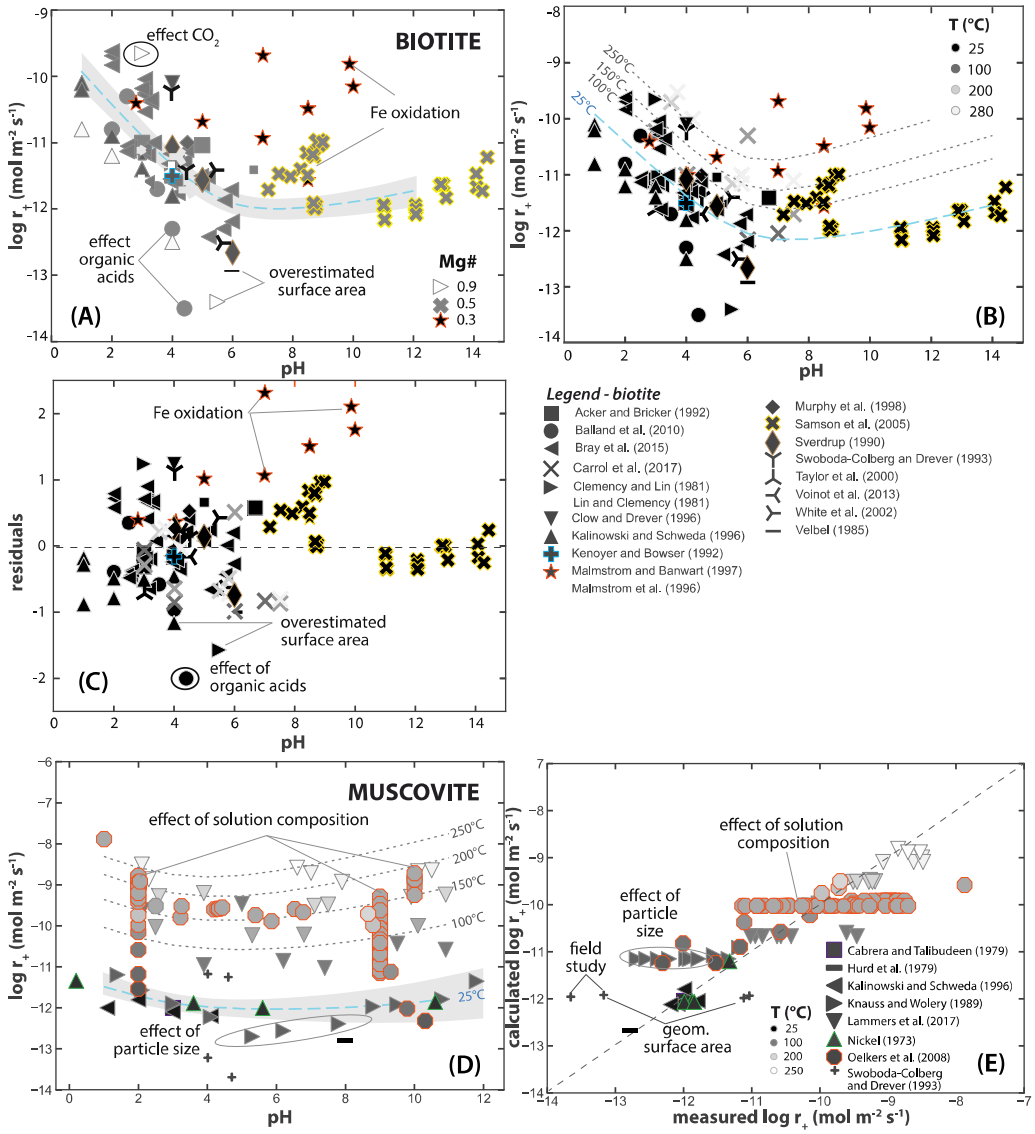


***Figure 7:*** *Far-from-equilibrium dissolution rates of mica minerals: comparison of* ***A****) measured biotite dissolution rates at 25 °C;* ***B****) comparison of experimentally measured biotite dissolution rates shown as symbols with rates generated using the regression equations generated in this study at temperatures from 25 to 280 °C, and* ***C****) residuals of the biotite regression analysis as a function of pH.* ***D-E)*** *Measured muscovite dissolution rates at 25 °C. The symbols represent experimentally measured rates, whereas the blue dashed curve represents rates calculated using the regression equation generated in this study. The symbol shape and outline indicate the source of the data. The shading of the symbol indicates the composition of biotites in* ***Figure 7A****, but the temperature of the measurement in* ***Figure 7B-7F****. The shaded regions in the plots illustrate the 95% confidence limits of the corresponding regression fits at 25 °C.*

**Figures 7D** and **7E** compare experimentally measured muscovite dissolution rates with those generated from the equations and parameters generated in this study. The dissolution rate equation for muscovite describes the experimentally measured rate data with an average difference of 0.55 log units; 50% of the experimental data are within 0.45 log units of the corresponding calculated rates. Less than 13% of the measured rates differ by more than one log unit from the corresponding calculated rates. Most of the rates exceeding this difference were reported by Knauss and Wolery

(1989) at intermediate pH; these rates may have been affected by the precipitation of secondary minerals.

The regression fit generated in the present study yields similar rates as the equations proposed by Kalinowski and Schweda (1996), Palandri and Kharaka (2004), and Lammers et al. (2017), with a difference of less than 0.5 log unit in corresponding rates. Moreover, the retrieved activation energies obtained in this study compare well with those of Lammers et al. (2017). At the same time, the activation energies of Palandri and Kharaka (2004) are substantially lower than those reported here. This difference is likely due to the former study having limited their regressed dataset to temperatures of 70 °C or less.

## 3.5 Olivines

Experimentally measured olivine dissolution rates have been reported over wide ranges of temperature, mineral, and aqueous solution composition. Most experimental results have been concentrated on the reactivity of Mg-rich olivines due to their dominance in natural systems and ease of acquisition. Rimstidt et al. (2012) and Oelkers et al. (2018) summarized and reviewed olivine dissolution rate data and compared previous rate equations describing these rates. Some datasets are available for fayalite, with less than 10 mol% MgO in this site. Regressions of the experimentally measured rates of the olivine minerals were performed assuming two parallel rate mechanisms, one dominating at acidic conditions and the second dominating at basic conditions.

### 3.5.1 Forsterite

Experimentally measured far-from-equilibrium forsterite dissolution rates have been collected from 16 studies reporting 583 rates. The majority of these studies quantified the reactivity of forsterite having from 91 to 93 mol% of MgO in its divalent metal site and at temperatures ranging from 25 to 150 °C (Luce et al., 1972; Bailey, 1974; Siegel and Pfannkuch, 1984; Grandstaff, 1986; Van Herk et al., 1989; Casey et al., 1993; Westrich et al., 1993; Chen and Brantley, 2000; Pokrovsky and Schott, 2000; Rosso and Rimstidt, 2000; Oelkers, 2001b; Golubev et al., 2005; Hänchen et al., 2006; Olsen, 2007; Prigiobbe et al., 2009; Shirokova et al., 2012; Olsen et al., 2015). Additionally, Bailey (1974), Wogelius and Walther (1991, 1992), Pokrovsky and Schott (2000), Golubev et al. (2005), and Prigiobbe et al. (2009) reported experimentally measured forsterite dissolution rates in the presence of organic acids and as a function of $CO_2$ up to 178 atm, and in the presence of bacteria. Forsterite dissolution rates decrease as the pH increases, from $10^{-7.2}$ mol $m^{-2}$ $s^{-1}$ at pH 1.8 to $10^{-10.4}$ mol $m^{-2}$ $s^{-1}$ at pH 11.9 at 25 °C. As observed for many silicates, the dissolution rates increase as temperature increases, with rates increasing by two orders of magnitude from 25 to 90 °C, and increasing by four orders of magnitude from 25 to 150 °C (Siegel and Pfannkuch, 1984; Van Herk et al., 1989; Wogelius and Walther, 1991, 1992; Casey et al., 1993; Jonckbloedt, 1998; Chen and Brantley, 2000; Oelkers, 2001b; Hänchen et al., 2006; Prigiobbe et al., 2009). Wogelius and Walther (1991) and Pokrovsky and

Schott (2000) suggested that the addition of $CO_2$ to the reactive aqueous fluid slows forsterite dissolution as the pH increases beyond pH 6. The experimental results of Wogelius and Walther (1991), however, exhibited non-stoichiometric release of metals to the aqueous phase. Therefore, the rates they reported may have been influenced by the formation of secondary minerals in their reactors. Dissolution rates reported by Pokrovsky and Schott (2000) were calculated based on Mg release rates and possibly could have been influenced by the formation of a brucite-leached layer or magnesite precipitation at the mineral surface (Olsen, 2007). More recently, Golubev et al. (2005) and Prigiobbe et al. (2009) observed no significant changes in forsterite dissolution rates with increasing $pCO_2$. These authors attribute the previous observations of the effect of aqueous $CO_2$ on rates to the change in pH of the aqueous fluid due to the $CO_2$ addition. According to the results of Shirokova et al. (2012), the presence of both live and dead bacteria increases somewhat olivine dissolution rates. There is also some experimental evidence that the presence of organic acids might affect olivine dissolution rates (Bailey, 1974; Wogelius and Walther, 1991), insufficient systematic data are available to quantify such effects. Hence, the results of the latter two studies were not considered in the data regression. The study of Siegel and Pfannkuch (1984) was not considered due to the contamination of the mineral structure, and experimental data from Grandstaff (1986) were not considered due to ambiguities in quantifying the surface area of their forsterite grains. Note that experimental datasets that were not considered in the regression, including data from Gradstaff (1977), Siegel and Pfannkuch (1984), and those affected by added organic acids and presence of $CO_2$, are marked in **Figure 8** and **Table S1 in Appendix**.

The regression of the existing results performed in this study differs insignificantly from the fit proposed by Rimstidt et al. (2012); therefore, we chose to adopt the Rimstidt et al. (2012) rate equation in this study. This equation suggests activation energy of 70.4 kJ $mol^{-1}$ at acid conditions and 60.9 kJ $mol^{-1}$ at basic conditions. These are within an upper limit of a previously published range for forsterite, comparable with corresponding values proposed by Olsen (2007). Rimstidt et al. (2012) noted that higher values of activation energy might be due to a heterogeneous distribution of rates over the pH and temperature range. The reaction order in this rate equation with respect to proton activity changes from 0.44 at acidic conditions to 0.22 at pH ~8.8 (Oelkers et al., 2018). This pH value corresponds approximately to the pH at which forsterite switches from preferential initial Si to preferential initial Mg release (Pokrovsky and Schott, 2000).

**Figure 8** shows a comparison between forsterite far-from-equilibrium dissolution rates generated from **Eq. (7)** and the parameters listed in **Table 2** with corresponding rates generated from experiments at temperatures from 25 to 150 °C. The scatter is evenly distributed across the range of temperature and pH. The average difference between measured and calculated rates is 0.28 log units. In total, 50% of the measured rates differ by 0.18 log units or less from their corresponding calculated values.

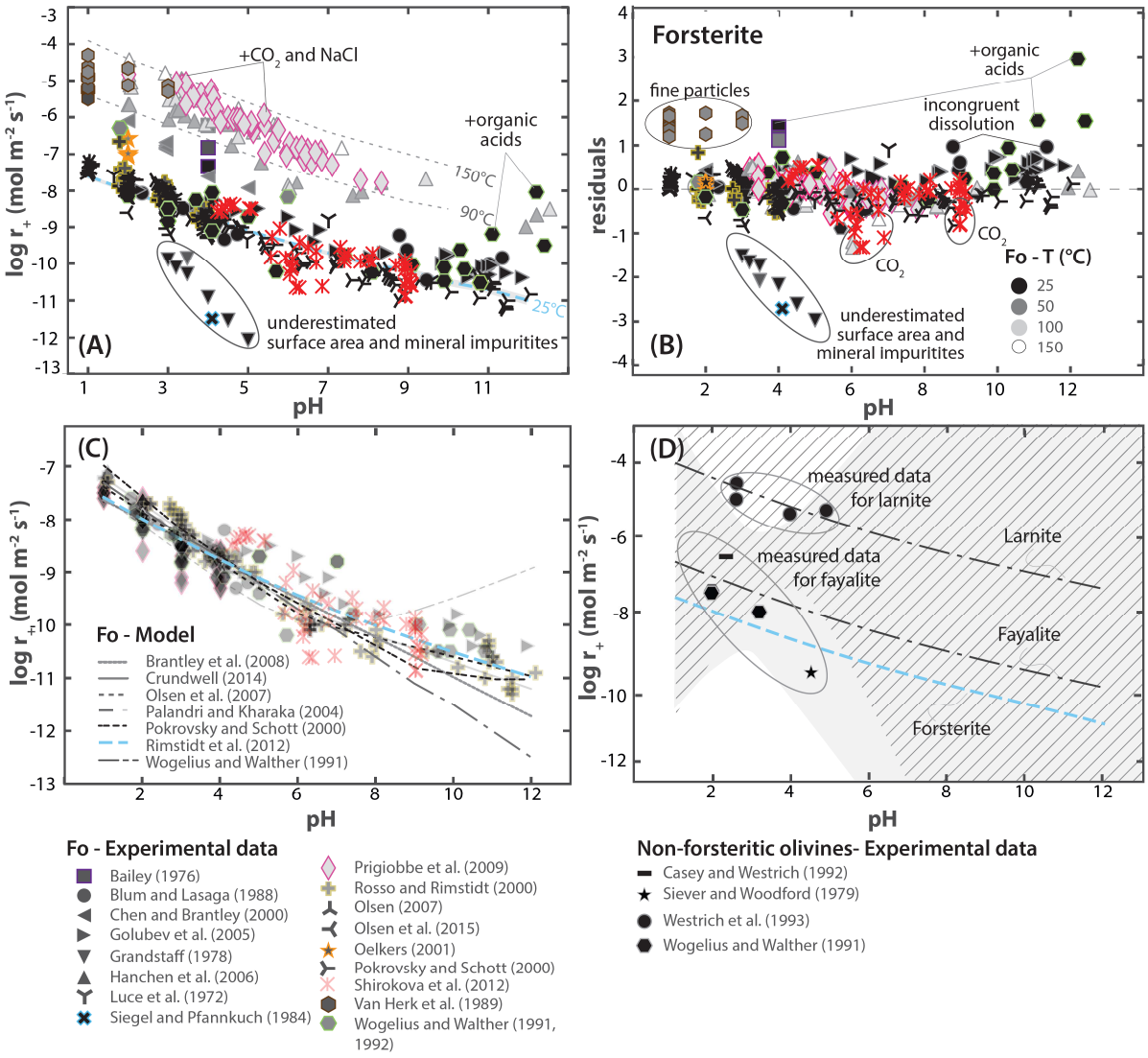


***Figure 8**: Far-from-equilibrium dissolution rates of olivine minerals: **A-B)** Comparison of experimentally measured forsterite dissolution rates with values calculated from **Eq. (7)** and the parameters listed in **Table 2** at temperatures from 25 to 150 °C as a function of pH; **C)** comparison of far-from-equilibrium forsterite dissolution rates calculated using equations and parameters available in the literature; **D)** comparison of measured far-from-equilibrium dissolution rates for selected olivine minerals with values calculated from **Eq. (7)** and the parameters listed in **Table 2** at 25 °C as a function of pH. The symbol shape and outline color indicate the source of the data, whereas the shading of the symbol indicates the experimental temperature, with black symbols being 25 °C. The shaded regions in the plots illustrate the 95% confidence limits of the corresponding regression fits at 25 °C.*

**Figure 8C** shows a comparison of forsterite far-from-equilibrium dissolution rates generated from **Eq. (7)** compared with previously suggested fit equations. The rate equations published in Wogelius and Walther (1991), Pokrovsky and Schott (2000), Palandri and Kharaka (2004), Olsen (2007), Brantley et al. (2008), Crundwell (2014) at acidic pH are similar to one another and to rates generated using **Eq. (7)**. At basic pH, the models of Wogelius and Walther (1991), Palandri and Kharaka (2004), and Brantley et al. (2008) differ by up to one order of magnitude from that adopted in this study, as some of these fits took into account experimental data from Pokrovsky and Schott

(2000). The rate equation of Wogelius and Walther (1991) took into account some experimental data obtained at non-steady-state conditions and hence overestimated forsterite dissolution rates by up to two orders of magnitude.

### 3.5.2 Non-forsteritic olivines

In comparison to forsterite, relatively few studies have reported the dissolution rates of olivines with non-forsteritic composition. Siever and Woodford (1979), Casey and Westrich (1992), and Wogelius and Walther (1992) reported the dissolution rates of fayalite from pH 2 to 4.5 at ambient temperature ranged from $10^{-6.52}$ to $10^{-9.60}$ mol $m^{-2}$ $s^{-1}$. Larnite dissolution rates reported in Westrich et al. (1993) for the same temperature and pH ranging from 2 to 4.9 are one to four orders of magnitude faster. Due to a scarcity of experimental data, activation energies and reaction orders for fayalite and larnite were taken to be identical to those of forsterite. Moreover, it is not possible to independently regress the fayalite and larnite dissolution rates at pH<5; therefore, activation energies and reaction orders for these minerals are taken from those of forsterite.

**Figure 8D** compares the calculated versus measured far-from-equilibrium dissolution rates for larnite and fayalite at a temperature of 25 °C with corresponding calculated rates. The large average difference between the calculated and measured rates for fayalite of 0.88 log units is caused by slower reported dissolution rates from Siever and Woodford (1979), possibly affected by iron oxidation and silica precipitation (Wogelius and Walther, 1992). The average difference between the calculated and measured rates for larnite is 0.23 log units, and 50% of the experimentally measured rates are within 0.22 log units of the corresponding calculated rates. Calculated dissolution rates for larnite compare well with the fit suggested in Westrich et al. (1993).

## 3.6 Pyroxenes

The pyroxene mineral structures are made up of linear chains of silica tetrahedra consisting of Si-O-Si bonds. These chains are held together in the pyroxene structure by divalent metal-oxygen bonds. Oelkers and Schott (2001) presented evidence that the dissolution mechanism of the pyroxene minerals consists first of the rapid exchange of the divalent metals near the mineral surface with protons in the aqueous phase, followed by the slow rate-limiting breaking of the Si-O bonds adjacent to the removed cations. This mechanism was further confirmed by Oelkers et al. (2009), who showed that the rapid exchange of divalent metals with the divalent cations at pyroxene surfaces occurs at fixed proportions over wide ranges of pH. Such studies suggest that the far-from-equilibrium rates of pyroxene dissolution in the absence of other accelerating aqueous species would be proportional to the aqueous activity ratio $a_{H^+}^2/a_{M^{2+}}$. The value of this ratio depends on the concentration of the $M^{2+}$ cation in the aqueous solution. Aqueous $M^{2+}$ cations form negligible hydroxide complexes. This implies that the aqueous activity ratio and thus the far-from-equilibrium dissolution rates of the pyroxenes will decrease monotonically with pH at constant $M^{2+}$ concentration.

885 The generation of an accurate expression describing the dissolution rates of the pyroxenes is
886 challenging due to the relative scarcity of experimental data and the large range of composition of
887 natural pyroxene samples. Brantley and Chen (1995) summarized the experimentally measured
888 dissolution rates available at the time of this publication. Most of the data have been reported for
889 acidic pH conditions. As previously mentioned for the case of amphiboles, the lack of experimentally
890 measured data at basic pH leads to significant uncertainties in the fit of the data at these conditions.
891 Similar to the amphiboles, Palandri and Kharaka (2004) proposed a two-term fit of the available data
892 where rates are pH-independent at basic conditions, while the fits of Knauss et al. (1993) and Brantley
893 et al. (2008) suggested that these rates continuously decrease with increasing pH. The current study
894 adopted the former approach as it provides a better description of the available experimental data.

895 **3.6.1 Clinopyroxenes**

896 The sources of experimentally measured far-from-equilibrium dissolution rates of diopside and
897 augite dissolution are summarized in **Table 7**. The dataset consists of 11 studies, of which the majority
898 focused on clinopyroxene dissolution at ambient temperature and over the pH range of 1 to 7. Some of
899 these studies reported pyroxene dissolution rates at pH up to 12 and, or temperatures up to 90 °C
900 (Schott and Berner, 1985; Knauss et al., 1993; Chen and Brantley, 1998; Golubev et al., 2005;
901 Stockmann et al., 2008; Daval et al., 2010). Several studies reported the effect of $CO_2$ and aqueous
902 organic acids on clinopyroxene dissolution rates. Knauss et al. (1993) reported diopside dissolution
903 rates in the presence of $10^{-3.5}$ to 1 atm $pCO_2$ for pH 1-12 and temperature range 1 to 70 °C. This study
904 suggested that diopside dissolution rates are not appreciably changed by the concentration of $CO_2$ in
905 the aqueous solution at these conditions.

906 Oxidation state may affect the dissolution rates of the iron-bearing pyroxenes. Siever and
907 Woodford (1979), Schott and Berner (1985), and White and Yee (1985) described the effect of iron
908 oxidation at 20 to 50 °C and pH range 1 to 9 for augite and other Fe-bearing pyroxenes at oxic and
909 anoxic conditions. They concluded that in comparison to anoxic conditions, pyroxene dissolution rates
910 at pH<6 decreased when exposed to air, which they explained by precipitation of less reactive iron
911 hydroxides on primary grains (Casey and Cheney, 1993). At pH>6, however, no effect of oxidation
912 state on rates was observed.

***Table 7:*** *Sources of experimentally measured clinopyroxene dissolution rates considered in this study.*

| | T<br>°C | pH | Exp Duration (d) | Mineral composition* (%) | Comments |
|---|---|---|---|---|---|
| ***Augite*** | | | | | |
| Schott and Berner (1985) | 20-72 | 6 | 16 | N/R | - |
| Siegel and Pfannkuch, (1984) | 22 | 4.1 | 29 | $En_{22}Fs_{44}Wo_{34}$ | +Al, Na in mineral structure |
| Sverdrup (1990) | 25 | 2.5-6.8 | 2-25 | $En_{45}Fs_{27.5}Wo_{27.5}$ | - |
| Sverdrup (1990) | 25 | 3.1-6.5 | 2-25 | $En_{51}Fs_{5}Wo_{44}$ | - |
| ***Diopside*** | | | | | |
| Chen and Brantley (1998) | 25-90 | 1.2-3.8 | 77 | $Wo_{44.45}En_{44.51}Fs_{111}$ | +Al in mineral structure |
| Daval et al. (2010) | 90 | 4.9-5.2 | 23-122 | $Wo_{51.1}En_{48.7}Fs_{0.2}$ | +Al in mineral structure |

| | | | | | |
|---|---|---|---|---|---|
| Eggleston et al. (1989) | 25 | 1.0 | 1 | $Wo_{51}En_{48}Fs_1$ | Effect of age |
| Golubev et al. (2005) | 25 | 1.0-11.8 | 1-6 | $Wo_{49.7}En_{49.2}Fs_1$ | +Al, Mn, Na, Ti, Cr in mineral structure; $+CO_2$ |
| Hoch et al. (1996) | 25 | 5.8 | 25-183 | $Wo_{49}En_{47}Fs_4$ | At atmospheric conditions, +Fe, Na, Al in the mineral structure |
| Knauss et al. (1993) | 25-70 | 2.0-12.0 | 60 | $Wo_{50}En_{46}Fs_4$ | +Al in mineral structure; $+CO_2$ |
| Schott et al. (1981) | 20-25 | 1.0-6.0 | 2-40 | $Wo_{51}En_{48}Fs_1$ | Non-stoichiometric dissolution, +Al in the mineral structure |
| Stockmann et al. (2008) | 25-70 | 4.3-8.5 | Up to 164 | $Wo_{50}En_{49}Fs_1$ | +Al, Cr, Mn, Na, Ti in mineral structure |

N/R = not reported
* Wo-wollastonite, En – enstatite, Fs- ferrosilite

Experimental data that were not included for the regression are marked in **Figure 9** and include datasets from Schott et al. (1981), Hoch et al. (1996), and Daval et al. (2010). The data of Hoch et al. (1996) were obtained from experiments on diopside containing substantial mineral impurities. The data of Schott et al. (1981) were obtained from experiments that did not attain a steady state. Finally, the data of Daval et al. (2010) were obtained at close to equilibrium conditions such that the chemical affinity term in **Eq. (7)** could influence the measured rates.

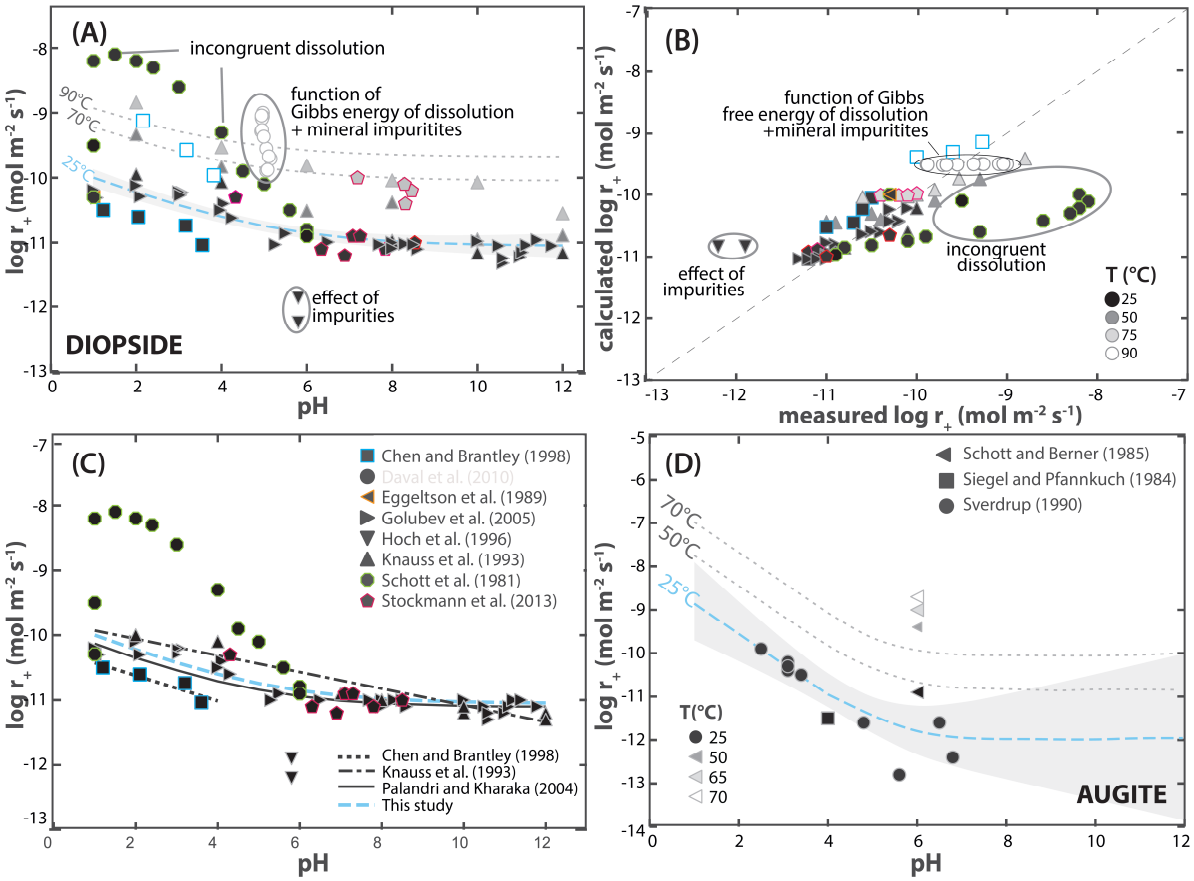


***Figure 9:*** *Far-from-equilibrium dissolution rates of diopside and augite:* ***A-B)*** *Comparison of measured experimental rates with rates calculated from* ***Eq. (7)*** *together with parameters listed in* ***Table 2*** *as a function of pH at temperatures from 25 to 90 °C. C) Comparison of the diopside dissolution rates generated from the equations and parameters generated in this study compared with the results of previously published rate equations.* ***D)*** *Comparison of measured augite experimental rates with rates calculated from* ***Eq. (7)*** *together with parameters listed in* ***Table 2*** *as a function of pH at temperatures from 25 to 70 °C. The symbol shape and*

*outline color indicate the source of the data, whereas the shading of the symbol indicates the experimental temperature, where black symbols being 25 °C. The shaded regions in the plots illustrate the 95% confidence limits of the corresponding regression fits at 25 °C.*

**Figure 9A-C** compares the calculated versus measured far-from-equilibrium dissolution rates for diopside at 25 to 90 °C. The average difference between the calculated and measured rates is 0.23 log units, and 50% of the experimentally measured rates are within 0.19 log units of the corresponding calculated rates. Rates generated using equations and parameters in this study are compared with the results of previously proposed diopside rate equations in **Figure 9C**. Despite the availability of more recent experimentally measured rates, the rate equations provide largely similar results. The present regression equation provides similar rates as the equations of Palandri and Kharaka (2004), while they differ by as much as 0.4 log units from those calculated using the equation proposed by Knauss et al. (1993). Measured far-from-equilibrium dissolution rates of augite are shown in **Figure 9D.** Rate parameters for augite were obtained from fitting the experimental data of Siegel and Pfannkuch (1984), Schott and Berner (1985), and Sverdrup (1990). The average difference between experimentally measured rates and corresponding values obtained using the regression equation is 0.68 log units. This relatively large difference likely stems at least in part from the varying composition of augite used in the experiments.

### 3.6.2 Orthopyroxenes

The sources of experimentally measured far-from-equilibrium dissolution rates of enstatite and bronzite dissolution are summarized in **Table 8**. The dataset consists of 10 studies, of which the majority focused on orthopyroxene dissolution at ambient temperature and over the pH range of 1 to 7. Some of these studies reported pyroxene dissolution rates at pH up to 12 and, or temperatures of up to 168 °C (Brady and Walther, 1989; Oelkers and Schott, 2001; Halder and Walther, 2011). Several studies reported the effect of $CO_2$ and aqueous organic acids on clinopyroxene dissolution rates. Bailey (1974) and Grandstaff (1977) reported bronzite and enstatite dissolution rates in the presence of aqueous organic acids for the pH range 1 to 4.1 and the temperature range 1 to 42 °C; however, they found no evidence that added organic acids affect dissolution rates of the pyroxenes. Schott and Berner (1983) reported on bronzite dissolution in the presence of atmospheric oxygen. They concluded that, as in the case of clinopyroxenes, the reactivity of orthopyroxenes at acidic pH up to pH 6 decreased when exposed to air.

**Figure 10A-C** compares the calculated versus measured rates for enstatite dissolution. The average difference between the calculated and measured rates is 0.32 log units, and 50% of the measured data are within 0.39 log units of their corresponding calculated values. Fewer than 5% of the measured rates are more than 1 log unit different from their corresponding calculated values. The fit

based on the pH polynomial in this study is close to the same quality as that based on a mechanistic model reported by Oelkers and Schott (2001).

***Table 8:*** *Sources of experimentally measured orthopyroxene dissolution rates considered in this study.*

| | T °C | pH | Exp Duration (d) | Mineral Composition | Comments |
|---|---|---|---|---|---|
| ***Bronzite*** | | | | | |
| Grandstaff (1977) | 1-42 | 1.2-4.1 | 2-22 | $En_{77}Fs_{21}Wo_2$ | $K_2SO_4$, $H_2SO_4$, $HNO_3$, $KNO_3$, +Al, Na in the mineral structure, + organic acids |
| Schott and Berner (1983) | 25 | 1.0-6.0 | 60 | $En_{89}Fs_{11}$ | +at atmospheric conditions |
| ***Enstatite*** | | | | | |
| Bailey (1974) | 25 | 4.0 | N/R | N/R | Added organic acids |
| Brady and Walther (1989) | 25 | 8.0-12.5 | N/R | N/R | |
| Ferruzzi (1993) | 25 | 2.0-7.0 | 62-84 | $En_{100}$ | 0.1M buffer solutions |
| Halder and Walther (2011) | 24 | 8.0-13.0 | 80-137 | $En_{100}$ | |
| Luce et al. (1972) | 25 | 1.6 | 1-4 | $En_{92.5}Fs_{7.5}$ | |
| Oelkers and Schott (2001) | 28-168 | 2.0-10.8 | 3-10.5 | $En_{85}Fs_{13.6}Wo_{0.4}$ | |
| Schott et al. (1981) | 22-72 | 1.0-6.0 | 2-40 | $En_{99.6}Fs_{0.4}$ | +Na, Al in mineral structure |
| Siegel and Pfannkuch (1984) | 22 | 4.0 | 29 | $En_{70}Fs_{28}Wo_{1.27}$ | +Na, Al in mineral structure |

N/R = not reported

The far-from-equilibrium dissolution rates of bronzite are shown in **Figure 10D.** The rate parameters for bronzite were obtained by fitting experimentally measured dissolution rates of Grandstaff (1977) and Schott and Berner (1983). The average difference between measured rates and those obtained from the regression equation is 0.17 log units, and 50% of the rates are within 0.08 log units of their corresponding calculated values. Rates calculated using the equations and parameters generated in the present study are slower than corresponding values generated using equations and parameters reported by Palandri and Kharaka (2004) at acidic conditions, as their regression considered only the experimental data of Sverdrup (1990).

**Figure 11** shows a comparison of the calculated far-from-equilibrium dissolution rates for clinopyroxene and orthopyroxene minerals generated from **Eq. (7)** together with the parameters listed in **Table 2** at 25 and 150 °C. The rates among the different pyroxenes range over roughly an order of magnitude at any single pH and temperature, with enstatite being the most reactive and bronzite the least reactive at acidic conditions, and augite being the least reactive and diopside the most reactive at basic conditions. The dissolution rates of augite appear to be most affected by pH variations. Such differences, however, may be due to minor inconsistencies among the dissolution rate data sets reported in the literature rather than distinct rate behaviors of the different pyroxenes, as these differences are largely within the uncertainties and scatter of the various experimentally measured dissolution rates.

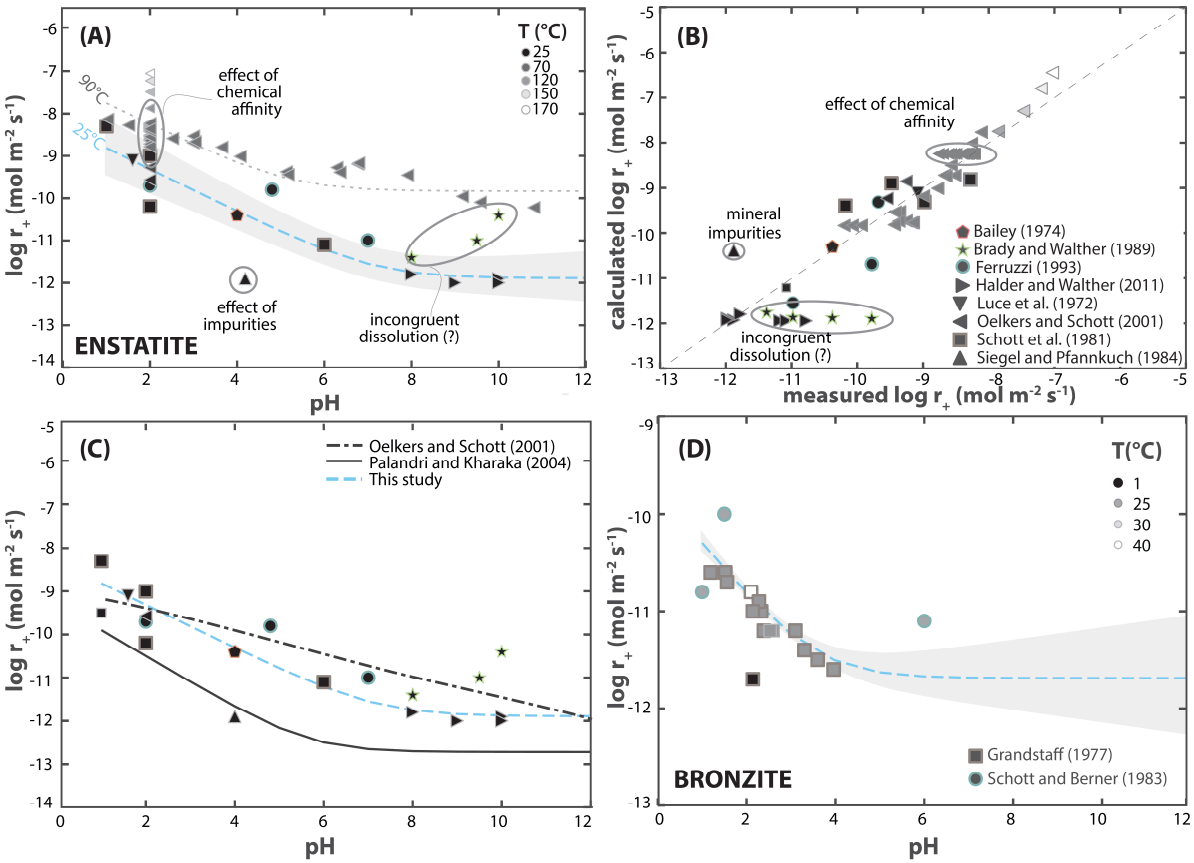


***Figure 10:*** *Far-from-equilibrium dissolution rates of enstatite and bronzite:* ***A and B)*** *Comparison of measured experimental rates with rates calculated from* ***Eq. (7)*** *together with parameters listed in* ***Table 2*** *as a function of pH at the indicated temperatures;* ***C)*** *comparison of the enstatite dissolution rates generated from the equations and parameters generated in this study compared with the results of previously published rate equations.* ***D)*** *Comparison of bronzite measured experimental rates with rates calculated from* ***Eq. (7)*** *together with parameters listed in* ***Table 2*** *as a function of pH at the indicated temperatures. The symbol shape and outline color indicate the source of the data, whereas the shading of the symbol indicates the experimental temperature, where black symbols being 25 °C. The shaded regions in the plots illustrate the 95% confidence limits of the corresponding regression fits at 25 °C.*

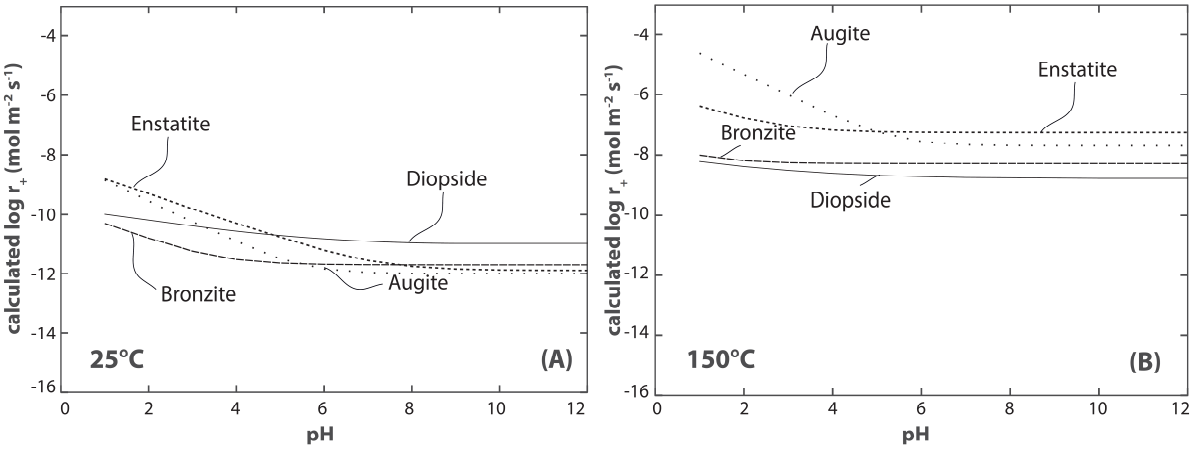


***Figure 11:*** *Comparison of the far-from-equilibrium dissolution rates of pyroxene minerals calculated using* ***Eq. (7)*** *together with the parameters listed in* ***Table 2*** *at* ***(A)*** *25 °C, and* ***(B)*** *150 °C.*

## 3.7 Quartz and other $SiO_2$ polymorphs

A large number of studies have reported the dissolution rates of quartz and other $SiO_2$ polymorphs. A summary of these studies is presented in **Table 9** and **Figure 12.** All silica polymorphs were regressed assuming pH-dependent dissolution rates at acidic and basic conditions.

### 3.7.1 Quartz

Experimentally measured dissolution rates of quartz have been previously compiled and reviewed in Dove (1994), Bickmore et al. (2006), and Rimstidt (2015). The experimental rate dataset in the present study includes 410 distinct rates presented in 24 publications. This dataset covers a temperature range of 25 to 430 °C and a pH range from 0 to 12.3. Schwartzentruber et al. (1987), Knauss and Wolery (1988), Brady and Walther (1990), and House and Orr (1992) investigated the effect of pH on quartz dissolution rates at 25 °C. Kamiya et al. (1974), Rimstidt and Barnes (1980), Bird et al. (1986), Brady and Walther (1989), Dove and Crerar (1990), Casey et al. (1990), Dove (1994, 1999), Hellmann (1994), Tester et al. (1994), Murphy et al. (1998), and Bickmore et al. (2006) reported quartz dissolution rates at temperatures up to 430 °C, and pH ranging from 0 to 12.3. Rates of quartz dissolution at 25 °C vary from $10^{-13.5}$ mol $m^{-2}$ $s^{-1}$ at pH 6 to up to $10^{-10}$ mol $m^{-2}$ $s^{-1}$ at pH of 12.3, and these rates increase by ~5 orders of magnitude by increasing temperature from 25 to 200 °C at constant pH. Dove and Crerar (1990), Dove (1994), and Dove and Nix (1997) reported on the effect of the presence of aqueous alkali metals on quartz dissolution rates. Kamiya and Shimokata (1974), Wollast and Chou (1988), Dove and Crerar (1990), Bennett (1991), Dove (1994), and Dove and Nix (1997) noted that the presence of aqueous sodium, potassium, magnesium, and/or calcium can enhance quartz dissolution rates by up to two orders of magnitude at temperatures ~25 ºC. In contrast, the presence of aqueous divalent or trivalent metals, such as iron or aluminum, tends to decrease quartz dissolution rates as such metals tend to precipitate on the quartz surface in the form of hydroxides or aluminosilicate. The presence of such aqueous cations can slow quartz dissolution rates by up to eight orders of magnitude (Lier et al., 1960; Hurd, 1973; Kamiya and Shimokata, 1974; Bennett, 1991). Additionally, Bennett et al. (1988) and Bennett (1991) reported that the presence of aqueous organic ligands could enhance quartz dissolution rates by up to four orders of magnitude. Due to the considerable effect of added (Na, K, Li)Cl, (Pb, Ca, Ba)$Cl_2$, $NaNO_3$, and organic ligands on quartz dissolution rates, these datasets were not considered in the regression calculations. Experimental data affected by the addition of these species are marked in **Figure 12** and **Table S1 in Appendix.** As the regression of data in the present study is limited to temperatures up to 350 °C, the quartz rates reported by Murphy and Helgeson (1989) were also excluded from the regression calculations. Moreover, the study of Kamiya et al. (1974) does not provide the BET surface areas of their quartz; therefore, this dataset is not included in the regression calculation.

**Figure 12A-C** shows a comparison of quartz dissolution rates generated using equations and parameters of this study with corresponding experimentally measured rates. Fifty percent of calculated

rates are within 0.56 log units of their corresponding measured values. Average difference between the logarithm of measured and calculated rates is 0.60. Much of this difference may stem from variations in dislocation density and sample preparation (Blum et al. 1990) or the identity of added acids (Dove, 1994, 1999). Moreover, some of the data presented in Rimstidt and Barnes (1980) and Tester et al. (1994) show scatter greater than one order of magnitude, potentially due to uncertainties in reactive fluid pH. The fit of quartz dissolution rates in this study differs somewhat from previous efforts. In the present study, far-from-equilibrium quartz dissolution rates were assumed to be composed of two distinct trends for acidic and basic conditions. In contrast, Knauss and Wolery (1988) and Tester et al. (1994) assumed the rates at acidic conditions were pH-independent, while Grigsby (1989) and Brantley et al. (2008) suggested pH-dependent dissolution at acidic conditions. This latter conclusion is consistent with the results of Pokrovsky et al. (2006) who successfully described measured quartz dissolution rates assuming these were controlled by a $>SiOH_2^+$ surface species. The rates generated by the regression calculation in this study agree well with the corresponding regressions of Grigsby (1989) and Brantley et al. (2008).

***Table 9:*** *Sources of experimentally measured silica polymorph dissolution rates considered in this study.*

| Reference | T | pH | Comments |
|---|---|---|---|
| | °C | | |
| ***Quartz*** | | | |
| Bennett (1991) | 25 | 1.1-7.0 | +NaCl |
| Bennett et al. (1988) | 25-70 | 1.1 – 7.0 | +NaCl |
| Berger et al. (1994) | 25-300 | 1.6-6.5 | +NaCl, $PbCl_2$, $Pb(NO_3)_2$, $NaNO_3$ |
| Bickmore et al. (2006) | 89-200 | 8.2-11.3 | +$NaNO_3$ |
| Blake and Walter (1999) | 70 | 6.0 | +Organic acids, NaCl |
| Blum et al. (1990) | 80 | 5.7 | Effect of heterogeneities in mineral structure |
| Bolt (1957) | 25 | 4.0-12.3 | |
| Casey et al. (1990) | 25-70 | 3.0 | Added 0.001 M NaCl |
| Dove (1994) | 200-300 | 1.5-9.1 | +NaCl |
| Dove (1999) | 175-290 | 5.7 | +Mg, Ca, Na, Ba |
| Dove and Crerar (1990) | 200-300 | 5.7 | +NaCl, KCl, $MgCl_2$ |
| Dove and Nix (1997) | 200 | 5.7 | +$MgCl_2$, $CaCl_2$, $BaCl_2$, LiCl, KCI, and NaCl |
| Grigsby (1989) | 25 | 0.0-4.5 | - |
| House and Orr (1992) | 25 | 4.4-10.5 | +NaCl, KCl |
| Knauss and Copenhaver (1995) | 70 | 4.0-9.5 | Effect of malonate |
| Knauss and Wolery (1986) | 70 | 7.6-11.7 | |
| Knauss and Wolery (1988) | 70 | 1.4-11.8 | |
| Murphy and Helgeson (1989) | 385-430 | 4.8-5.3 | |
| Pokrovsky et al. (2006) | 25 | 0.0-2.9 | +$NaNO_3$/$HNO_3$ |
| Rimstidt and Barnes (1980) | 105-305 | 5.7 | pH not monitored/reported |
| Schwartzentruber et al. (1987) | 90 | 9.5-11.4 | +NaCl |
| Tester et al. (1994) | 25-200 | 6 | pH not monitored/reported |
| Wollast and Chou (1988) | 25 | 1.3-12.3 | +NaCl |
| ***$SiO_2$(am)*** | | | |
| Elmer and Nordberg (1958) | 95 | 7.0 | |
| Icenhower and Dove (2000) | 60-250 | 5.7 | 0-0.15 M NaCl |
| Loucaide et al. (2008) | 25 | 6.3-8.1 | 0-50 % seawater fraction, + NaCl, KCl, $MgCl_2$, $CaCl_2$; diatom frustules, phytoliths, two diatomaceous lake sediments, a siliceous ooze, diatomite deposit, and a synthetic amorphous silica |
| Mazer and Walther (1994) | 40-85 | 7.0 | |
| Niibori et al. (2000) | 33 | 13.0 | +NaOH, synthetic $SiO_2$ |
| Pokrovsky et al. (2006) | 25 | 0-1.92 | Constant IS 1M |
| Rimstidt and Barnes (1980) | 25 | 7.0 | |
| Seidel et al. (1997) | 25 | 7.0 | Monospheres; +NaCl |
| Van Cappellen and Qiu (1997) | 5-35 | 6.0-9.0 | Biogenic $SiO_2$ |

### 3.7.2 Other $SiO_2$ polymorphs

Experimentally measured dissolution rates of amorphous $SiO_2$ have been reported over the temperature and pH range of 18 to 290 °C and 4 to 9, respectively (Rimstidt and Barnes,1980; Mazer and Walther, 1994; Van Cappellen and Qiu, 1997; Pokrovsky et al., 2006). Amorphous silica dissolution rates in the absence of rate accelerating cations were found to vary from $10^{-11.8}$ mol $m^{-2}$ $s^{-1}$ at pH 6.0 to $10^{-10.4}$ mol $m^{-2}$ $s^{-1}$ at pH 8.0. Icenhower and Dove (2000) and Loucaide et al. (2008) reported the dissolution rates of synthetic and biogenic amorphous $SiO_2$ in aqueous NaCl solutions at temperatures from 25 to 290 °C. These studies show that amorphous $SiO_2$ dissolution rates increase with increasing salinity. Notably, the addition of 0.05 M NaCl to the reactive aqueous solution was found to increase rates by up to a factor of 21 compared to rates in deionized water (Icenhower and Dove, 2000), while the apparent activation energy remains unaltered by the presence of these rate accelerating cations (Icenhower and Dove, 2000). Such observations are coherent with results from experimental studies describing quartz dissolution in the presence of NaCl (Dove and Crerar, 1990; Dove, 1994; Dove and Nix, 1997). In all cases, amorphous $SiO_2$ dissolution rates are independent of the origin of the silica and method of rate measurement (Icenhower and Dove, 2000).

**Figure 12** compares measured $SiO_2$ polymorph dissolution rates at 25 °C with corresponding rates obtained from **Eq. (7)** and parameters listed in **Table 2**. While there are sufficient measured rates to quantify relatively precisely quartz dissolution rates over wide ranges of pH and temperature, fewer dissolution rates have been published on amorphous $SiO_2$ or cristobalite. It is reasonable to assume, however, that amorphous silica and cristobalite dissolution rates follow similar trends as quartz, although the dissolution rates of quartz are ~10 times slower due to differences in surface energy and mineral structure (Icenhower and Dove, 2000). Therefore, the activation energies and reaction order of amorphous $SiO_2$ were assumed to be the same as those for quartz, while the pre-exponential factor for amorphous $SiO_2$ at acidic conditions was set to be 10 times faster than that of quartz as suggested in Icenhower and Dove (2000). Owing to the lack of available experimental data the rates of both forms of cristobalite, whose crystalline structure consists of Si-O bonds were assumed to be the same as those of quartz.

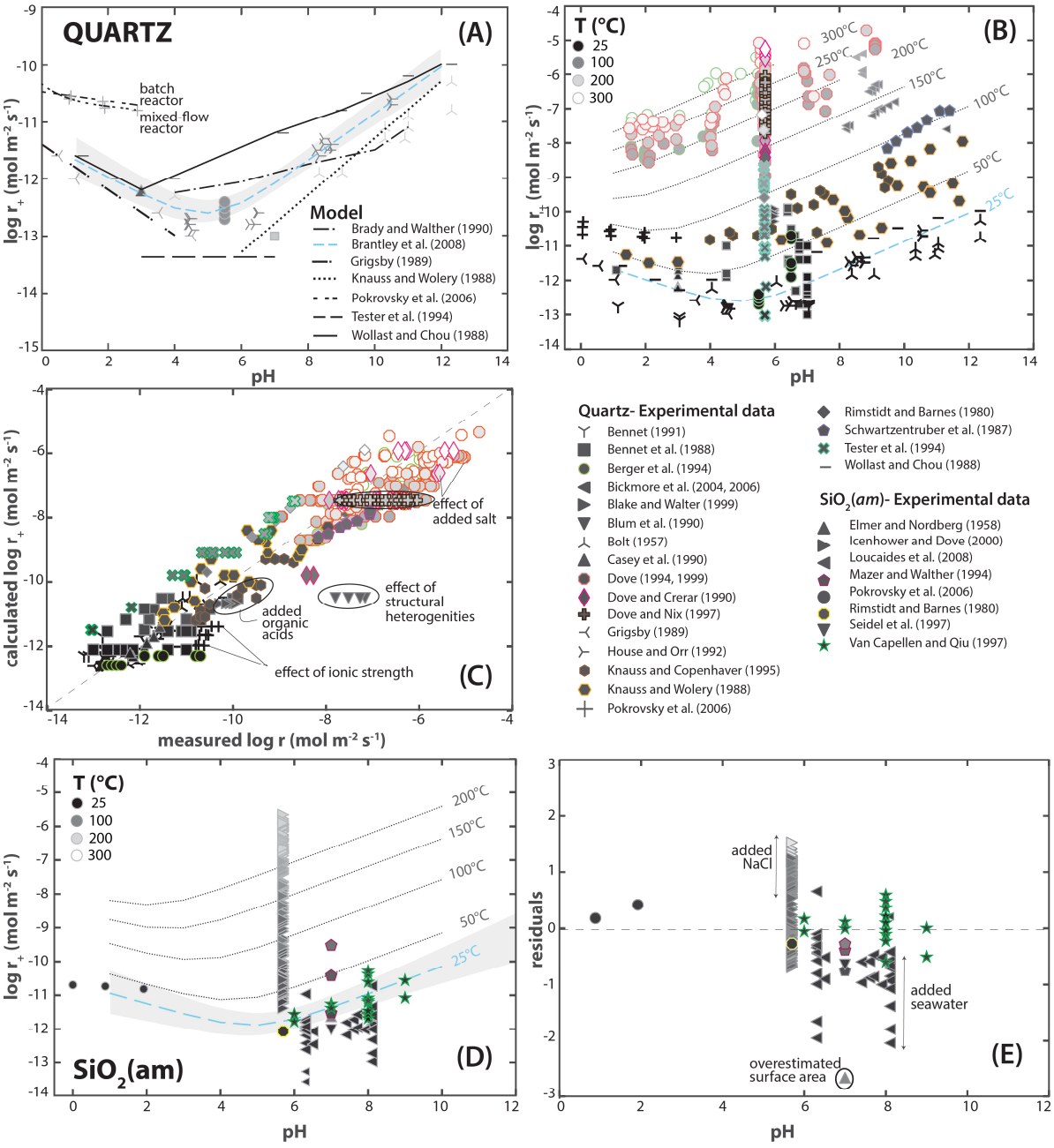


***Figure 12:*** *Far-from-equilibrium dissolution rates of $SiO_2$ polymorphs:* ***A)*** *Comparison of 25 °C quartz dissolution rates calculated with parameters regressed in this study as shown with the solid curve with previous regression equations shown in non-solid curves and measured rate data shown as symbols.* ***B-C)*** *Comparison of measured experimental quartz dissolution rates shown as symbols with rates calculated using* ***Eq. (7)*** *with parameters from* ***Table 2*** *as a function of pH at a temperature range from 25 to 300 °C.* ***D-E)*** *Comparison of measured amorphous silica dissolution rates with those calculated from* ***Eq. (7)*** *and parameters from* ***Table 2*** *as a function of pH at a temperature range from 25 to 200 °C. The symbol shape and outline color indicate the source of the data, whereas the shading of the symbol indicates the experimental temperature, where black symbols are 25 °C. The shaded regions in the plots illustrate the 95% confidence limits of the corresponding regression fits at 25 °C.*

**Figures 12 D** and **E** show calculated amorphous $SiO_2$ dissolution rates displayed as a function of temperature and pH compared with experimental data from Rimstidt and Barnes (1980), Mazer and Walther (1994), Van Cappellen and Qiu (1997), Icenhower and Dove (2000), and Pokrovsky et al.

(2006). Fifty percent of the calculated rates are within 0.27 log units of their corresponding measured rate, with an average difference of 0.30 log units.

# 4. Discussion

This article provides a compilation of experimentally measured dissolution rates and regression equations describing the dissolution rates of 27 primary silicate minerals. Rates in this study were normalized to the initial mineral-fluid interfacial surface area measured by the BET technique. As such, any application of these rates to natural systems must take into account the differences between BET surface area and that of the natural system and any changes in this surface area over time. This may depend significantly on the hydrology of the system and the effect of biotic or abiotic mineral surface coatings. The rate equations generated in this study were added into the thermodynamic database *carbfix.dat* (Voigt et al. 2018) in the form of RATE blocks. This database can thus be directly used in the PHREEQC geochemical software (**Table 2** and **Appendix B**) and can be readily adapted for other software such as TOUGHREACT. However, aqueous solubilities for some of the minerals, and notably solid solutions including andesine, bytownite, labradorite, oligoclase, ferroactinolite, riebeckite, glaucophane, augite, and bronzite are missing in the *carbfix.dat* database. This has been resolved in the version of the kinetic database for PHREEQC by calculating the saturation index of these phases by assuming the ideal mixing of appropriate endmembers.

**Table 10** provides a summary of the temperature and pH range of the experimental data considered in the regression calculations of this study. Within the temperature and pH range listed in this table, the equations and parameters presented in this study provide rates that can be considered interpolations. It seems reasonable to use the regression equations to estimate the dissolution rates of the primary silicate minerals beyond these limits, over temperatures ranging from 0 to 300 °C and pH from 1 to 12. Nevertheless, it should be kept in mind that the likely uncertainties in the rates will increase as one extrapolates rates beyond the limits of the experimental data.

What is clear when reviewing this effort to create a consistent mineral dissolution rate database is that, despite decades of experimental studies, large uncertainties remain. A typical difference between computed and measured rates is on the order of 0.5 log units. The average differences between measured and calculated rates tend to increase with the number of studies. In addition, effects on rates other than temperature and pH could be of one order of magnitude or greater. These observations suggest that there are large uncertainties when attempting to quantify the temporal evolution of any natural water-rock system. It should also not be overlooked that all rates in this study are normalized to a water-mineral interfacial surface area. This surface area may be challenging to determine unambiguously due to preferential fluid flow paths and the opening and closing of fractures in subsurface rocks. As a result, calculations made using the regression calculations reported in this study

should be considered provisional estimates until a more accurate mineral-fluid database can be developed.

**Table 10:** Summary of pH and T conditions for regressed mineral dissolution rates where data were available

| | | T (°C) | | pH range | | Quality | Comments |
|---|---|---|---|---|---|---|---|
| | | Min | max | Min | Max | of the fit* | |
| ***Amphiboles*** | | | | | | | |
| | Anthophyllite | 25 | 100 | 1 | 12 | 0.090 | |
| | Ferroactinolite | 20 | 250 | 1 | 12 | - | -due to the lack of experimental data ferroactinolite dissolution rates and kinetic parameters (*A, E, n*) are assumed to equal those of tremolite due to their similar structures and compositions |
| | Glaucophane | 25 | 25 | 2 | 12 | 0.07 | -the thermodynamics of this mineral was not included in the *carbfix.dat* database, its stability in the RATE block of the database is based on the ideal mixing of its Na-Mg endmembers |
| | Hornblende | 25 | 25 | 2 | 12 | 0.13 | -assumed mineral composition of Mg-endmember ($Ca_2(Mg_4Al)(Si_7Al)O_{22}(OH)_2$) -the thermodynamics of this mineral is not included in the *carbfix.dat* database, its stability in the RATE block of the database is based on the ideal mixing of its Ca-Mg endmembers |
| | Riebeckite | 20 | 250 | 1 | 12 | - | -due to the lack of experimental data, the dissolution rates and kinetic parameters (*A, n, E*) of this mineral were adopted from tremolite due to their similar structures and compositions -the thermodynamics of this mineral is not included in the *carbfix.dat* database, its stability in the RATE block in the database is based on the ideal mixing of its Na-Fe endmembers |
| | Tremolite | 20 | 250 | 1 | 12 | 0.28 | |
| ***Feldspars*** | | | | | | | |
| | Andesine | 5 | 300 | 1 | 12 | 0.42 | -the thermodynamics for this mineral is not included in the *carbfix.dat* database, its stability is computed in the RATE block of the database assuming ideal mixing between albite and anorthite |
| | Anorthite | 5 | 300 | 1 | 12 | 0.41 | |
| | Albite | 5 | 300 | 1 | 12 | 0.54 | |
| | Bytownite | 5 | 300 | 1 | 12 | 0.56 | -the thermodynamics for this mineral is not included in the *carbfix.dat* database, its stability is computed in the RATE block of the database assuming ideal mixing between albite and anorthite |
| | K-feldspar | 25 | 100 | 1 | 12 | 0.40 | |
| | Labradorite | 5 | 300 | 1 | 12 | 0.55 | -the thermodynamics for this mineral is not included in the *carbfix.dat* database, its stability is computed in the RATE block of the database assuming ideal mixing between albite and anorthite |
| | Oligoclase | 5 | 300 | 1 | 12 | 0.50 | -the thermodynamics for this mineral is not included in the *carbfix.dat* database, its stability is computed in the RATE block of the database assuming ideal mixing between albite and anorthite |
| | Sanidine | 25 | 100 | 1 | 12 | - | -due to the lack of experimental data the rates and kinetic parameters (*A, E, n*) are adopted from K-feldspar |
| ***Glass*** | | | | | | | |
| | Basalt | 7 | 300 | 0 | 12 | 0.44 | |
| | Rhyolite | 25 | 200 | 1 | 12 | 0.22 | |
| ***Mica*** | | | | | | | |
| | Annite | 25 | 280 | 1 | 14 | 0.35 | -no visible trend between Mg-rich and Fe-rich biotit dissolution -due to lack of data the kinetic parameters (*A, n, E*) for annite and phlogopite were set equal to those of |
| | Biotite | 25 | 280 | 1 | 14 | | |
| | Phlogopite | 25 | 280 | 1 | 14 | | |

| | | | | | | | |
|---|---|---|---|---|---|---|---|
| | | | | | | | biotite. |
| | Muscovite | 25 | 250 | 1 | 12 | 0.45 | |
| ***Olivines*** | | | | | | | |
| | Fayalite | 25 | 25 | 0 | 12 | 0.60 | -due to a lack of experimental data at pH>4.5 and temperature > 25 °C the kinetic parameters (*A, E, n*) for this mineral was set equal to those of forsterite |
| | Forsterite | 7 | 300 | 0 | 12 | 0.18 | |
| | Larnite | 25 | 25 | 0 | 12 | 0.22 | -due to a lack of experimental data at pH>4.5 and temperature > 25 °C the kinetic parameters (*A, E, n*) for this mineral was set equal to those of forsterite |
| ***Pyroxenes*** | | | | | | | |
| | Augite | 20 | 25 | 2 | 12 | 0.32 | -the thermodynamics for this mineral is not included in the *carbfix.dat* database; its stability is computed in the RATE block of the database assuming ideal mixing between pyroxene Ca-Fe-Mg endmembers |
| | Bronzite | 1 | 100 | 2 | 12 | 0.08 | -the thermodynamics of this mineral is not included in the *carbfix.dat* database; its stability is computed in the RATE block of the database assuming ideal mixing between pyroxene Ca-Fe-Mg endmembers |
| | Diopside | 25 | 50 | 2 | 12 | 0.19 | |
| | Enstatite | 25 | 100 | 2 | 12 | 0.39 | |
| ***$SiO_2$ polymorphs*** | | | | | | | |
| | Cristobalite (alpha) | 1 | 25 | 1 | 12 | - | -due to lack of experimental data, reaction orders are assumed to be the same as those of amorphous silica |
| | Cristobalite (beta) | 1 | 25 | 1 | 12 | | |
| | Quartz | 25 | 300 | 0 | 12 | 0.56 | |
| | $SiO_2$(am) | 25 | 200 | 1 | 12 | 0.27 | -due to lack of data, reaction orders and pre-exponential factors are derived based on the assumption that rates for amorphous silica are ~ ten times faster than those of quartz, as suggested in Icenhower and Dove (2000) |

***** Median of residuals in log units

# 5. Conclusions

This study is the first of at least three contributions generating a comprehensive and internally consistent database of the dissolution rates of the rock-forming minerals. It is anticipated that the resulting database, made available in the readily applied form will provide a benchmark for comparing directly the results of temporal geochemical modeling calculations performed using various reactive transport algorithms in a variety of natural and geoengineered systems. Despite these efforts, considerable uncertainties remain. At present, the ability to quantify in a consistent manner the effects of fluid ionic strength, the presence of organic and inorganic aqueous species, the biotic activity, mineral coatings, and mineral surface area in natural systems is hindered by lack of consistent observations and/or theories. Nevertheless, it is anticipated that the compilation of rates presented in these studies, together with the comparison of computational results with both laboratory experiments and field observations, will lead to the continuous improvement of our ability to describe accurately geochemical processes as a function of distance and time.

# Acknowledgments

This research has been carried out within the CarbFix2 and GECO projects that have received funding from the European Union's Horizon 2020 research and innovation program under grant agreements No 764760 and number 818169, respectively. EHO would like to dedicate this work to the memory of William M. Murphy, who was both a trusted friend and one of the pioneers in interpreting and quantifying reaction rates through his pioneering work at Prediction Central, Berkeley, California, in the 1980s.

# References

Aagaard, P., Helgeson, H.C., 1977. Thermodynamic and kinetic constraints on the dissolution of feldspars. Geol Soc Am Abstr Programs U. S. 9:7.

Aagaard, P., Helgeson, H.C., 1982. Thermodynamic and kinetic constraints on reaction rates among minerals and aqueous solutions; I, Theoretical considerations. Am. J. Sci. 282, 237–285. https://doi.org/10.2475/ajs.282.3.237

Acker, J.G., Bricker, O.P., 1992. The influence of pH on biotite dissolution and alteration kinetics at low temperature. Geochim. Cosmochim. Acta 56, 3073–3092. https://doi.org/10.1016/0016-7037(92)90290-Y

Amrhein, C., Suarez, D.L., 1988. The use of a surface complexation model to describe the kinetics of ligand-promoted dissolution of anorthite. Geochim. Cosmochim. Acta 52, 2785–2793. https://doi.org/10.1016/0016-7037(88)90146-9

Amrhein, C., Suarez, D.L., 1992. Some factors affecting the dissolution kinetics of anorthite at 25 °C. Geochim. Cosmochim. Acta 56, 1815–1826. https://doi.org/10.1016/0016-7037(92)90312-7

Bailey, A., 1974. Effects of temperature on the reaction of silicates with aqueous solutions in the low temperature range. Presented at the International Symposium on Water-Rock Interaction (1st), Praha, pp. 375–380.

Balland, C., Poszwa, A., Leyval, C., Mustin, C., 2010. Dissolution rates of phyllosilicates as a function of bacterial metabolic diversity. Geochim. Cosmochim. Acta 74, 5478–5493. https://doi.org/10.1016/j.gca.2010.06.022

Banfield, J.F., Jones, B.F., Veblen, D.R., 1991. An AEM-TEM study of weathering and diagenesis, Abert Lake, Oregon: I. Weathering reactions in the volcanics. Geochim. Cosmochim. Acta 55, 2781–2793. https://doi.org/10.1016/0016-7037(91)90444-A

Beig, M.S., Lüttge, A., 2006. Albite dissolution kinetics as a function of distance from equilibrium: Implications for natural feldspar weathering. Geochim. Cosmochim. Acta 70, 1402–1420. https://doi.org/10.1016/j.gca.2005.10.035

Bénézeth, P., Palmer, D.A., Wesolowski, D.J., 2008. Dissolution/precipitation kinetics of boehmite and gibbsite: Application of a pH-relaxation technique to study near-equilibrium rates. Geochim. Cosmochim. Acta 72, 2429–2453. https://doi.org/10.1016/j.gca.2008.02.019

Bennett, P.C., 1991. Quartz dissolution in organic-rich aqueous systems. Geochim. Cosmochim. Acta 55, 1781–1797. https://doi.org/10.1016/0016-7037(91)90023-X

Bennett, P.C., Melcer, M.E., Siegel, D.I., Hassett, J.P., 1988. The dissolution of quartz in dilute aqueous solutions of organic acids at 25 °C. Geochim. Cosmochim. Acta 52, 1521–1530. https://doi.org/10.1016/0016-7037(88)90222-0

Berg, A., Banwart, S.A., 2000. Carbon dioxide mediated dissolution of Ca-feldspar: implications for silicate weathering. Chem. Geol. 163, 25–42. https://doi.org/10.1016/S0009-2541(99)00132-1

Berger, G., Cadore, E., Schott, J., Dove, P.M., 1994. Dissolution rate of quartz in lead and sodium electrolyte solutions between 25 and 300 °C: Effect of the nature of surface complexes and reaction affinity. Geochim. Cosmochim. Acta 58, 541–551. https://doi.org/10.1016/0016-7037(94)90487-1

Berner, R.A., Holdren, G.R., 1979. Mechanism of feldspar weathering—II. Observations of feldspars from soils. Geochim. Cosmochim. Acta 43, 1173–1186. https://doi.org/10.1016/0016-7037(79)90110-8

Berner, R.A., Lasaga, A.C., Garrels, R.M., 1983. The carbonate-silicate geochemical cycle and its effect on atmospheric carbon dioxide over the past 100 million years. Am. J. Sci. 283, 641–683. https://doi.org/10.2475/ajs.283.7.641

Bertier, P., Swennen, R., Laenen, B., Lagrou, D., Dreesen, R., 2006. Experimental identification of $CO_2$–water–rock interactions caused by sequestration of $CO_2$ in Westphalian and Buntsandstein sandstones of the Campine Basin (NE-Belgium). J. Geochem. Explor., GEOFLUIDS V: 5th International Conference on Fluid Evolution, Migration and Interaction in Sedimentary Basins and Orogenic Belts 89, 10–14. https://doi.org/10.1016/j.gexplo.2005.11.005

Bevan, J., Savage, D., 1989. The effect of organic acids on the dissolution of K-feldspar under conditions relevant to burial diagenesis. Mineral. Mag. 53, 415–425. https://doi.org/10.1180/minmag.1989.053.372.02

Bickmore, B.R., Nagy, K.L., Gray, A.K., Brinkerhoff, A.R., 2006. The effect of $Al(OH)_4^-$ on the dissolution rate of quartz. Geochim. Cosmochim. Acta 70, 290–305. https://doi.org/10.1016/j.gca.2005.09.017

Bird, G., Boon, J., Stone, T., 1986. Silica transport during steam injection into oil sands: 1. Dissolution and precipitation kinetics of quartz: New results and review of existing data. Chem. Geol. 54, 69–80. https://doi.org/10.1016/0009-2541(86)90072-0

Blake, R.E., Walter, L.M., 1999. Kinetics of feldspar and quartz dissolution at 70–80 °C and near-neutral pH: Effects of organic acids and NaCl. Geochim. Cosmochim. Acta 63, 2043–2059. https://doi.org/10.1016/S0016-7037(99)00072-1

Blum, A.E., Stillings, L.L., 1995. Chapter 7. Feldspar Dissolution Kinetics, in Chemical Weathering Rates of Silicate Minerals. De Gruyter. https://doi.org/10.1515/9781501509650-009

Blum, A.E., Yund, R.A., Lasaga, A.C., 1990. The effect of dislocation density on the dissolution rate of quartz. Geochim. Cosmochim. Acta 54, 283–297. https://doi.org/10.1016/0016-7037(90)90318-F

Bolt, G., 1957. Determination of the charge density of silica sois. J. Phys. Chem. 61, 1166.

Bourcier, W., 1990. A kinetic model for borosilicate glass dissolution based on the dissolution affinity of a surface layer. Materials Research Society Symposium Proceedings 176:209-216.

Brady, P.V., 1991. The effect of silicate weathering on global temperature and atmospheric $CO_2$. J. Geophys. Res. Solid Earth 96, 18101–18106. https://doi.org/10.1029/91JB01898

Brady, P.V., Carroll, S.A., 1994. Direct effects of $CO_2$ and temperature on silicate weathering: Possible implications for climate control. Geochim. Cosmochim. Acta 58, 1853–1856. https://doi.org/10.1016/0016-7037(94)90543-6

Brady, P.V., Walther, J.V., 1989. Controls on silicate dissolution rates in neutral and basic pH solutions at 25 °C. Geochim. Cosmochim. Acta 53, 2823–2830. https://doi.org/10.1016/0016-7037(89)90160-9

Brady, P.V., Walther, J.V., 1990. Kinetics of quartz dissolution at low temperatures. Chem. Geol. 82, 253–264. https://doi.org/10.1016/0009-2541(90)90084-K

Brantley, S.L., 2003. 5.03 - Reaction Kinetics of Primary Rock-forming Minerals under Ambient Conditions, in: Holland, H.D., Turekian, K.K. (Eds.), Treatise on Geochemistry. Pergamon, Oxford, pp. 73–117. https://doi.org/10.1016/B0-08-043751-6/05075-1

Brantley, S.L., Chen, Y., 1995. Chemical weathering rates of pyroxenes and amphiboles. Rev. Mineral. Geochem. 31, 119–172.

Brantley, S., Kubicki, J., White, A. (Eds.), 2008. Kinetics of Water-Rock Interaction. Springer-Verlag, New York. https://doi.org/10.1007/978-0-387-73563-4

Bray, A., Oelkers, E., Bonneville, S.C., Wolff-Boenisch, D., Potts, N., Fones, G., Benning, L., 2015. The effect of pH, grain size, and organic ligands on biotite weathering rates. Geochim. Cosmochim. Acta 56. https://doi.org/10.1016/j.gca.2015.04.048

Brunauer, S., Emmett, P.H., Teller, E., 1938. Adsorption of Gases in Multimolecular Layers. J. Am. Chem. Soc. 60, 309–319. https://doi.org/10.1021/ja01269a023

Burch, T.E., Nagy, K.L., Lasaga, A.C., 1993. Free energy dependence of albite dissolution kinetics at 80 °C and pH 8.8. Chem. Geol., Geochemical kinetics of mineral-water reactions in the field and the laboratory 105, 137–162. https://doi.org/10.1016/0009-2541(93)90123-Z

Busenberg, E., Clemency, C.V., 1976. The dissolution kinetics of feldspars at 25 °C and 1 atm $CO_2$ partial pressure. Geochim. Cosmochim. Acta 40, 41–49. https://doi.org/10.1016/0016-7037(76)90192-7

Cabrera, F., Talibudeen, O., 1979. The Release of Aluminum from Aluminosilicate Minerals. II. Acid-Base Potentiometric Titrations. Clays Clay Miner. 27, 113–118. https://doi.org/10.1346/ccmn.1979.0270206

Carroll, S., Knauss, K., 2001. Experimental Determination of Ca-Silicate Dissolution Rates: A Source of Calcium for Geologic $CO_2$ Sequestration. DOENETL First Natl. Conf. Carbon Sequestration Wash. DC.

Carroll, S., Smith, M.M., Lammers, K., 2017. Chlorite, Biotite, Illite, Muscovite and Feldspar Dissolution Kinetics at Variable pH and Temperatures up to 280 ºC (No. 910). DOE Geothermal Data Repository; Lawrence Livermore National Lab. (LLNL), Livermore, CA (United States). https://doi.org/10.15121/1441454

Casey, W.H., Cheney, M.A., 1993. Brønsted reactions on oxide mineral surfaces and the temperature-dependence of their dissolution rates. Aquat. Sci. 55, 304–313. https://doi.org/10.1007/BF00877275

Casey, W.H., Lasaga, A.C., Gibbs, G.V., 1990. Mechanisms of silica dissolution as inferred from the kinetic isotope effect. Geochim. Cosmochim. Acta 54, 3369–3378. https://doi.org/10.1016/0016-7037(90)90291-R

Casey, W.H., Sposito, G., 1992. On the temperature dependence of mineral dissolution rates. Geochim. Cosmochim. Acta 56, 3825–3830. https://doi.org/10.1016/0016-7037(92)90173-G

Casey, W.H., Westrich, H.R., 1992. Control of dissolution rates of orthosilicate minerals by divalent metal–oxygen bonds. Nature 355, 157–159. https://doi.org/10.1038/355157a0

Casey, W.H., Westrich, H.R., Banfield, J.F., Ferruzzi, G., Arnold, G.W., 1993. Leaching and reconstruction at the surfaces of dissolving chain-silicate minerals. Nature 366, 253–256. https://doi.org/10.1038/366253a0

Casey, W.H., Westrich, H.R., Holdren, G.R., 1991. Dissolution rates of plagioclase at pH = 2 and 3. Am. Mineral. 76, 211–217.

Chadwick, O.A., Chorover, J., 2001. The chemistry of pedogenic thresholds. Geoderma, Developments and Trends in Soil Science 100, 321–353. https://doi.org/10.1016/S0016-7061(01)00027-1

Chen, Y., Brantley, S.L., 1997. Temperature- and pH-dependence of albite dissolution rate at acid pH. Chem. Geol. 135, 275–290. https://doi.org/10.1016/S0009-2541(96)00126-X

Chen, Y., Brantley, S.L., 1998. Diopside and anthophyllite dissolution at 25° and 90 °C and acid pH. Chem. Geol. 147, 233–248. https://doi.org/10.1016/S0009-2541(98)00016-3

Chen, Y., Brantley, S.L., 2000. Dissolution of forsteritic olivine at 65 °C and pH 2. Chem. Geol. 165, 267–281. https://doi.org/10.1016/S0009-2541(99)00177-1

Chou, L., Wollast, R., 1984. Study of the weathering of albite at room temperature and pressure with a fluidized bed reactor. Geochim. Cosmochim. Acta 48, 2205–2217. https://doi.org/10.1016/0016-7037(84)90217-5

Chou, L., Wollast, R., 1985. Steady-state kinetics and dissolution mechanisms of albite. Am. J. Sci. 285, 963–993. https://doi.org/10.2475/ajs.285.10.963

Clemency, C.V., Lin, F.-C., 1981. Dissolution Kinetics of Phlogopite. II. Open System Using an Ion-Exchange Resin. Clays Clay Miner. 29, 107–112. https://doi.org/10.1346/CCMN.1981.0290204

Clow, D.W., Drever, J.I., 1996. Weathering rates as a function of flow through an alpine soil. Chem. Geol., Chemical And Biological Control On Mineral Growth And Dissolution Kinetics, American Chemical Society Meeting 132, 131–141. https://doi.org/10.1016/S0009-2541(96)00048-4

Coker, E.N., Rees, L.V.C., 2005. Kinetics of ion exchange in quasi-crystalline aluminosilicate zeolite precursors. Microporous Mesoporous Mater. 84, 171–178. https://doi.org/10.1016/j.micromeso.2005.05.028

Colella, C., 1996. Ion exchange equilibria in zeolite minerals. Miner. Deposita 31, 554–562. https://doi.org/10.1007/BF00196136

Colman, S.M., 1982. Chemical weathering of basalts and andesites; evidence from weathering rinds (No. 1246), Professional Paper. U.S. G.P.O.,. https://doi.org/10.3133/pp1246
Critelli, T., Marini, L., Schott, J., Mavromatis, V., Apollaro, C., Rinder, T., De Rosa, R., Oelkers, E.H., 2014. Dissolution rates of actinolite and chlorite from a whole-rock experimental study of metabasalt dissolution from 2≤pH≤12 at 25 °C. Chem. Geol. 390, 100–108. https://doi.org/10.1016/j.chemgeo.2014.10.013
Crooks, J.E., El-Daly, H., El-Sheikh, M.Y., Habib, A.-F.M., Zaki, A.B., 1993. Kinetics of ion-exchange on montmorillonite clays. Int. J. Chem. Kinet. 25, 161–168. https://doi.org/10.1002/kin.550250304
Crovisier, J.L., Advocat, T., Petit, J.C., Fritz, B., 1988. Alteration of Basaltic Glass in Iceland as a Natural Analogue for Nuclear Waste Glasses: Geochemical Modelling with DISSOL. MRS Online Proc. Libr. Arch. 127. https://doi.org/10.1557/PROC-127-57
Crovisier, J.L., Honnorez, J., Eberhart, J.P., 1987. Dissolution of basaltic glass in seawater: Mechanism and rate. Geochim. Cosmochim. Acta 51, 2977–2990. https://doi.org/10.1016/0016-7037(87)90371-1
Crundwell, F.K., 2014. The mechanism of dissolution of forsterite, olivine and minerals of the orthosilicate group. Hydrometallurgy 150, 68–82. https://doi.org/10.1016/j.hydromet.2014.09.006
Crundwell, F.K., 2015. The mechanism of dissolution of the feldspars: Part I. Dissolution at conditions far from equilibrium. Hydrometallurgy 151, 151–162. https://doi.org/10.1016/j.hydromet.2014.10.006
Daux, V., Guy, C., Advocat, T., Crovisier, J.-L., Stille, P., 1997. Kinetic aspects of basaltic glass dissolution at 90 °C: role of aqueous silicon and aluminium. Chem. Geol. 142, 109–126. https://doi.org/10.1016/S0009-2541(97)00079-X
Daval, D., Hellmann, R., Corvisier, J., Tisserand, D., Martinez, I., Guyot, F., 2010. Dissolution kinetics of diopside as a function of solution saturation state: Macroscopic measurements and implications for modeling of geological storage of $CO_2$. Geochim. Cosmochim. Acta 74, 2615–2633. https://doi.org/10.1016/j.gca.2010.02.003
Declercq, J., Diedrich, T., Perrot, M., Gislason, S.R., Oelkers, E.H., 2013. Experimental determination of rhyolitic glass dissolution rates at 40–200 °C and 2. Geochim. Cosmochim. Acta 100, 251–263. https://doi.org/10.1016/j.gca.2012.10.006
Dehouck, E., Gaudin, A., Mangold, N., Lajaunie, L., Dauzères, A., Grauby, O., Le Menn, E., 2014. Weathering of olivine under $CO_2$ atmosphere: A martian perspective. Geochim. Cosmochim. Acta 135, 170–189. https://doi.org/10.1016/j.gca.2014.03.032
De Yoreo, J. J., Vekilov, P.G., 2003. Principles of crystal nucleation and growth. Rev. Min. Geochem. 54, 57-93.
Diedrich, T., Schott, J., Oelkers, E.H., 2014. An experimental study of tremolite dissolution rates as a function of pH and temperature: Implications for tremolite toxicity and its use in carbon storage. Mineral. Mag. 78, 1449–1464. https://doi.org/10.1180/minmag.2014.078.6.12
Dove, P.M., 1994. The dissolution kinetics of quartz in sodium chloride solutions at 25 degrees to 300 degrees C. Am. J. Sci. 294, 665–712. https://doi.org/10.2475/ajs.294.6.665
Dove, P.M., 1999. The dissolution kinetics of quartz in aqueous mixed cation solutions. Geochim. Cosmochim. Acta 63, 3715–3727. https://doi.org/10.1016/S0016-7037(99)00218-5
Dove, P.M., Crerar, D.A., 1990. Kinetics of quartz dissolution in electrolyte solutions using a hydrothermal mixed flow reactor. Geochim. Cosmochim. Acta 54, 955–969. https://doi.org/10.1016/0016-7037(90)90431-J
Dove, P.M., Nix, C.J., 1997. The influence of the alkaline earth cations, magnesium, calcium, and barium on the dissolution kinetics of quartz. Geochim. Cosmochim. Acta 61, 3329–3340. https://doi.org/10.1016/S0016-7037(97)00217-2
Drever, J.I., 1988. The geochemistry of natural waters, 2nd ed. ed. Prentice Hall, Englewood Cliffs, N.J.
Drummond, D., De Jonge, A., Rees, L.V.C., 1983. Ion-exchange kinetics in zeolite A. J. Phys. Chem. 87, 1967–1971. https://doi.org/10.1021/j100234a027
Dyer, A., 2007. Chapter 16 - Ion-Exchange Properties of Zeolites and Related Materials, in: Čejka, J., van Bekkum, H., Corma, A., Schüth, F. (Eds.), Studies in Surface Science and Catalysis,

Introduction to Zeolite Science and Practice. Elsevier, pp. 525–553. https://doi.org/10.1016/S0167-2991(07)80804-4
Eggleston, C.M., Hochella, M.F., George, P.A., 1989. Sample preparation and aging effects on the dissolution rate and surface composition of diopside. Geochim. Cosmochim. Acta 53, 797–804. https://doi.org/10.1016/0016-7037(89)90026-4
Eggleton, R.A., 1987. Weathering of Basalt: Changes in Rock Chemistry and Mineralogy. Clays Clay Miner. 35, 161–169. https://doi.org/10.1346/CCMN.1987.0350301
Elmer, T.H., Nordberg, M.E., 1958. Solubility of Silica in Nitric Acid Solutions. J. Am. Ceram. Soc. 41, 517–520. https://doi.org/10.1111/j.1151-2916.1958.tb12907.x
Ferruzzi, G., 1993. The character and rates of dissolution of pyroxenes and pyroxenoids. University of California, Davis.
Fleer, V.N., 1982. Dissolution kinetics of anorthite ($CaAl_2Si_2O_8$) and synthetic strontium feldspar ($SrAl_2Si_2O_8$) in aqueous solutions at temperatures below 1000 ºC: with applications to the geological disposal of radioactive nuclear wastes. Pennsylvania State University, United States.
Furrer, G., Stumm, W., 1986. The coordination chemistry of weathering: I. Dissolution kinetics of δ-Al2O3 and BeO. Geochim. Cosmochim. Acta 50, 1847–1860. https://doi.org/10.1016/0016-7037(86)90243-7
Ganor, J., Reznik, I.J., Rosenberg, Y.O., 2009. Organics in Water-Rock Interactions. Rev. Mineral. Geochem. 70, 259–369. https://doi.org/10.2138/rmg.2009.70.7
Gautier, J.-M., Oelkers, E.H., Schott, J., 1994. Experimental study of K-feldspar dissolution rates as a function of chemical affinity at 150 °C and pH 9. Geochim. Cosmochim. Acta 58, 4549–4560. https://doi.org/10.1016/0016-7037(94)90190-2
Gautier, J.-M., Oelkers, E.H., Schott, J., 2001. Are quartz dissolution rates proportional to BET surface areas? Geochim. Cosmochim. Acta 65, 1059-1070.
Gislason, S.R., Arnorsson, S., Armannsson, H., 1996. Chemical weathering of basalt in Southwest Iceland; effects of runoff, age of rocks and vegetative/glacial cover. Am. J. Sci. 296, 837–907. https://doi.org/10.2475/ajs.296.8.837
Gislason, S.R., Eugster, H.P., 1987. Meteoric water-basalt interactions. II: A field study in N.E. Iceland. Geochim. Cosmochim. Acta 51, 2841–2855. https://doi.org/10.1016/0016-7037(87)90162-1
Gislason, S.R., Oelkers, E.H., 2003. Mechanism, rates, and consequences of basaltic glass dissolution: II. An experimental study of the dissolution rates of basaltic glass as a function of pH and temperature. Geochim. Cosmochim. Acta 67, 3817–3832. https://doi.org/10.1016/S0016-7037(03)00176-5
Gislason, S.R., Wolff-Boenisch, D., Stefansson, A., Oelkers, E.H., Gunnlaugsson, E., Sigurdardottir, H., Sigfusson, B., Broecker, W.S., Matter, J.M., Stute, M., 2010. Mineral sequestration of carbon dioxide in basalt: A pre-injection overview of the CarbFix project. Int. J. Greenh. Gas Control 4, 537–545. https://doi.org/10.1016/j.ijggc.2009.11.013
Goldberg, D.S., Takahashi, T., Slagle, A.L., 2008. Carbon dioxide sequestration in deep-sea basalt. Proc. Natl. Acad. Sci. 105, 9920–9925. https://doi.org/10.1073/pnas.0804397105
Golubev, S.V., Pokrovsky, O.S., Schott, J., 2005. Experimental determination of the effect of dissolved $CO_2$ on the dissolution kinetics of Mg and Ca silicates at 25 °C. Chem. Geol., Geochemical Aspects of $CO_2$ sequestering 217, 227–238. https://doi.org/10.1016/j.chemgeo.2004.12.011
Gordon, S.J., Brady, P.V., 2002. In situ determination of long-term basaltic glass dissolution in the unsaturated zone. Chem. Geol., Geochemistry of Crustal Fluids-Fluids in the Crust and Chemical Fluxes at the Earth's Surface 190, 113–122. https://doi.org/10.1016/S0009-2541(02)00113-4
Grandstaff, D.E., 1977. Some kinetics of bronzite orthopyroxene dissolution. Geochim. Cosmochim. Acta 41, 1097–1103. https://doi.org/10.1016/0016-7037(77)90104-1
Grandstaff, D.E., 1986. The dissolution rate of forsteritic olivine from Hawaiian beach sand., in: Rates of Chemical Weathering of Rocks and Minerals,. Academic Press, Orlando, Florida, pp. 41–59.

1410 Grigsby, C.O., 1989. Kinetics of rock-water reactions. Chemical Engineering Department,
1411 Massachusetts Institute of Technology, Cambridge, MA.
1412 Gudbrandsson, S., Wolff-Boenisch, D., Gislason, S.R., Oelkers, E.H., 2014. Experimental
1413 determination of plagioclase dissolution rates as a function of its composition and pH at 22 °C.
1414 Geochim. Cosmochim. Acta 139, 154–172. https://doi.org/10.1016/j.gca.2014.04.028
1415 Guy, C., 1989. Mechanimes de dissolution des solides dans les solutions hydrothermales deduits du
1416 comportement des verres basaltiques et de calcites deformees. Universite Paul Sabatier,
1417 Toulouse, France.
1418 Guyot, F., Daval, D., Dupraz, S., Martinez, I., Ménez, B., Sissmann, O., 2011. $CO_2$ geological storage:
1419 The environmental mineralogy perspective. Comptes Rendus Geosci. 343, 246–259.
1420 https://doi.org/10.1016/j.crte.2010.12.007
1421 Halder, S., Walther, J.V., 2011. Far from equilibrium enstatite dissolution rates in alkaline solutions at
1422 earth surface conditions. Geochim. Cosmochim. Acta 75, 7486–7493.
1423 https://doi.org/10.1016/j.gca.2011.09.013
1424 Hänchen, M., Prigiobbe, V., Storti, G., Seward, T.M., Mazzotti, M., 2006. Dissolution kinetics of
1425 fosteritic olivine at 90-150 °C including effects of the presence of $CO_2$. Geochim.
1426 Cosmochim. Acta 70, 4403–4416. https://doi.org/10.1016/j.gca.2006.06.1560
1427 Hausrath, E.M., Brantley, S.L., 2010. Basalt and olivine dissolution under cold, salty, and acidic
1428 conditions: What can we learn about recent aqueous weathering on Mars? J. Geophys. Res.
1429 Planets 115. https://doi.org/10.1029/2010JE003610
1430 Hausrath, E. M., Treiman, A. h., Vicenzi, E., Bish, D. l., Blake, D., Sarrazin, P., Hoehler, T.,
1431 Midtkandal, I., Steele, A., Brantley, S. l., 2008. Short- and Long-Term Olivine Weathering in
1432 Svalbard: Implications for Mars. Astrobiology 8, 1079–1092.
1433 https://doi.org/10.1089/ast.2007.0195
1434 Helgeson, H.C., Murphy, W.M., Aagaard, P., 1984. Thermodynamic and kinetic constraints on
1435 reaction rates among minerals and aqueous solutions. II. Rate constants, effective surface area,
1436 and the hydrolysis of feldspar. Geochim. Cosmochim. Acta 48, 2405–2432.
1437 https://doi.org/10.1016/0016-7037(84)90294-1
1438 Hellmann, R., 1994. The albite-water system: Part I. The kinetics of dissolution as a function of pH at
1439 100, 200 and 300 °C. Geochim. Cosmochim. Acta 58, 595–611. https://doi.org/10.1016/0016-
1440 7037(94)90491-X
1441 Hellmann, R., Eggleston, C., Hochella, M., Crerar, D.A., 1989. Altered layers on dissolving albite.
1442 Part 1. Results. Water-Rock Interact. 293–296.
1443 Hellmann, R., Tisserand, D., 2006. Dissolution kinetics as a function of the Gibbs free energy of
1444 reaction: An experimental study based on albite feldspar. Geochim. Cosmochim. Acta 70,
1445 364–383. https://doi.org/10.1016/j.gca.2005.10.007
1446 Hoch, A.R., Reddy, M.M., Drever, J.I., 1996. The effect of iron content and dissolved $O_2$ on
1447 dissolution rates of clinopyroxene at pH 5.8 and 25 °C: Preliminary results. Chem. Geol.,
1448 Chemical And Biological Control On Mineral Growth And Dissolution Kinetics, American
1449 Chemical Society Meeting 132, 151–156. https://doi.org/10.1016/S0009-2541(96)00050-2
1450 Hodson, M.E., 2003. The influence of Fe-rich coatings on the dissolution of anorthite at pH 2.6.
1451 Geochim. Cosmochim. Acta 67, 3355–3363. https://doi.org/10.1016/S0016-7037(02)01370-4
1452 Holdren, G.R., Speyer, P.M., 1985. Reaction rate-surface area relationships during the early stages of
1453 weathering I. Initial observations. Geochim. Cosmochim. Acta 49, 675-681.
1454 Holdren, G.R., Speyer, P.M., 1987. Reaction rate-surface area relationships during the early stages of
1455 weathering. II. Data on eight additional feldspars. Geochim. Cosmochim. Acta 51, 2311–
1456 2318. https://doi.org/10.1016/0016-7037(87)90284-5
1457 House, W.A., Orr, D.R., 1992. Investigation of the pH dependence of the kinetics of quartz dissolution
1458 at 25 °C. J. Chem. Soc. Faraday Trans. 88, 233–241. https://doi.org/10.1039/FT9928800233
1459 Hurd, D.C., 1973. Interactions of biogenic opal, sediment and seawater in the Central Equatorial
1460 Pacific. Geochim. Cosmochim. Acta 37, 2257–2282. https://doi.org/10.1016/0016-
1461 7037(73)90103-8
1462 Hurd, D.C., Fraley, C., Fugate, J.K., 1979. Silica Apparent Solubilities and Rates of Dissolution and
1463 Precipitation, in: Chemical Modeling in Aqueous Systems, ACS Symposium Series. American
1464 Chemical Society, pp. 413–445. https://doi.org/10.1021/bk-1979-0093.ch021

Icenhower, J.P., Dove, P.M., 2000. The dissolution kinetics of amorphous silica into sodium chloride solutions: effects of temperature and ionic strength. Geochim. Cosmochim. Acta 64, 4193–4203. https://doi.org/10.1016/S0016-7037(00)00487-7

Jantzen, C.M., Plodinec, M.J., 1984. Thermodynamic model of natural, medieval and nuclear waste glass durability. J. Non-Cryst. Solids, Proceedings of the International Conference on Glass in Planetary and Geological Phenomena 67, 207–223. https://doi.org/10.1016/0022-3093(84)90151-0

Jercinovic, M.J., Kaser, S.A., Ewing, R.C., Lutze, W., 1990. Comparison of surface layers formed on synthetic basaltic glass, French R7T7 and HMI borosilicate nuclear waste form glasses - Materials Interface Interactions Tests, Waste Isolation Pilot Plant. Sci. Basis Nucl. Waste Manag. 13.

Jonckbloedt, R.C.L., 1998. Olivine dissolution in sulphuric acid at elevated temperatures—implications for the olivine process, an alternative waste acid neutralizing process. J. Geochem. Explor. 62, 337–346. https://doi.org/10.1016/S0375-6742(98)00002-8

Kalinowski, B.E., Schweda, P., 1996. Kinetics of muscovite, phlogopite, and biotite dissolution and alteration at pH 1-4, room temperature. Geochim. Cosmochim. Acta 60, 367–385. https://doi.org/10.1016/0016-7037(95)00411-4

Kamiya, H., Ozaki, A., Imahashi, M., 1974. Dissolution rate of powdered quartz in acid solution. Geochem. J. 8, 21–26. https://doi.org/10.2343/geochemj.8.21

Kamiya, H., Shimokata, K., 1974. The role of the salts in the dissolution of powdered quartz., in: International Symposium on Water-Rock Interaction. Czechoslovakia, pp. 426–429.

Kampman, N., Bickle, M., Becker, J., Assayag, N., Chapman, H., 2009. Feldspar dissolution kinetics and Gibbs free energy dependence in a CO2-enriched groundwater system, Green River, Utah. Earth Planet. Sci. Lett. 284, 473–488. https://doi.org/10.1016/j.epsl.2009.05.013

Karkhanis, S.N., Bancroft, G.M., Fyfe, W.S., Brown, J.D., 1980. Leaching behaviour of rhyolite glass. Nature 284, 435–437. https://doi.org/10.1038/284435a0

Kenoyer, G.J., Bowser, C.J., 1992. Groundwater chemical evolution in a sandy silicate aquifer in northern Wisconsin: 2. Reaction modeling. Water Resour. Res. 28, 591–600. https://doi.org/10.1029/91WR02303

King, H.E., Plümper, O., Putnis, A., 2010. Effect of Secondary Phase Formation on the Carbonation of Olivine. Environ. Sci. Technol. 44, 6503–6509. https://doi.org/10.1021/es9038193

Knauss, K.G., Copenhaver, S.A., 1995. The effect of malonate on the dissolution kinetics of albite, quartz, and microcline as a function of pH at 70 °C. Appl. Geochem. 10, 17–33. https://doi.org/10.1016/0883-2927(94)00045-8

Knauss, K.G., Nguyen, S.N., Weed, H.C., 1993. Diopside dissolution kinetics as a function of pH, $CO_2$, temperature, and time. Geochim. Cosmochim. Acta 57, 285–294. https://doi.org/10.1016/0016-7037(93)90431-U

Knauss, K.G., Wolery, T.J., 1986. Dependence of albite dissolution kinetics on pH and time at 25 °C and 70 °C. Geochim. Cosmochim. Acta 50, 2481–2497. https://doi.org/10.1016/0016-7037(86)90031-1

Knauss, K.G., Wolery, T.J., 1988. The dissolution kinetics of quartz as a function of pH and time at 70 °C. Geochim. Cosmochim. Acta 52, 43–53. https://doi.org/10.1016/0016-7037(88)90055-5

Knauss, K.G., Wolery, T.J., 1989. Muscovite dissolution kinetics as a function of pH and time at 70 °C. Geochim. Cosmochim. Acta 53, 1493–1501. https://doi.org/10.1016/0016-7037(89)90232-9

Köhler, S.J., Bosbach, D., Oelkers, E.H., 2005. Do clay mineral dissolution rates reach steady state? Geochim. Cosmochim. Acta 69, 1997–2006.

Köhler, P., Abrams, J.F., Völker, C., Hauck, J., Wolf-Gladrow, D.A., 2013. Geoengineering impact of open ocean dissolution of olivine on atmospheric $CO_2$ , surface ocean pH and marine biology. Environ. Res. Lett. 8, 014009. https://doi.org/10.1088/1748-9326/8/1/014009

Kump, L.R., Brantley, S.L., Arthur, M.A., 2000. Chemical Weathering, Atmospheric $CO_2$, and Climate. Annu. Rev. Earth Planet. Sci. 28, 611–667. https://doi.org/10.1146/annurev.earth.28.1.611

Lagache, M., 1965. Contribution à l'étude de l'altération des feldspaths, dans l'eau entre 100 et 200° C, sous diverses pressions de $CO_2$ et application à la synthèse des minéraux argileux. Bull. Minéralogie 88, 223–253. https://doi.org/10.3406/bulmi.1965.5840

Lammers, K., Smith, M.M., Carroll, S.A., 2017. Muscovite dissolution kinetics as a function of pH at elevated temperature. Chem. Geol. 466, 149–158. https://doi.org/10.1016/j.chemgeo.2017.06.003

Lasaga, A.C., 1981. Rate laws of chemical reactions. Rev Miner. U. S. 8.

Lasaga, A.C., Soler, J.M., Ganor, J., Burch, T.E., Nagy, K.L., 1994. Chemical weathering rate laws and global geochemical cycles. Geochim. Cosmochim. Acta 58, 2361–2386. https://doi.org/10.1016/0016-7037(94)90016-7

Li, Z., Guo, J., Dong, Z., Chen, J., 2018. Insight into interactions of olivine-sc$CO_2$-water system at 140 °C and 15 MPa during $CO_2$ mineral sequestration. Geosci. Front., Reliability Analysis of Geotechnical Infrastructures 9, 1945–1955. https://doi.org/10.1016/j.gsf.2017.12.008

Lichtner, P. C., 2016. Kinetic rate laws invariant to scaling the mineral formula unit. Am. J. Sci., 316, 437-469.

Lier, J.A.V., Bruyn, P.L.D., Overbeek, J.Th.G., 1960. The Solubility of Quartz. J. Phys. Chem. 64, 1675–1682. https://doi.org/10.1021/j100840a017

Lin, F.-C., Clemency, C.V., 1981. Dissolution Kinetics of Phlogopite. I. Closed System. Clays Clay Miner. 29, 101–106. https://doi.org/10.1346/CCMN.1981.0290203

Loucaide, S., Cappelle, P.V., Behrends, T., 2008. Dissolution of biogenic silica from land to ocean: Role of salinity and pH. Limnol. Oceanogr. 53, 1614–1621. https://doi.org/10.4319/lo.2008.53.4.1614

Lu, P., Fu, Q., Seyfried, W.E., Hedges, S.W., Soong, Y., Jones, K., Zhu, C., 2013. Coupled alkali feldspar dissolution and secondary mineral precipitation in batch systems – 2: New experiments with supercritical $CO_2$ and implications for carbon sequestration. Appl. Geochem., Geochemical Aspects of Geologic Carbon Storage 30, 75–90. https://doi.org/10.1016/j.apgeochem.2012.04.005

Luce, R.W., Bartlett, R.W., Parks, G.A., 1972. Dissolution kinetics of magnesium silicates. Geochim. Cosmochim. Acta 36, 35–50. https://doi.org/10.1016/0016-7037(72)90119-6

Maher, K., Steefel, C.I., White, A.F., Stonestrom, D.A., 2009. The role of reaction affinity and secondary minerals in regulating chemical weathering rates at the Santa Cruz Soil Chronosequence, California. Geochim. Cosmochim. Acta 73, 2804–2831. https://doi.org/10.1016/j.gca.2009.01.030

Malmström, M., Banwart, S., 1997. Biotite dissolution at 25 °C: The pH dependence of dissolution rate and stoichiometry. Geochim. Cosmochim. Acta 61, 2779–2799. https://doi.org/10.1016/S0016-7037(97)00093-8

Malmström, M., Banwart, S., Duro, L., Wersin, P., Bruno, J., 1995. Biotite and chlorite weathering at 25 degrees C: the dependence of pH and (bi)carbonate on weathering kinetics, dissolution stoichiometry, and solubility; and the relation to redox conditions in granitic aquifers (No. 0284–3757). Sweden.

Malmström, M., Banwart, S., Lewenhagen, J., Duro, L., Bruno, J., 1996. The dissolution of biotite and chlorite at 25 °C in the near-neutral pH region. J. Contam. Hydrol., Migration 93 21, 201–213. https://doi.org/10.1016/0169-7722(95)00047-X

Malow, G., Lutze, W., Ewing, R.C., 1984. Alteration effects and leach rates of basaltic glasses: Implications for the long-term stability of nuclear waste form borosilicate glasses. J. Non-Cryst. Solids, Proceedings of the International Conference on Glass in Planetary and Geological Phenomena 67, 305–321. https://doi.org/10.1016/0022-3093(84)90156-X

Manley, E.P., Evans, L.J., 1986. Dissolution of feldspars by low molecular-weight aliphatic and aromatic acids. Soil Sci. 141, 106–112.

Marini, L., 2007. Geological Sequestration of Carbon Dioxide: Thermodynamics, Kinetics, and Reaction Path Modeling, Developments in Geochemistry. Elsevier Science.

Mast, A., M., Drever, J.I., 1987. The effect of oxalate on the dissolution rates of oligoclase and tremolite. Geochim. Cosmochim. Acta 51, 2559–2568. https://doi.org/10.1016/0016-7037(87)90306-1

Matter, J.M., Kelemen, P.B., 2009. Permanent storage of carbon dioxide in geological reservoirs by mineral carbonation. Nat. Geosci. 2, 837–841. https://doi.org/10.1038/ngeo683

Matter, J.M., Stute, M., Snæbjörnsdottir, S.Ó., Oelkers, E.H., Gislason, S.R., Aradottir, E.S., Sigfusson, B., Gunnarsson, I., Sigurdardottir, H., Gunnlaugsson, E., Axelsson, G., Alfredsson, H.A., Wolff-Boenisch, D., Mesfin, K., Taya, D.F. de la R., Hall, J., Dideriksen, K., Broecker, W.S., 2016. Rapid carbon mineralization for permanent disposal of anthropogenic carbon dioxide emissions. Science 352, 1312–1314. https://doi.org/10.1126/science.aad8132

Matter, J.M., Takahashi, T., Goldberg, D., 2007. Experimental evaluation of in situ $CO_2$-water-rock reactions during $CO_2$ injection in basaltic rocks: Implications for geological $CO_2$ sequestration. Geochem. Geophys. Geosystems 8. https://doi.org/10.1029/2006GC001427

Mazer, J.J., Walther, J.V., 1994. Dissolution kinetics of silica glass as a function of pH between 40 and 85 °C. J. Non-Cryst. Solids 170, 32–45. https://doi.org/10.1016/0022-3093(94)90100-7

McGrail, B.P., Schaef, H.T., Ho, A.M., Chien, Y.-J., Dooley, J.J., Davidson, C.L., 2006. Potential for carbon dioxide sequestration in flood basalts. J. Geophys. Res. Solid Earth 111. https://doi.org/10.1029/2005JB004169

Morgenstein, M.E., Shettel, D.L., 1993. Volcanic Glass as a Natural Analog for Borosilicate Waste Glass. MRS Online Proc. Libr. Arch. 333. https://doi.org/10.1557/PROC-333-605

Murphy, S.F., Brantley, S.L., Blum, A.E., White, A.F., Dong, H., 1998. Chemical Weathering in a Tropical Watershed, Luquillo Mountains, Puerto Rico: II. Rate and Mechanism of Biotite Weathering. Geochim. Cosmochim. Acta 62, 227–243. https://doi.org/10.1016/S0016-7037(97)00336-0

Murphy, W.M., Helgeson, H.C., 1987. Thermodynamic and kinetic constraints on reaction rates among minerals and aqueous solutions. III. Activated complexes and the pH-dependence of the rates of feldspar, pyroxene, wollastonite, and olivine hydrolysis. Geochim. Cosmochim. Acta 51, 3137–3153. https://doi.org/10.1016/0016-7037(87)90124-4

Murphy, W.M., Helgeson, H.C., 1989. Thermodynamic and kinetic constraints on reaction rates among minerals and aqueous solutions; IV, Retrieval of rate constants and activation parameters for the hydrolysis of pyroxene, wollastonite, olivine, andalusite, quartz, and nepheline. Am. J. Sci. 289, 17–101. https://doi.org/10.2475/ajs.289.1.17

Nagy, K.L., 1995. Dissolution and precipitation kinetics of sheet silicates. Rev. Mineral. Geochem. 31, 173–233.

Nesbitt, H.W., Wilson, R.E., 1992. Recent chemical weathering of basalts. Am. J. Sci. 292, 740–777. https://doi.org/10.2475/ajs.292.10.740

Nickel, E., 1973. Experimental dissolution of light and heavy minerals in comparison with weathering and intrastratal solution. Contrib. Sedimentol. 1, 1–68.

Niibori, Y., Kunita, M., Tochiyama, O., Chida, T., 2000. Dissolution Rates of Amorphous Silica in Highly Alkaline Solution. J. Nucl. Sci. Technol. 37, 349–357. https://doi.org/10.1080/18811248.2000.9714905

Niles, P.B., Michalski, J., Ming, D.W., Golden, D.C., 2017. Elevated olivine weathering rates and sulfate formation at cryogenic temperatures on Mars. Nat. Commun. 8, 998. https://doi.org/10.1038/s41467-017-01227-7

Oelkers, E.H., 2001a. General kinetic description of multioxide silicate mineral and glass dissolution. Geochim. Cosmochim. Acta 65, 3703–3719. https://doi.org/10.1016/S0016-7037(01)00710-4

Oelkers, E.H., 2001a. An experimental study of forsterite dissolution rate as a function of temperature band aqueous Mg and Si concentration. Chem. Geol. 148, 485–494.

Oelkers, E.H., Schott, J., 2001. An experimental study of enstatite dissolution rates as a function of pH, temperature, and aqueous Mg and Si concentration, and the mechanism of pyroxene/pyroxenoid dissolution. Geochim. Cosmochim. Acta 65, 1219–1231. https://doi.org/10.1016/S0016-7037(00)00564-0

Oelkers, E.H., Cole, D.R., 2008. Carbon Dioxide Sequestration A Solution to a Global Problem. Elements 4, 305–310. https://doi.org/10.2113/gselements.4.5.305

Oelkers, E.H., Declercq, J., Saldi, G.D., Gislason, S.R., Schott, J., 2018. Olivine dissolution rates: A critical review. Chem. Geol. 500, 1–19. https://doi.org/10.1016/j.chemgeo.2018.10.008

Oelkers, E.H., Gislason, S.R., 2001. The mechanism, rates and consequences of basaltic glass dissolution: I. An experimental study of the dissolution rates of basaltic glass as a function of aqueous Al, Si and oxalic acid concentration at 25 °C and pH = 3 and 11. Geochim. Cosmochim. Acta 65, 3671–3681. https://doi.org/10.1016/S0016-7037(01)00664-0

Oelkers, E.H., Golubev, S.V., Chairat, C., Pokrovsky, O.S., Schott, J., 2009. The surface chemistry of multi-oxide silicates. Geochim. Cosmochim. Acta 73, 4617–4634. https://doi.org/10.1016/j.gca.2009.05.028

Oelkers, E.H., Schott, J., 1995. Experimental study of anorthite dissolution and the relative mechanism of feldspar hydrolysis. Geochim. Cosmochim. Acta 59, 5039–5053. https://doi.org/10.1016/0016-7037(95)00326-6

Oelkers, E.H., Schott, J., 1998. Does organic acid adsorption affect alkali-feldspar dissolution rates? Chem. Geol. 151, 235–245. https://doi.org/10.1016/S0009-2541(98)00082-5

Oelkers, E.H., Schott, J., 1999. Experimental study of kyanite dissolution rates as a function of chemical affinity and solution composition. Geochim. Cosmochim. Acta 63, 785–797. https://doi.org/10.1016/S0016-7037(98)00294-

Oelkers, E.H., Schott, J., 2005. Geochemical aspects of $CO_2$ sequestration. Chem. Geol., Geochemical Aspects of $CO_2$ sequestering 217, 183–186. https://doi.org/10.1016/j.chemgeo.2004.12.006

Oelkers, E.H., Schott, J., Devidal, J.-L., 1994. The effect of aluminum, pH, and chemical affinity on the rates of aluminosilicate dissolution reactions. Geochim. Cosmochim. Acta 58, 2011–2024. https://doi.org/10.1016/0016-7037(94)90281-X

Oelkers, E.H., Schott, J., Devidal, J.-L., 2001. On the interpretation of closed system mineral dissolution experiments: Comment on "Mechanism of kaolinite dissolution at room temperature and pressure Part II: Kinetic study" by Hurtas et al., (1999). Geochim. Cosmochim. Acta 65, 4429-2232.

Oelkers, E.H., Schott, J., Gauthier, J.-M., Herrero-Roncal, T., 2008. An experimental study of the dissolution mechanism and rates of muscovite. Geochim. Cosmochim. Acta 72, 4948–4961. https://doi.org/10.1016/j.gca.2008.01.040

Olsen, A.A., 2007. Forsterite Dissolution Kinetics: Applications and Implications for Chemical Weathering. Virginia Polytechnic Institute and State University, Blacksburg, Virginia, United States.

Olsen, A.A., Hausrath, E.M., Rimstidt, J.D., 2015. Forsterite dissolution rates in Mg-sulfate-rich Mars-analog brines and implications of the aqueous history of Mars. J. Geophys. Res. Planets 120, 388–400. https://doi.org/10.1002/2014JE004664

Olsen, A.A., Rimstidt, D.J., 2008. Oxalate-promoted forsterite dissolution at low pH. Geochim. Cosmochim. Acta 72, 1758–1766. https://doi.org/10.1016/j.gca.2007.12.026

Oxburgh, R., Drever, J.I., Sun, Y.-T., 1994. Mechanism of plagioclase dissolution in acid solution at 25 °C. Geochim. Cosmochim. Acta 58, 661–669. https://doi.org/10.1016/0016-7037(94)90496-0

Palandri, J., Kharaka, Y., 2004. A Compilation of Rate Parameters of Water-Mineral Interaction Kinetics for Application to Geochemical Modeling 1068, 71.

Parkhurst, D.L., Appelo, C.A.J., 1999. User's guide to PHREEQC (Version 2) : a computer program for speciation, batch-reaction, one-dimensional transport, and inverse geochemical calculations (USGS Numbered Series No. 99–4259), Water-Resources Investigations Report. U.S. Geological Survey: Earth Science Information Center, Open-File Reports Section.

Petit, J.-C., Mea, G.D., Dran, J.-C., Magonthier, M.-C., Mando, P.A., Paccagnella, A., 1990. Hydrated-layer formation during dissolution of complex silicate glasses and minerals. Geochim. Cosmochim. Acta 54, 1941–1955. https://doi.org/10.1016/0016-7037(90)90263-K

Plodinec, M.J., Wicks, G.G., 1993. Applicatons of Hydration Thermodynamics to In-Situ Test Results. MRS Proc. 333, 145. https://doi.org/10.1557/PROC-333-145

Pokrovsky, O.S., Golubev, S.V., Mielczarski, J.A., 2006. Kinetic evidences of the existence of positively charged species at the quartz-aqueous solution interface. J. Colloid Interface Sci. 296, 189–194. https://doi.org/10.1016/j.jcis.2005.09.001

Pokrovsky, O.S., Golubev, S.V., Schott, J., Castillo, A., 2009. Calcite, dolomite and magnesite dissolution kinetics in aqueous solutions at acid to circumneutral pH, 25 to 150 °C and 1 to 55 atm $pCO_2$: New constraints on $CO_2$ sequestration in sedimentary basins. Chem. Geol., $CO_2$

geological storage: Integrating geochemical, hydrodynamical, mechanical and biological processes from the pore to the reservoir scale 265, 20–32. https://doi.org/10.1016/j.chemgeo.2009.01.013
Pokrovsky, O.S., Schott, J., 2000. Kinetics and mechanism of forsterite dissolution at 25 °C and pH from 1 to 12. Geochim. Cosmochim. Acta 64, 3313–3325. https://doi.org/10.1016/S0016-7037(00)00434-8
Pokrovsky, O.S., Schott, J., 2004. Experimental study of brucite dissolution and precipitation in aqueous solutions: surface speciation and chemical affinity control. Geochim. Cosmochim. Acta 68, 31–45. https://doi.org/10.1016/S0016-7037(03)00238-2
Prigiobbe, V., Costa, G., Baciocchi, R., Hänchen, M., Mazzotti, M., 2009. The effect of $CO_2$ and salinity on olivine dissolution kinetics at 120 °C. Chem. Eng. Sci. 64, 3510–3515. https://doi.org/10.1016/j.ces.2009.04.035
Rimstidt, J.D., 2015. Rate equations for sodium catalyzed quartz dissolution. Geochim. Cosmochim. Acta 167, 195–204. https://doi.org/10.1016/j.gca.2015.07.030
Rimstidt, J.D., Barnes, H.L., 1980. The kinetics of silica-water reactions. Geochim. Cosmochim. Acta 44, 1683–1699. https://doi.org/10.1016/0016-7037(80)90220-3
Rimstidt, J.D., Brantley, S.L., Olsen, A.A., 2012. Systematic review of forsterite dissolution rate data. Geochim. Cosmochim. Acta 99, 159–178. https://doi.org/10.1016/j.gca.2012.09.019
Rose, N.M., 1991. Dissolution rates of prehnite, epidote, and albite. Geochim. Cosmochim. Acta, The Macalpine Hills Lunar Meteorite Consortium 55, 3273–3286. https://doi.org/10.1016/0016-7037(91)90488-Q
Ross, G., 1967. Kinetics of acid dissolution of an orthochlorite mineral. Can. J. Chem. 45, 3031–3034. https://doi.org/10.1139/v67-491
Rosso, J., Rimstidt, J.D., 2000. A high-resolution study of forsterite dissolution rates. Geochim. Cosmochim. Acta 64, 797–811. https://doi.org/10.1016/S0016-7037(99)00354-3
Samson, S.D., Nagy, K.L., Cotton, W.B., 2005. Transient and quasi-steady-state dissolution of biotite at 22–25 °C in high pH, sodium, nitrate, and aluminate solutions. Geochim. Cosmochim. Acta 69, 399–413. https://doi.org/10.1016/j.gca.2004.07.005
Schaef, H.T., McGrail, B.P., 2009. Dissolution of Columbia River Basalt under mildly acidic conditions as a function of temperature: Experimental results relevant to the geological sequestration of carbon dioxide. Appl. Geochem. 24, 980–987. https://doi.org/10.1016/j.apgeochem.2009.02.025
Schaef, H.T., McGrail, B.P., Owen, A.T., 2009. Basalt- $CO_2$–$H_2O$ interactions and variability in carbonate mineralization rates. Energy Procedia, Greenhouse Gas Control Technologies 9 1, 4899–4906. https://doi.org/10.1016/j.egypro.2009.02.320
Schaef, H.T., McGrail, B.P., Owen, A.T., 2010. Carbonate mineralization of volcanic province basalts. Int. J. Greenh. Gas Control, The Ninth International Conference on Greenhouse Gas Control Technologies 4, 249–261. https://doi.org/10.1016/j.ijggc.2009.10.009
Schnoor, J.L., 1990. Kinetics of chemical weathering: A comparison of laboratory and field weathering rates, in: Aquatic Chemical Kinetics : Reaction Rates of Processes in Natural Waters. Wiley, New York, USA, pp. 475–504.
Schott, J., Berner, R.A., 1983. X-ray photoelectron studies of the mechanism of iron silicate dissolution during weathering. Geochim. Cosmochim. Acta 47, 2233–2240. https://doi.org/10.1016/0016-7037(83)90046-7
Schott, J., Berner, R.A., 1985. Dissolution Mechanisms of Pyroxenes and Olivines During Weathering, in: Drever, J.I. (Ed.), The Chemistry of Weathering, Nato ASI Series. Springer Netherlands, Dordrecht, pp. 35–53. https://doi.org/10.1007/978-94-009-5333-8_3
Schott, J., Berner, R.A., Sjöberg, E.L., 1981. Mechanism of pyroxene and amphibole weathering - I. Experimental studies of iron-free minerals. Geochim. Cosmochim. Acta 45, 2123–2135. https://doi.org/10.1016/0016-7037(81)90065-X
Schott, J., Oelkers, E.H., 1995. Dissolution and crystallization rates of silicate minerals as a function of chemical affinity. Pure Appl. Chem. 67, 903–910. https://doi.org/10.1351/pac199567060903

1733 Schott, J., Pokrovsky, O.S., Oelkers, E.H., 2009. The Link Between Mineral Dissolution/Precipitation
1734 Kinetics and Solution Chemistry. Rev. Mineral. Geochem. 70, 207–258.
1735 https://doi.org/10.2138/rmg.2009.70.6
1736 Schott, J., Pokrovsky, O.S., Spalla, O., Devreaux, F., Gloter, A., Mielczarski, J. A.,2012. Formation,
1737 growth and transformation of leached layers during silicate minerals dissolution: the example
1738 of wollastonite. Geochim. Cosmochim. Acta 98, 259-281.
1739 Schwartzentruber, J., Fürst, W., Renon, H., 1987. Dissolution of quartz into dilute alkaline solutions at
1740 90 °C: A kinetic study. Geochim. Cosmochim. Acta 51, 1867–1874.
1741 https://doi.org/10.1016/0016-7037(87)90177-3
1742 Schweda, P., 1989. Kinetics of alkali feldspar dissolution at low temperature, in: Proceeding of the 6th
1743 International Symposium on Water-Rock Interaction. AA Balkema, Rotterdam, pp. 609–612.
1744 Schweda, P., 1990. Kinetics and mechanisms of alkali feldspar dissolution at low temperatures.
1745 Stockholm University, Fakulty of Science, Department of Geology and Geochemistry,
1746 Stockholm, Sweden.
1747 Seidel, A., Löbbus, M., Vogelsberger, W., Sonnefeld, J., 1997. The kinetics of dissolution of silica
1748 'Monospher' into water at different concentrations of background electrolyte. Solid State Ion.,
1749 International Symposium on the Reactivity of Solids 101–103, 713–719.
1750 https://doi.org/10.1016/S0167-2738(97)00289-0
1751 Shirokova, L.S., Bénézeth, P., Pokrovsky, O.S., Gerard, E., Ménez, B., Alfredsson, H., 2012. Effect of
1752 the heterotrophic bacterium Pseudomonas reactans on olivine dissolution kinetics and
1753 implications for $CO_2$ storage in basalts. Geochim. Cosmochim. Acta 80, 30–50.
1754 https://doi.org/10.1016/j.gca.2011.11.046
1755 Shoji, S., Tohoku U., Nanzyo, M., Shirato, Y., Ito, T., 1993. Chemical kinetics of weathering in young
1756 andisols from northeastern Japan using soil age normalized to 10 ºC. Soil Sci. USA.
1757 Siegel, D.I., Pfannkuch, H.O., 1984. Silicate mineral dissolution at pH 4 and near standard temperature
1758 and pressure. Geochim. Cosmochim. Acta 48, 197–201. https://doi.org/10.1016/0016-
1759 7037(84)90362-4
1760 Siever, R., Woodford, N., 1979. Dissolution kinetics and the weathering of mafic minerals. Geochim.
1761 Cosmochim. Acta 43, 717–724. https://doi.org/10.1016/0016-7037(79)90255-2
1762 Sissmann, O., Brunet, F., Martinez, I., Guyot, F., Verlaguet, A., Pinquier, Y., Daval, D., 2014.
1763 Enhanced Olivine Carbonation within a Basalt as Compared to Single-Phase Experiments:
1764 Reevaluating the Potential of $CO_2$ Mineral Sequestration. Environ. Sci. Technol. 48, 5512–
1765 5519. https://doi.org/10.1021/es405508a
1766 Sissmann, O., Daval, D., Brunet, F., Guyot, F., Verlaguet, A., Pinquier, Y., Findling, N., Martinez, I.,
1767 2013. The deleterious effect of secondary phases on olivine carbonation yield: Insight from
1768 time-resolved aqueous-fluid sampling and FIB-TEM characterization. Chem. Geol. 357, 186–
1769 202. https://doi.org/10.1016/j.chemgeo.2013.08.031
1770 Sposito, G., 1981. Cation exchange in soils: An historical and theoretical perspective. Chem. Soil
1771 Environ. 40, 13–30.
1772 Stillings, L.L., Brantley, S.L., 1995. Feldspar dissolution at 25 °C and pH 3: Reaction stoichiometry
1773 and the effect of cations. Geochim. Cosmochim. Acta 59, 1483–1496.
1774 https://doi.org/10.1016/0016-7037(95)00057-7
1775 Stillings, L.L., Drever, J.I., Brantley, S.L., Sun, Y., Oxburgh, R., 1996. Rates of feldspar dissolution at
1776 pH 3–7 with 0–8 m M oxalic acid. Chem. Geol., Chemical And Biological Control On
1777 Mineral Growth And Dissolution Kinetics, American Chemical Society Meeting 132, 79–89.
1778 https://doi.org/10.1016/S0009-2541(96)00043-5
1779 Stockmann, G.J., Shirokova, L.S., Pokrovsky, O.S., Bénézeth, P., Bovet, N., Gislason, S.R., Oelkers,
1780 E.H., 2012. Does the presence of heterotrophic bacterium Pseudomonas reactans affect
1781 basaltic glass dissolution rates? Chem. Geol. 296–297, 1–18.
1782 https://doi.org/10.1016/j.chemgeo.2011.12.011
1783 Stockmann, G., Wolff-Boenisch, D., Gíslason, S.R., Oelkers, E.H., 2008. Dissolution of diopside and
1784 basaltic glass: the effect of carbonate coating. Mineral. Mag. 72, 135–139.
1785 https://doi.org/10.1180/minmag.2008.072.1.135

1786 Stopar, J.D., Jeffrey Taylor, G., Hamilton, V.E., Browning, L., 2006. Kinetic model of olivine
1787 dissolution and extent of aqueous alteration on mars. Geochim. Cosmochim. Acta, A Special
1788 Issue Dedicated to Larry A. Haskin 70, 6136–6152. https://doi.org/10.1016/j.gca.2006.07.039
1789 Stumm, W., Furrer, G., Kunz, B., 1983. The role of surface coordination in precipitation and
1790 dissolution of mineral phase. Croat. Chem. Acta. 58,593-611.
1791 Stumm, W., Wieland, E., 1990. Dissolution of oxide and silicate minerals: rates depend on surface
1792 speciation. In: Aquatic Chemical Kinetics. Stumm W (ed) John Wiley, New York, p 367-400.
1793 Sun, Y., 1994. The effect of pH and oxalate ion on the dissolution rates of plagioclase feldspar. MS
1794 thesis, University of Wyoming, Laramie, WY.
1795 Sverdrup, H.U., 1990. The Kinetics of Base Cation Release Due to Chemical Weathering. Lund
1796 University Press, Lund, Sweden.
1797 Swoboda-Colberg, N.G., Drever, J.I., 1993. Mineral dissolution rates in plot-scale field and laboratory
1798 experiments. Chem. Geol., Geochemical kinetics of mineral-water reactions in the field and
1799 the laboratory 105, 51–69. https://doi.org/10.1016/0009-2541(93)90118-3
1800 Talman, S.J., Nesbitt, H. W., 1988. Dissolution of populations of ultrafine grains with applications to
1801 feldspars. Geochim. Cosmochim. Acta 52, 1967-1471.
1802 Tan, K.H., 1980. The release of silicon, aluminum, and potassium during decomposition of soil
1803 minerals by humic acid. Soil Sci. 129.
1804 Taylor, A.S., Blum, J.D., Lasaga, A.C., 2000. The dependence of labradorite dissolution and Sr
1805 isotope release rates on solution saturation state. Geochim. Cosmochim. Acta 64, 2389–2400.
1806 https://doi.org/10.1016/S0016-7037(00)00361-6
1807 Temkin, M.I., 1963. Kinetics of stationary reactions. Dokl. Akad. Nauk SSSR 156–159.
1808 Tester, J.W., Worley, W.G., Robinson, B.A., Grigsby, C.O., Feerer, J.L., 1994. Correlating quartz
1809 dissolution kinetics in pure water from 25 to 625 °C. Geochim. Cosmochim. Acta 58, 2407–
1810 2420. https://doi.org/10.1016/0016-7037(94)90020-5
1811 Townsend, R.P., 1991. Chapter 10 Ion Exchange in Zeolites, in: van Bekkum, H., Flanigen, E.M.,
1812 Jansen, J.C. (Eds.), Studies in Surface Science and Catalysis, Introduction to Zeolite Science
1813 and Practice. Elsevier, pp. 359–390. https://doi.org/10.1016/S0167-2991(08)63608-3
1814 Tutolo, B.M., Luhmann, A.J., Kong, X.-Z., Saar, M.O., Seyfried, W.E., 2015. $CO_2$ sequestration in
1815 feldspar-rich sandstone: Coupled evolution of fluid chemistry, mineral reaction rates, and
1816 hydrogeochemical properties. Geochim. Cosmochim. Acta 160, 132–154.
1817 https://doi.org/10.1016/j.gca.2015.04.002
1818 Ullman, W.J., Welch, S.A., 2002. Organic ligands and feldspar dissolution. Water-Rock Interact. Ore
1819 Depos. Environ. Geochem. Tribute David Crearar 3–35.
1820 Van Cappellen, P., Qiu, L., 1997. Biogenic silica dissolution in sediments of the Southern Ocean. II.
1821 Kinetics. Deep Sea Res. Part II Top. Stud. Oceanogr., Antares I: France JGOFS in the Indian
1822 Sector of the Southern Ocean; Benthic and Water Column Processes 44, 1129–1149.
1823 https://doi.org/10.1016/S0967-0645(96)00112-9
1824 Van Hees, P.A.W., Lundström, U.S., Mörth, C.-M., 2002. Dissolution of microcline and labradorite in
1825 a forest O horizon extract: the effect of naturally occurring organic acids. Chem. Geol. 189,
1826 199–211. https://doi.org/10.1016/S0009-2541(02)00141-9
1827 Van Herk, J., Pietersen, H.S., Schuiling, R.D., 1989. Neutralization of industrial waste acids with
1828 olivine — The dissolution of forsteritic olivine at 40–70 °C. Chem. Geol., Water-rock
1829 interaction 76, 341–352. https://doi.org/10.1016/0009-2541(89)90102-2
1830 Velbel, M.A., 1985. Geochemical mass balances and weathering rates in forested watersheds of the
1831 Southern Blue Ridge. Am. J. Sci. 285, 904–930.
1832 Velbel, M.C., 1993. Temperature dependence of silicate weathering in nature: how strong a feedback
1833 on long-term accumulation of atmospheric $CO_2$ and global greenhouse warming. Geology 21,
1834 1059–1062.
1835 Velbel, M.A., 2014. Etch-pit size, dissolution rate, and time in the experimental dissolution of olivine:
1836 Implications for estimating olivine lifetime at the surface of Mars. Am. Mineral. 99, 2227–
1837 2233. https://doi.org/10.2138/am-2014-4654
1838 Voigt, M., Marieni, C., Clark, D.E., Gíslason, S.R., Oelkers, E.H., 2018. Evaluation and refinement of
1839 thermodynamic databases for mineral carbonation. Energy Procedia 146, 81–91.
1840 https://doi.org/10.1016/j.egypro.2018.07.012

Voinot, A., Lemarchand, D., Collignon, C., Granet, M., Chabaux, F., Turpault, M.-P., 2013. Experimental dissolution vs. transformation of micas under acidic soil conditions: Clues from boron isotopes. Geochim. Cosmochim. Acta 117, 144–160.

Walther, J.V., Wood, B.J., 1986. Mineral-fluid reaction rates. In: Walther, J.V., Wood, B.J. (eds) Fluid-rock interactions during metamorphism. Adv. Phys. Geochem. 5, Springer, New York Berlin Heidelberg, pp 194–211

Wang, T., Wang, H., Zhang, F., Xu, T., 2013. Simulation of $CO_2$–water–rock interactions on geologic $CO_2$ sequestration under geological conditions of China. Mar. Pollut. Bull. 76, 307–314. https://doi.org/10.1016/j.marpolbul.2013.08.014

Welch, S.A., Ullman, W.J., 1993. The effect of organic acids on plagioclase dissolution rates and stoichiometry. Geochim. Cosmochim. Acta 57, 2725–2736. https://doi.org/10.1016/0016-7037(93)90386-B

Welch, S.A., Ullman, W.J., 1996. Feldspar dissolution in acidic and organic solutions: Compositional and pH dependence of dissolution rate. Geochim. Cosmochim. Acta 60, 2939–2948. https://doi.org/10.1016/0016-7037(96)00134-2

Westrich, H.R., Cygan, R.T., Casey, W.H., Zemitis, C., Arnold, G.W., 1993. The dissolution kinetics of mixed-cation orthosilicate minerals. Am. J. Sci. 293, 869–893. https://doi.org/10.2475/ajs.293.9.869

White, A.F., 1983. Surface chemistry and dissolution kinetics of glassy rocks at 25 °C. Geochim. Cosmochim. Acta 47, 805–815. https://doi.org/10.1016/0016-7037(83)90114-X

White, A., Blum, A., Schulz, M., Huntington, T., Peters, N., Stonestrom, D., 2002. Chemical weathering of the Panola Granite: Solute and regolith elemental fluxes and the weathering rate of biotite. Water-Rock Interact. Ore Depos. Environ. Geochem. Tribute David Crerar 7.

White, A.F., Brantley, S.L., 1995. Chemical weathering rates of silicate minerals; an overview. Rev. Mineral. Geochem. 31, 1–22.

White, A.F., Yee, A., 1985. Aqueous oxidation-reduction kinetics associated with coupled electron-cation transfer from iron-containing silicates at 25 °C. Geochim. Cosmochim. Acta 49, 1263–1275. https://doi.org/10.1016/0016-7037(85)90015-8

Whitworth, T.M., 1998. Clay minerals: Ion exchange, in: Geochemistry. Springer Netherlands, Dordrecht, pp. 85–87. https://doi.org/10.1007/1-4020-4496-8_56

Wieland, E., Werhli, B., Stumm, W., 1988. The coordination chemistry of weathering: III. A generalization on the dissolution rates of minerals. Geochim. Cosmochim. Acta 52, 1969-1981.

Wogelius, R.A., Walther, J.V., 1991. Olivine dissolution at 25 °C: Effects of pH, $CO_2$, and organic acids. Geochim. Cosmochim. Acta USA 55:4. https://doi.org/10.1016/0016-7037(91)90153-V

Wogelius, R.A., Walther, J.V., 1992. Olivine dissolution kinetics at near-surface conditions. Chem. Geol. 97, 101–112. https://doi.org/10.1016/0009-2541(92)90138-U

Wolff-Boenisch, D., Gislason, S.R., Oelkers, E.H., Putnis, C.V., 2004. The dissolution rates of natural glasses as a function of their composition at pH 4 and 10.6, and temperatures from 25 to 74 °C. Geochim. Cosmochim. Acta 68, 4843–4858. https://doi.org/10.1016/j.gca.2004.05.027

Wollast, R., Chou, L., 1988. Rate Control of Weathering of Silicate Minerals at Room Temperature and Pressure, in: Lerman, A., Meybeck, M. (Eds.), Physical and Chemical Weathering in Geochemical Cycles, NATO ASI Series. Springer Netherlands, Dordrecht, pp. 11–32. https://doi.org/10.1007/978-94-009-3071-1_2

Xiao, Z., Jonckbloedt, R.C.L., Schuiling, R.D., 1999. Neutralization of waste acids with olivine dissolution in organically contaminated acids. Chem Erde 59, 33–45.

Xiao, M., Yuan, X., Cheng, D., Wu, S., Cao, Z., Tang, Y., Xie, Z., 2018. Feldspar Dissolution and Its Influence on Reservoirs: A Case Study of the Lower Triassic Baikouquan Formation in the Northwest Margin of the Junggar Basin, China [WWW Document]. Geofluids. https://doi.org/10.1155/2018/6536419

Xu, T., Sonnenthal, E., Spycher, N., Pruess, K., 2006. TOUGHREACT-A Simulation Program for Non-Isothermal Multiphase Reactive Geochemical Transport in Variably Saturated Geologic Media: Applications to Geothermal Injectivity and $CO_2$ Geological Sequestration. Comput Geosci 32, 145–165. https://doi.org/10.1016/j.cageo.2005.06.014

Xu, T., Spycher, N., Sonnenthal, E., Zhang, G., Zheng, L., Pruess, K., 2011. TOUGHREACT Version 2.0: A simulator for subsurface reactive transport under non-isothermal multiphase flow conditions. Comput. Geosci., 2009 Transport of Unsaturated Groundwater and Heat Symposium 37, 763–774. https://doi.org/10.1016/j.cageo.2010.10.007

Zaidi, S., 2012. Zeolites as inorganic ion exchangers for environmental applications: An overview, in: Ion Exchange Technology II: Applications. pp. 183–215. https://doi.org/10.1007/978-94-007-4026-6_9

Zhang, H., Bloom, P.R., Nater, E.A., 1990. Morphology and Chemistry of Hornblende Dissolution Products in Acid Solutions. Scientific Journal Series Paper no. 16275, Minnesota Agricultural Experiment Station, University of Minnesota, St. Paul, MN 55108. in: Douglas, L.A. (Ed.), Developments in Soil Science. Elsevier, pp. 551–556. https://doi.org/10.1016/S0166-2481(08)70372-6

Zhang, Y., Hu, B., Teng, Y., Tu, K., Zhu, C., 2019. A library of BASIC scripts of reaction rates for geochemical modeling using PHREEQC. Comput. Geosci. 133, 104316. https://doi.org/10.1016/j.cageo.2019.104316

## Appendix A- Summary of previously published data

**Table S1:** Experimental dataset for dissolution of selected silicate minerals discussed here.

## Appendix B – Kinetic database

**B1.** Version for PHREEQC software with RATES blocks.

**B2**. Readme file with a description of the parameters used in the database.

## Appendix C – Example application of kinetic database for mineral dissolution in PHREEQC geochemical model

**Ex1**: Quartz dissolution at 25 °C and pH from 2 to 10.

**Ex2**: Comparison of the kinetic parameters presented in Palandri and Kharaka (2004) and here using an example of albite dissolution at 25 °C.

**Ex3**: Forsterite dissolution in the presence of $CO_2$.